

USE OF BORON COMPOUNDS AS SYNERGISTIC FLAME RETARDANT IN LOW
DENSITY POLYETHYLENE – ETHYLENE VINYL ACETATE BLENDS AND
NANOCOMPOSITES

A THESIS SUBMITTED TO
THE GRADUATE SCHOOL OF NATURAL AND APPLIED SCIENCES
OF
MIDDLE EAST TECHNICAL UNIVERSITY

BY

ESİN İBİBKAN

IN PARTIAL FULFILLMENT OF THE REQUIREMENTS
FOR
THE DEGREE OF MASTER OF SCIENCE
IN
POLYMER SCIENCE AND TECHNOLOGY

JUNE 2013

Approval of the Thesis:

**USE OF BORON COMPOUNDS AS SYNERGISTIC FLAME RETARDANT IN
LOW DENSITY POLYETHYLENE – ETHYLENE VINYL ACETATE BLENDS
AND NANOCOMPOSITES**

submitted by **ESİN İBİBİKCAN** in partial fulfillment of the requirements for the degree
of **Master of Science in Department of Polymer Science and Technology, Middle
East Technical University** by,

Prof. Dr. Canan Özgen
Dean, Graduate School of **Natural and Applied Sciences**

Prof. Dr. Teoman Tinçer
Head of Department, **Polymer Science and Technology**

Prof. Dr. Cevdet Kaynak
Supervisor, **Metallurgical and Materials Eng. Dept. METU**

Examining Committee Members:

Prof. Dr. Teoman Tinçer
Chemistry Department, METU

Prof. Dr. Cevdet Kaynak
Metallurgical and Materials Engineering Department, METU

Prof. Dr. Göknur Bayram
Chemical Engineering Department, METU

Prof. Dr. Necati Özkan
Polymer Science and Technology Department, METU

Assist. Prof. Dr. Y. Eren Kalay
Metallurgical and Materials Engineering Department, METU

Date:
28.06.2013

I hereby declare that all information in this document has been obtained and presented in accordance with academic rules and ethical conduct. I also declare that, as required by these rules and conduct, I have fully cited and referenced all material and results that are not original to this work.

Name, Last name: Esin İbikcan

Signature:

ABSTRACT

USE OF BORON COMPOUNDS AS SYNERGISTIC FLAME RETARDANT IN LOW DENSITY POLYETHYLENE – ETHYLENE VINYL ACETATE BLENDS AND NANOCOMPOSITES

İbibikcan, Esin

M.Sc., Department of Polymer Science and Technology

Supervisor: Prof. Dr. Cevdet Kaynak

June 2013, 80 pages

It is known that for the production of halogen-free cable insulation materials based on polyethylene, very high amounts of traditional metal hydroxide flame retardants such as 65 wt% aluminum hydroxide (ATH) is required to fulfill international directives. Thus, flammability studies investigating synergistic compounds and contribution of nanomaterials have been crucial.

Therefore, the first purpose of this thesis was to reveal possible synergism of three boron compounds zinc borate (ZB), boron oxide (BO) and boric acid (BA) on the flame retardancy of two cable insulation materials; low density polyethylene (LDPE) and its blend with ethylene vinyl acetate (EVA) both loaded with ATH. The second purpose of this thesis was to investigate contribution of nanoclays when used alone, and together with ATH, and also together with ATH-ZB synergistic system.

For these purposes, materials were compounded by melt mixing method with a laboratory scale twin-screw extruder, while specimens were shaped by compression and injection molding. Flammability properties of the specimens were investigated by using Limiting Oxygen Index (LOI), UL-94 Vertical Burning and Mass Loss Cone Calorimeter (MLC) analyses. Other characterization techniques required in this thesis were; X-ray diffraction analysis (XRD), scanning and transmission electron microscopy (SEM and TEM), thermogravimetric analysis (TGA) and tensile tests.

Flammability tests in the first part of this study simply revealed that replacement of certain amount of ATH with boron compounds could lead to certain levels of synergism in many flame retardancy parameters. Residue analyses revealed that these improvements were basically due to further contribution of boron compounds to the physical barrier mechanism of ATH in both gas and condensed phases.

Analyses in the second part of this study indicated that even use of nanoclays alone could improve many flammability parameters including peak heat release rate, time to ignition

and fire growth index. Contributions of nanoclays were much more significant when they were incorporated together with traditional ATH or together with synergistic ATH-ZB system. Residue analysis revealed that contribution of nanoclays to the flame retardancy mechanisms of ATH and ZB was mainly by formation of strong and tough char structure via well-dispersed and intercalated/exfoliated silicate layers shielding the underlying polymer matrices from heat and mass transfer.

Keywords: Flame Retardancy, Low Density Polyethylene, Ethylene Vinyl Acetate, Aluminum Hydroxide, Zinc Borate, Boron Oxide, Boric Acid, Nanoclays

ÖZ

BOR BİLEŞİKLERİNİN DÜŞÜK YOĞUNLUKLU POLİETİLEN – ETİLEN VİNİL ASETAT KARIŞIMLARI VE NANOKOMPOZİTLERİNDE SİNERJİSTİK ALEV GECİKTİRİCİ OLARAK KULLANILMASI

İbibikcan, Esin
Yüksek Lisans, Polimer Bilim ve Teknolojisi Bölümü
Tez Yöneticisi: Prof. Dr. Cevdet Kaynak

Haziran 2013, 80 sayfa

Bilindiği üzere uluslararası yönergelerde gerekli olan alevlenme dayanımı düzeyini sağlayabilmek için polietilen bazlı halojen içermeyen kablo yalıtım malzemelerinde çok yüksek oranlarda geleneksel metal hidroksit alev geciktiricilerin kullanılması gerekmektedir, örneğin ağırlıkça %65 civarında alüminyum trihidroksit (ATH). Bu yüzden, alevlenme dayanımı ile ilgili araştırmalarda olası sinerjistik bileşiklerin ve nanomalzemelerin katkılarının incelenmesi çok önemli olmaktadır.

Dolayısıyla, bu tezin birinci amacı, ATH ile birlikte üç bor bileşiğinin; çinko borat (ZB), bor oksit (BO) ve borik asidin (BA) iki kablo yalıtım malzemesinin; düşük yoğunluklu polietilen (LDPE) ve onun etilen vinil asetat (EVA) ile karışımının alevlenme dayanımına olan olası sinerjistik etkilerini ortaya çıkarmaktır. Bu tezin ikinci amacı ise, nanokillerin hem tek başlarına, hem ATH ile birlikte, hem de ATH-ZB sinerjistik sistemi ile birlikte kullanıldıklarında oluşan katkılarını incelemektir.

Bu amaçlar için, malzemeler laboratuvar boyutlu çift vidalı ekstrüder ile eriyik halde karıştırma yöntemi ile hazırlanmış, numuneler ise basınçlı kalıplama ve enjeksiyon kalıplama yöntemleri ile şekillendirilmiştir. Numunelerin alevlenme dayanımları Oksijen Limiti İndeksi (LOI), UL- 94 Dikey yanma testleri ve Kütle Kaybı Konik Kalorimetre (MLC) analizleri ile incelenmiştir. Bu tezde gerekli olan diğer karakterizasyon teknikleri ise şunlardır; X-ışını kırınımı analizi (XRD), taramalı ve geçirimli elektron mikroskobu (SEM and TEM), termogravimetrik analiz (TGA) ve çekme testleri.

Bu çalışmanın ilk kısmında yapılan alevlenme dayanımı testleri, belli miktarlardaki ATH yerine bor bileşiklerinin kullanılmasının birçok alevlenme dayanımı parametresinde belli derecelerde sinerjik iyileşmelerin sağlanabileceğini ortaya çıkarmıştır. Kalıntı analizleri bu iyileşmelerin özellikle bor bileşiklerinin ATH'nin hem gaz hem de katı fazdaki fiziksel bariyer mekanizmasına ek katkısından dolayı olduğunu göstermiştir.

Bu çalışmanın ikinci kısmında yapılan analizler ise, nanokillerin tek başlarına kullanıldıklarında bile birçok alevlenme dayanımı parametresini iyileştirdiğini göstermiştir, örneğin ısı açığa çıkma hızı tavan değeri, tutuşma süresi ve yangın büyüme indeksi. Nanokillerin katkılarının geleneksel ATH ile birlikte ya da sinerjistik ATH-ZB sistemi ile birlikte kullanıldıklarında çok daha ileri düzeyde olduğu gözlemlenmiştir. Kalıntı analizleri nanokillerin ATH ve ZB'nin alevlenme dayanımı mekanizmalarına özellikle iyi dağılmış ve interkale/eksfoliye olmuş silika katmanları sayesinde güçlü ve tok kül yapısı oluşturarak katkıda bulduklarını ortaya çıkarmıştır. Böylece bu kül yapısı altındaki polimer matrisini ısı ve kütle transferinden korumaktadır.

Anahtar Sözcükler: Alevlenme Dayanımı, Düşük Yoğunluklu Polietilen, Etilen Vinil Asetat, Aluminyum Hidroksit, Çinko Borat, Bor Oksit, Borik Asit, Nanokiller

to my precious family

ACKNOWLEDGEMENTS

First and foremost, I would like to express my sincere gratitude to my supervisor Prof. Dr. Cevdet Kaynak for his support, guidance, advice, encouragement and patience throughout this dissertation.

I would like to gratefully acknowledge BOREN National Boron Research Institute for the grant with the project number 2009-Ç-0236, and ETI Mine Works Inc. for supplying boron compounds and the facilities used for their characterization.

I would like to acknowledge all the technical staff and administrative board of the Metallurgical and Materials Engineering Department for supplying all the research facilities required in this thesis. I would also like to thank to METU Central Laboratory for TEM analyses.

I want to thank my laboratory mates, Ayşe Çağıl Özkaraca, Seçil Şankal, Nihat Ali Işırtman and Bengü Melike Sipahioğlu for their sincere friendship, support and encouragement.

My sincere thanks go to the very best of friends, Simla Tanrıverdi, Melis Baltalı, Ela Uysal and my cousin Zeynep Çekinmez for helping me get through the difficult times, and for all the support, entertainment and caring they have provided for many years.

I would like to express my deepest gratitude to my mother Günseli İbibikcan, my father Nafi İbibikcan and my brother Cenk İbibikcan. I thank them for giving me wholehearted love without return and for believing in me. This thesis would certainly be not possible without their support.

My special thanks go to Barışcan Özkasnaklı for his endless love, encouragement, patience and never-ending support. Words are not enough to express my deep gratitude; just I can thank him from the bottom of my heart for being in my life.

TABLE OF CONTENTS

ABSTRACT	v
ÖZ	vii
ACKNOWLEDGEMENTS	x
TABLE OF CONTENTS	xi
LIST OF TABLES	xiii
LIST OF FIGURES	xiv
NOMENCLATURE	xvi
CHAPTERS	
1. INTRODUCTION	1
1.1 LDPE, EVA, their Blends and Nanocomposites.....	1
1.1.1 LDPE and EVA.....	1
1.1.2 Blends of LDPE and EVA	2
1.1.3 Clay Nanocomposites of LDPE and EVA	3
1.2 Flammability of Polymers.....	5
1.2.1 Flammability Tests.....	7
1.2.2 Flame Retardancy Mechanisms	11
1.2.3 Traditional Metal Hydroxide Flame Retardants and Boron Compounds... 13	
1.3 Literature Survey	14
1.3.1 Studies on the Flammability of LDPE and/or EVA Matrices with ATH and Boron Compounds	14
1.3.2 Studies on the Flammability of Clay Nanocomposites of LDPE and/or EVA Matrices with ATH.....	16
1.4 Aim of the Study	18
2. EXPERIMENTAL WORK	21
2.1 Materials Used	21
2.2 Production of the Specimens.....	23
2.3 Flammability Tests of the Specimens	25
2.4 Other Tests and Analysis	25
3. RESULTS AND DISCUSSION	27
3.1 Synergistic Effects of Three Boron Compounds with ATH in LDPE and LDPE/EVA Matrices	27
3.1.1 Thermal Decomposition of ATH and Boron Compounds	27
3.1.2 UL-94 and LOI Flammability Tests.....	30
3.1.3 Mass Loss Cone Calorimetry	32
3.1.4 Thermogravimetric Analysis	37
3.1.5 Residue Analysis	41
3.1.6 Mechanical Behavior	45
3.2 Contribution of Nanoclays with ATH and Zinc Borate in LDPE and LDPE/EVA	

Matrices.....	50
3.2.1 Nanocomposite Formation	50
3.2.2 UL-94 and LOI Flammability Tests	54
3.2.3 Mass Loss Cone Calorimetry	55
3.2.4 Thermogravimetric Analysis.....	60
3.2.5 Residue Analysis	64
3.2.6 Mechanical Behavior.....	69
4. CONCLUSIONS	75
REFERENCES	77

LIST OF TABLES

TABLES

Table 1.1 Classifications of UL94 Vertical Burning test	9
Table 2.1 Chemical structure of the materials used	22
Table 2.2 Designations and compositions (wt%) of the specimens	24
Table 3.1 Thermal degradation parameters of ATH and boron compounds determined from TG and DTG curves	28
Table 3.2 Results of UL-94 and LOI flammability tests	31
Table 3.3 Mass Loss Cone Calorimeter parameters of the specimens	34
Table 3.4 Thermal degradation parameters of the specimens determined from TG and DTG curves	38
Table 3.5 Mechanical properties of the specimens	47
Table 3.6 Results of UL-94 and LOI flammability tests	54
Table 3.7 Mass Loss Cone Calorimeter parameters of the specimens (under 50 kW/m ² heat flux)	57
Table 3.8 Thermal degradation parameters determined from TG and DTG curves.....	61
Table 3.9 Mechanical properties of the specimens	71

LIST OF FIGURES

FIGURES

Figure 1.1 Chain configuration of LDPE	1
Figure 1.2 Polymerization of EVA copolymer.....	2
Figure 1.3 Crystal structure of montmorillonite clay	3
Figure 1.4 Three typical structures of polymer nanocomposites.....	4
Figure 1.5 Combustion cycle of polymers	5
Figure 1.6 Three basic stages of polymer combustion	6
Figure 1.7 Experimental set-up of Limiting Oxygen Index test.....	7
Figure 1.8 Experimental set-up of UL-94 Vertical Burning test.....	9
Figure 1.9 Experimental set-up of Mass Loss Cone Calorimeter test	11
Figure 3.1 (a) Thermogravimetric (TG) and (b) Differential Thermogravimetric (DTG) curves of ATH and boron compounds	29
Figure 3.2 (a) Heat Release Rate and (b) Mass Loss Rate curves of the specimens with LDPE matrix	35
Figure 3.3 (a) Heat Release Rate and (b) Mass Loss Rate curves of the specimens with LDPE/EVA matrix	36
Figure 3.4 (a) Thermogravimetric (TG) and (b) Differential Thermogravimetric (DTG) curves of the specimens with LDPE matrix	39
Figure 3.5 (a) Thermogravimetric (TG) and (b) Differential Thermogravimetric (DTG) curves of the specimens with LDPE/EVA matrix.....	40
Figure 3.6 Macroscale appearances of the surface char layers of MLC specimens with LDPE matrix; (a) LDPE-ATH65, (b) LDPE-ATH55-ZB10, (c) LDPE-ATH55-BO10, (d) LDPE-ATH55-BA10	41
Figure 3.7 Macroscale appearances of the surface char layers of MLC specimens with LDPE/EVA matrix; (a) LDPE/EVA-ATH65, (b) LDPE/EVA-ATH55-ZB10, (c) LDPE/EVA-ATH55-BO10, (d) LDPE/EVA-ATH55-BA10.....	42
Figure 3.8 XRD patterns of the chars of the MLC specimens with LDPE matrix .	43
Figure 3.9 XRD patterns of the chars of the MLC specimens with LDPE/EVA matrix..	44
Figure 3.10 Tensile stress-strain curves of the specimens with LDPE matrix	46
Figure 3.11 Tensile stress-strain curves of the specimens with LDPE/EVA matrix.....	46
Figure 3.12 SEM fractographs of the specimens with LDPE matrix; (a) LDPE, (b) LDPE-ATH65, (c) LDPE-ATH55-ZB10, (d) LDPE-ATH55-BO10, (e) LDPE-ATH55-BA10	48
Figure 3.13 SEM fractographs of the specimens with LDPE/EVA matrix; (a) LDPE/EVA, (b) LDPE/EVA-ATH65, (c) LDPE/EVA-ATH55-ZB10, (d) LDPE/EVA-ATH55-BO10, (e) LDPE/EVA-ATH55-BA10.....	49
Figure 3.14 XRD patterns of nanocomposite specimens with (a) LDPE matrix and (b) LDPE/EVA matrix	51
Figure 3.15 TEM images showing (a) uniform distribution, (b) and (c) intercalated and partly exfoliated structure of NC silicate layers in LDPE matrix.....	52

Figure 3.16 TEM images showing (a) uniform distribution, (b) and (c) intercalated and partly exfoliated structure of NC silicate layers in LDPE/EVA matrix	53
Figure 3.17 (a) Heat Release Rate and (b) Mass Loss Rate curves of the specimens with LDPE matrix	58
Figure 3.18 (a) Heat Release Rate and (b) Mass Loss Rate curves of the specimens with LDPE/EVA matrix.....	59
Figure 3.19 (a) Thermogravimetric (TG) and (b) Differential Thermogravimetric (DTG) curves of the specimens with LDPE matrix.....	62
Figure 3.20 (a) Thermogravimetric (TG) and (b) Differential Thermogravimetric (DTG) curves of the specimens with LDPE/EVA matrix.....	63
Figure 3.21 SEM images showing surface char barriers of the specimens with LDPE matrix after LOI test; (a)LDPE-NC, (b)LDPE-ATH60-NC, (c)LDPE-ATH50-ZB-NC ..	65
Figure 3.22 Macroscale appearances of the surface char layers of MLC specimens with LDPE matrix; (a) LDPE, (b) LDPE-NC, (c) LDPE-ATH65, (d) LDPE-ATH60-NC, (e) LDPE-ATH55-ZB, (f) LDPE-ATH50-ZB-NC.....	66
Figure 3.23 XRD patterns of the chars of the MLC nanocomposite specimens with LDPE matrix	67
Figure 3.24 XRD patterns of the chars of the MLC nanocomposite specimens with LDPE/EVA matrix.....	68
Figure 3.25 Tensile stress-strain curves of the specimens with LDPE matrix.....	70
Figure 3.26 Tensile stress-strain curves of the specimens with LDPE/EVA matrix	70
Figure 3.27 SEM fractographs of the specimens with LDPE matrix; (a) LDPE, (b) LDPE-NC, (c) LDPE-ATH65, (d) LDPE-ATH60-NC, (e) LDPE-ATH55-ZB, (f) LDPE-ATH50-ZB-NC.....	72
Figure 3.28 SEM fractographs of the specimens with LDPE matrix; (a) LDPE/EVA, (b) LDPE/EVA-NC, (c) LDPE/EVA-ATH65, (d) LDPE/EVA-ATH60-NC, (e) LDPE/EVA-ATH55-ZB, (f) LDPE/EVA-ATH50-ZB-NC.....	73

NOMENCLATURE

% Residue at 600°C	:	% char yield at 600 °C
2θ	:	XRD diffraction angle
ATH	:	aluminum trihydroxide
BA	:	boric acid
BO	:	boron oxide
DTG	:	differential thermogravimetric
EVA	:	ethylene vinyl acetate
FGI	:	Fire Growth Index
LDPE	:	low density polyethylene
LOI	:	limiting oxygen index
MDH	:	magnesium dihydroxide
MLC	:	mass loss cone calorimeter
NC	:	nanoclay
PHRR	:	Peak Heat Release Rate
SEM	:	scanning electron microscopy
T_{10wt%}	:	thermal degradation temperature for 10% mass loss
T_{50wt%}	:	thermal degradation temperature for 50% mass loss
T_{DTG-Peak 1}	:	first peak temperature in DTG curve
T_{DTG-Peak 2}	:	second peak temperature in DTG curve
T_{DTG-Peak 3}	:	third peak temperature in DTG curve
TEM	:	transmission electron microscopy
TG	:	thermogravimetric
THE	:	Total Heat Evolved
THE/TML	:	Total Heat Evolved/Total Mass Loss
TTI	:	Time To Ignition
UL-94	:	Underwriters Laboratories vertical burning test standard
XRD	:	X-ray diffraction analysis
ZB	:	zinc borate

CHAPTER 1

INTRODUCTION

1.1 LDPE, EVA, their Blends and Nanocomposites

1.1.1 LDPE and EVA

Polyethylene (PE), also known as polythene is a thermoplastic polymer. It is the polymer of ethylene ($\text{CH}_2=\text{CH}_2$) and produced under high temperature and pressure. The catalyst used during production is chosen by considering desired properties of the end-use product.

Low density polyethylene (LDPE) is formed via free radical polymerization under 150-350 MPa pressure and at 80-300°C in the presence of a radical initiator azobisisobutyronitrile (AIBN). LDPE, which was the first polyethylene developed, has from two to eight carbon atom length alkyl branch groups (Figure 1.1). LDPE is a semi-rigid, tough, flexible polymer having resistance to chemicals and moisture. It can be easily processed by most methods and used at standard service temperatures. Moreover, LDPE has excellent electrical insulation ability. These properties make LDPE a widely used polymeric material in many application areas, such as packaging, films, rigid containers, toys and for insulation of wires and cables [1, 2].



Figure 1.1 Chain configuration of LDPE

LDPE undergoes thermo-oxidative degradation by random chain scission [3]. Jana et al. [4] revealed that according to TG and DTG curves initial decomposition temperature of LDPE is around 305°C above which free radicals are generated. These radicals lead to sequential degradation and breakdown of the covalent C-C bond at a higher temperature.

Ethylene vinyl acetate (EVA) copolymer is produced from ethylene and vinyl acetate monomers (Figure 1.2). EVA copolymer is formed at 50-80°C under 2-8 MPa pressure via solution, suspension, emulsion or bulk polymerization [5]. Vinyl acetate content could be between 10 to 40% by weight. When the vinyl acetate content increases, tensile strength, resistance to heat and chemicals, and barrier properties of the polymer decrease. EVA copolymer is a clear, flexible and soft thermoplastic. It is flexible even at low temperatures, has high friction coefficient and resistance to chemicals. EVA can also accept high filler loadings. Application areas of EVA copolymer include packaging, adhesives, stretch films, shoe soles, disposable medical equipment, flexible toys and wire insulation [1].

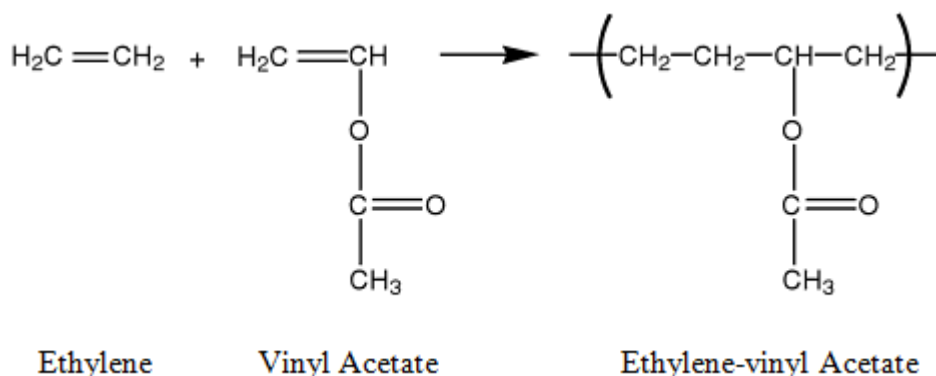


Figure 1.2 Polymerization of EVA copolymer

Thermal decomposition of EVA occurs in two steps. In the first step (around 350°C), it loses acetic acid and unsaturated polyenes are formed. In the second step (around 450°C), random chain scission of the remaining material proceeds, resulting in the formation of unsaturated vapour species, such as butane and ethylene [3].

1.1.2 Blends of LDPE and EVA

Blending two or more polymers is one of the most widely used technique to improve properties of the end-use product. In this respect, blends of LDPE and EVA are widely used in cable industry as the insulation coating. Another important application of these blends are shrinkable films and multilayer packaging [6].

Advantages of EVA over LDPE are its better flexibility even at low temperatures, better weather resistance, higher friction coefficient and ability of accepting higher filler

loadings. On the other hand, LDPE has improved chemical resistance, barrier properties and creep resistance [1]. Considering these properties of LDPE and EVA, it can be said that products made from LDPE/EVA blends would have many improved properties.

Takidis et al. [7] showed that during blending, both composition and process temperature are very important factors affecting compatibility of LDPE and EVA domains. They also suggested that mixing temperature should be higher than 180°C to achieve certain improvement in mechanical properties.

1.1.3 Clay Nanocomposites of LDPE and EVA

Polymer nanocomposites which have attracted attention in recent years are described as the materials which reinforcing nanoscale particles are dispersed in a polymer matrix. Polymer nanocomposites show tremendous improvements in many properties including mechanical, barrier, optical, thermal stability, fire retardancy, etc. [8, 9].

Nanoclays are one of the most widely investigated commercially available nanoparticles. Silica and alumina are the essential constituents of the montmorillonite clays. As shown in Figure 1.3, crystal structure of montmorillonite clay consists of two tetrahedral silicate layers sandwiching one octahedral alumina layer. The thickness of one montmorillonite clay sheet formed by these three layers is around 1 nm. In the natural state of montmorillonite clays, Na⁺ cations (or other cations such as K⁺) reside in the galleries between the layers [8].

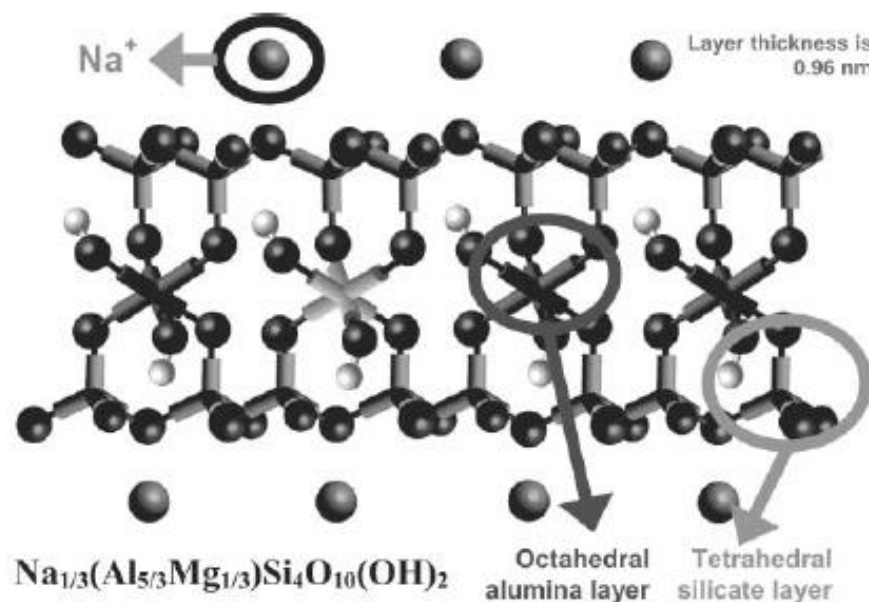


Figure 1.3 Crystal structure of montmorillonite clay [8]

In order to produce nanocomposites, clays should be organically modified. Because, clays are hydrophilic materials, they should be made organophilic in order to provide compatibility with hydrophobic polymers. Organic modification is also necessary to increase the interlayer distance required for intercalation [8, 10]. Natural silicate layers are usually compatible with the very polar polymers. Organic treatment of layered silicates is generally made with alkylammonium salts via cation exchange reaction. During this process, inorganic cations in the clay galleries should be exchanged with the desired organic cations, so that the clay would be tailored as organophilic [8, 11].

Organically modified layered silicates are dispersed in polar polymers while they are not compatible with nonpolar olefin polymers. Solvent mixing, in-situ polymerization and melt compounding are three methods used to disperse layered silicates in nonpolar polymers. On the other hand, in recent studies maleic anhydride is added as a compatibilizer to produce nonpolar olefin/clay nanocomposites [12].

Structure and accordingly properties of polymer/clay nanocomposites are influenced by the nature of used components and preparation method. There are three types of structures as shown in Figure 1.4. In the “phase separated (unmixed) structure”, polymer chains cannot penetrate between the silicate layers. Thus, the distance between the layers do not change leading to no improvements in the properties of the composite. When polymer chains intercalate between the silicate layers, then the distance between the layers increases leading to ordered multilayer structure which is called “intercalated structure”. An “exfoliated structure” can be obtained by the complete and uniform dispersion of silicate layers randomly in a polymer matrix [13].

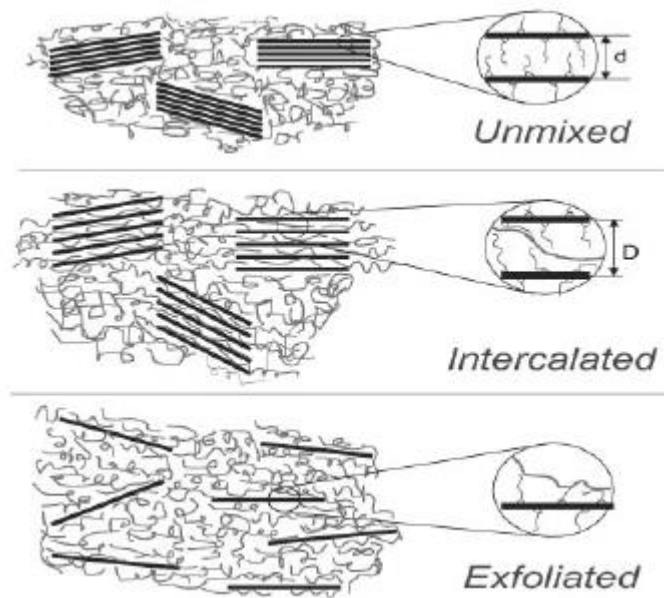


Figure 1.4 Three typical structures of polymer nanocomposites [8]

Nonpolar backbone of polyethylene induces difficulties in dispersion of layered silicates. Therefore, it may be necessary to use a compatibilizer for efficient intercalation. For instance, in the study of Zhang and Wilkie [14] maleic anhydride was used as a compatibilizer for the organically modified clay in LDPE matrix. They revealed that presence of maleic anhydride provided better intercalation. Morawiec et al. [10] also used maleic anhydride compatibilizer for the effective intercalation/exfoliation of silicate layers in LDPE. On the other hand, Zanetti and Costa [15] used EVA as a compatibilizer in LDPE matrix to obtain intercalated nanocomposite structure.

1.2 Flammability of Polymers

Despite their many advantages such as; low weight and ease of processing, polymers are very flammable materials due to their chemical structure consisting of mainly carbon and hydrogen. There are three parameters in the combustion cycle of polymers; heat, combustible and combustive (Figure 1.5). Combustion reaction starts with a heat source. Heat source increases temperature of the combustible (polymeric material) leading to start of bond scission at high temperatures. Then, volatile fractions of the combustible diffuse into the air and form combustible gaseous mixture. Finally, when ignition temperature is reached, or even at lower temperature with an external energy, combustible gaseous mixture ignites [16].

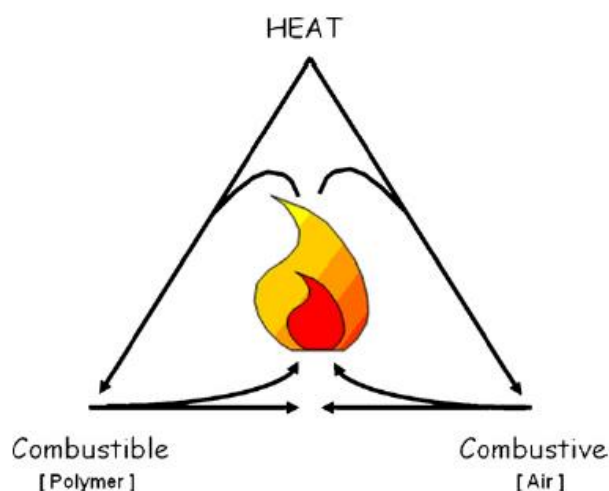


Figure 1.5 Combustion cycle of polymers [16]

Combustion of polymers takes place basically at three stages as shown in Figure 1.6 [17]:

- *Ignition*: the onset of flaming combustion which involves an ignition source, small length scale (cm), ambient temperatures around 600-700 K (in the range of ignition temperatures) and high ventilation.

- *Developing fire*: flaming combustion continues with an external heat flux of around 20-60 kW/m², larger length scale (dm-m), ambient temperatures around 700-900 K (above the ignition temperature) and still high ventilation.
- *Fully developed fire*: final stage of flame combustion with a high external heat flux (larger than 50 kW/m²), large length scales (larger than m), ambient temperatures above auto-ignition temperatures (higher than 900 K), and low ventilation.

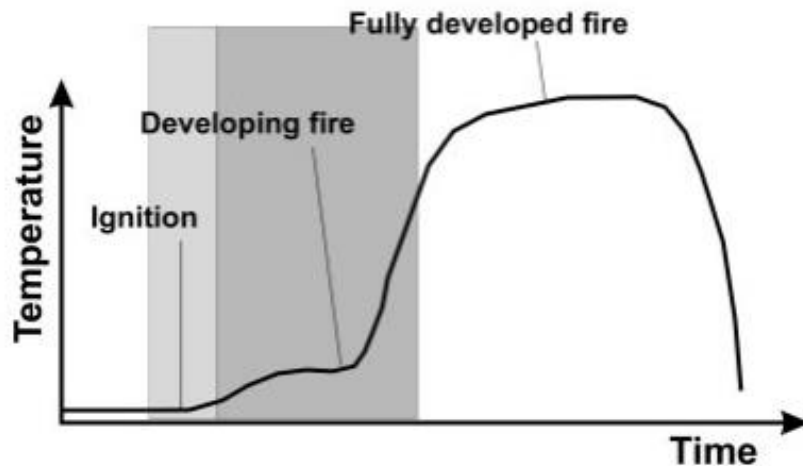


Figure 1.6 Three basic stages of polymer combustion [17]

During combustion process several chemical and physical reactions occur in solid, gaseous and interfacial phases. The amount of energy that initiates the polymer decomposition varies with the physical characteristic of the polymer. For example, semi-crystalline thermoplastic polymers soften, melt, and then drip upon heating. On the other hand, amorphous thermoplastics and most of the thermosets directly go into thermal decomposition because of the absence of melting point. Polymers degrade thermally via an endothermic reaction. The energy required for that endothermic reaction should be larger than the binding energy between covalently linked atoms. Decomposition process depends on weak bonds and presence or absence of oxygen in solid and gas phases. When a polymer is heated its chains start to break down which is called pyrolysis. This bond breakage results in the formation of volatile fuel molecules. There are basically four types of thermal decomposition mechanisms for polymers:

- (i) **End-chain scission (unzipping)**: Monomer units are removed at chain ends.
- (ii) **Random-chain scission**: Chain breaks at random locations along its length.
- (iii) **Chain-stripping**: Side groups attached to the backbone are cleaved.
- (iv) **Cross-linking**: Bonds are created between two polymer chains.

End-chain scission and random-chain scission result in generation of monomers or oligomers while chain stripping and cross-linking mechanisms result in char formation. Char formation is very important in thermal decomposition rate because chars can act as

barriers between polymer surface and volatile fragments and oxygen in air. Thermal decomposition of polymers generally takes place with more than one mechanism mentioned above [16, 18].

1.2.1 Flammability Tests

Flammability of polymers is generally characterized by three standardized techniques based upon ignitability, flame spread and heat release properties of polymers; i.e. limiting oxygen index test, UL-94 vertical burning test and cone calorimeter.

(i) Limiting Oxygen Index (LOI) Test

Limiting oxygen index (LOI) test is a small scale flammability test utilized to observe flammability behavior of polymeric materials. LOI test is conducted according to standard of *ISO 4589 Determination of Burning Behavior by Oxygen Index*.

The schematic representation of LOI test setup is given in Figure 1.7. The specimen is put into holder which is covered by insulating glass chimney. Then, the mixture of oxygen and nitrogen with a determined oxygen percent is introduced through the ignited specimen at the room temperature. LOI value of the specimen is the minimum oxygen concentration which retains the combustion more than 3 minutes or consumes more than 50 mm of the specimen during combustion. In order to obtain LOI value, the mixture of oxygen and nitrogen with various oxygen concentrations are introduced through the specimen.

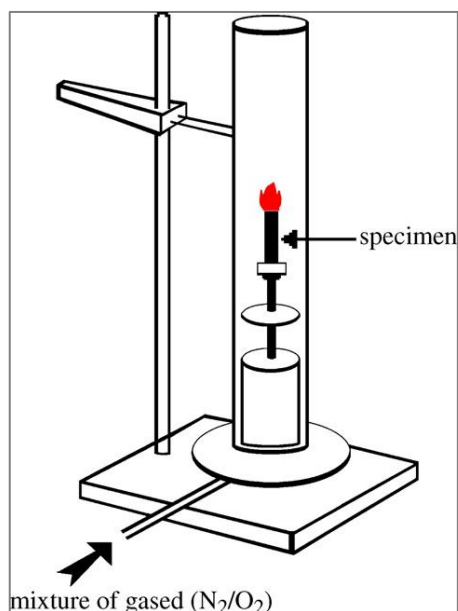


Figure 1.7 Experimental set-up of Limiting Oxygen Index test [16]

Since the atmosphere has 21% oxygen concentration, the materials having LOI values lower than 21% are considered as highly flammable. On the other hand, the materials with more than 27-28% LOI values could be considered as having self-extinguishing characteristic.

(ii) UL-94 Vertical Burning Test

This test is considered as one of the simplest small scale flammability tests in polymer industry. Its standard, *UL-94 Tests for Flammability of Plastic Materials for Parts in Devices and Appliances*, is developed by Underwriters Laboratories (USA).

In UL-94 vertical burning test, a specimen with the dimensions of 125 ± 5 mm long, 13.0 ± 0.5 mm wide, and thickness of 1.3 mm or 3.2 mm put into holder in vertical position and a piece of cotton is placed under it. The schematic representation of UL-94 vertical burning test setup is shown in Figure 1.8. The bottom of the specimen is ignited with the flame of burner for 10 seconds and extinguishment time (after flame time, t_1) of the specimen is measured. Then, the same procedure is repeated for the second time by recording second after flame time (t_2) and afterglow time (t_3) which is the time required for the fire glow to disappear. According to behavior of the specimen throughout combustion, it obtains several ratings which are tabulated in Table 1.1. For instance, in case that the specimen extinguishes in less than 10 seconds (t_1 and $t_2 < 10$ seconds), it means the specimen passes UL-94 test with the best rating of V-0. These materials are considered to have self-extinguishing characteristic. On the other hand, the specimens which could not extinguish within 30 seconds, fail in UL-94 vertical burning test indicating poor flame retardancy.

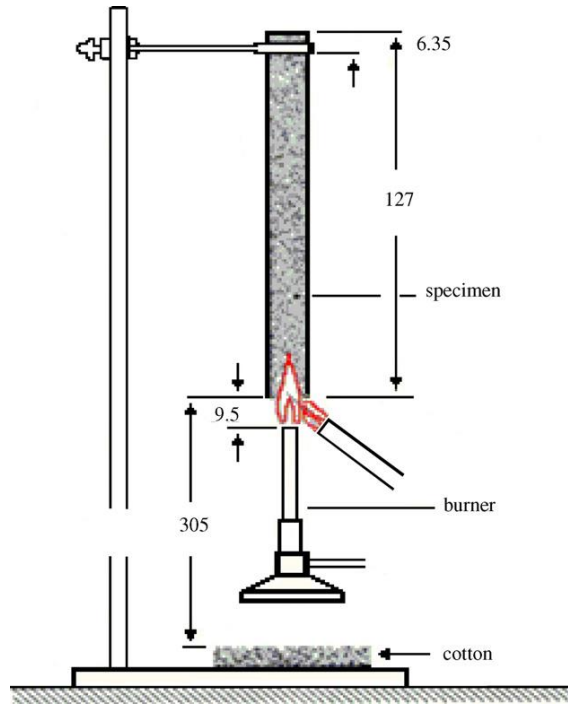


Figure 1.8 Experimental set-up of UL-94 Vertical Burning test [16]

Table 1.1 Classifications of UL-94 Vertical Burning test

Criteria	Ratings			
	V-0	V-1	V-2	Fail
After flame time of each individual specimen t_1 or t_2	$\leq 10s$	$\leq 30s$	$\leq 30s$	$> 30s$
Total afterflame time for 5 specimens ($t_1 + t_2$)	$\leq 50s$	$\leq 250s$	$\leq 250s$	
Afterflame plus afterglow time for each individual specimen after the second application ($t_2 + t_3$)	$\leq 30s$	$\leq 60s$	$\leq 60s$	
Afterflame or afterglow of any specimen up to the holding clamp	No	No	No	
Cotton indicator ignited by flaming particle or drops	No	No	Yes	

(iii) Mass Loss Cone Calorimeter Test

Heat release measurements by cone calorimeters are accepted to be one of the most reliable methods to gain information about flammability of polymeric materials. The name “cone” is due to the conic shape of the heaters. Large scale Cone Calorimeters utilizing oxygen consumption method works by correlating mass of oxygen consumed to the heat released from the specimen. However, in this study a variant of cone calorimeter which is called Mass Loss Cone Calorimeter (MLC) is utilized according to the standard *ISO 13927 Simple Heat Release Test Using a Conical Radiant Heater and a Thermopile Detector*.

In MLC test, external heat flux is brought towards to a specimen having 100x100x4 mm dimensions by conic heaters to measure temperature and mass of the specimen simultaneously (Figure 1.9). Temperature is measured by thermopiles which are located in the chimney while the mass is recorded by the load cell. The outputs of thermopiles are obtained in millivolts which are converted to heat release rate data (kW/m^2) by the help of calibration graph. In our study, the propane gas with a known calorific value is burned to obtain calibration graph.

There are several parameters that can be obtained from the curves of MLC test which give information about flammability of the materials such as:

Peak Heat Release Rate (PHRR) (kW/m^2): the maximum quantity of heat released from the specimen.

Total Heat Evolved (THE) (MJ/m^2): the area under the Heat Release Rate vs. time curve.

Time to Ignition (TTI) (s): the time between sparking and ignition of a material under external irradiation.

Time to Peak Heat Release Rate (TTP) (s): the time elapsed up to peak heat release rate.

FGI (Fire Growth Index): contribution of a material to fire propagation; ratio of PHRR to TTI.

FIGRA (Fire Growth Rate Index): contribution of a material to fire propagation rate; ratio of PHRR to TTP.

Char yield (wt %): weight percent of solid fire residue of a material measured at flame-out.

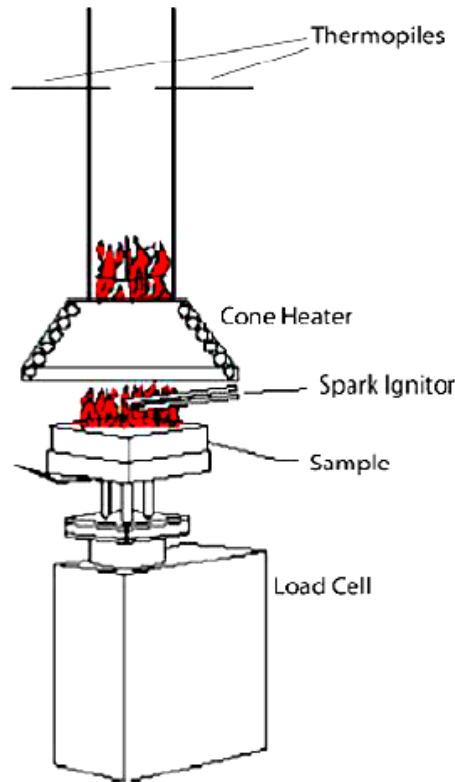


Figure 1.9 Experimental set-up of Mass Loss Cone Calorimeter test [16]

1.2.2 Flame Retardancy Mechanisms

Flame retardancy is an important aspect in polymer science and technology because of wide use of plastics in industry under flammable conditions. Flame retardant systems break down the combustion cycle by physically or by chemical reactions and repress or even terminate this process.

(i) Physical Action

Flame retardant systems act as physically in three ways.

- *By forming a protective layer*

A protective layer which acts as a barrier between gas and solid phases can be formed by some flame retardant additives such as; phosphorus, boric acid based, inorganic borates, silicon compounds and low melting glasses. In the gas phase combustion takes place, while in the solid phase thermal degradation occurs. This layer prevents transfer of heat, combustible gases and oxygen between gas and solid phases. Therefore, thermal degradation of the material is reduced and the “fuel” for combustion is decreased.

- *By cooling*

Some flame retardant additives such as; hydrated metals decompose endothermally and decrease the temperature below combustion temperature of the polymer. For instance, aluminum trihydroxide and magnesium dihydroxide having chemically bonded hydroxyl groups start liberated as water during endothermic reactions at about 200°C and 300°C, respectively. Therefore, they cool down the reaction medium and retard combustion of the material.

- *By dilution*

Inert substances and some flame retardant additives after decomposition lead to formation of inert gases, such as NH₃, CO₂ and H₂O. These inert gases dilute combustible gaseous mixture leading to lowered possibility of ignition.

(ii) **Chemical Action**

Flame retardant systems may also act chemically in the condensed and gas phases.

- *Reaction in gas phase*

In gas phase, flame retardant additives release radicals such as gaseous Cl•, Br•. These radicals can react with highly energetic and reactive species (H•, OH•) forming less energetic halogen radicals and molecules. With this alteration of the degradation pathway, radical concentration drop off, thus heat producing combustion processes decreases.

- *Reaction in condensed phase*

In condensed phase, flame retardants can accelerate breaking down of polymer causing melting and dripping away from the flame. Melamine cyanurate is one of the most widely used flame retardant additive causing dripping. Aliphatic bromines are also used to create same effect in foamed polystyrenes and thin films of polypropylene.

Flame retardants can also cause formation of a carbonaceous char or vitreous layer on the polymer surface. This can occur when a fire retardant removes the side chains and generates double bonds in the polymer. These double bonds give crosslinks, resulting in the formation of char. This char or vitreous layer can act as an insulating barrier in between flame zone and polymer.

There are also intumescent systems in which swelling of the surface layer of polymer is sustained via blowing agents. Char produced can provide insulation and slow down heat transfer from the exposed side to the unexposed side of polymer [16, 19].

1.2.3 Traditional Metal Hydroxide Flame Retardants and Boron Compounds

(i) Metal Hydroxides

Aluminum trihydroxide (ATH) and magnesium dihydroxide (MDH) are the most widely used traditional metal hydroxide flame retardant additives. These additives decompose endothermically and at the end of the reaction H_2O is released. Decomposition reaction occurs at temperatures around or above the polymer processing temperature. During combustion, temperature of the polymer material decreases due to the endothermic reaction and, liberated water molecules dilute the combustion fuel and act as gaseous barrier. Moreover, metal oxide which is the product of the decomposition reaction forms a thermally insulating protective layer, e.g. alumina (Al_2O_3) layer if ATH is used.

Decomposition reactions of the widely used metal hydroxides are:



ATH starts decomposition at about 180°C - 200°C whereas MDH starts decomposition above 300°C . Therefore, ATH can be used for the polymers having low processing temperatures (e.g. LDPE and EVA), while MDH can be used for the polymers having higher processing temperatures. MDH also maintains its flame retardant action up to 400°C , above which exothermic reaction starts.

(ii) Boron Compounds

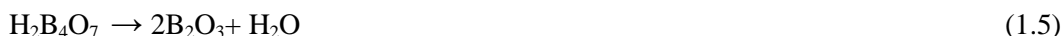
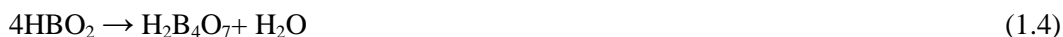
• Zinc Borate

Depending on its chemical composition, zinc borates have different dehydration temperatures. The commercial zinc borate with the formula of $2\text{ZnO}_3\text{B}_2\text{O}_3 \cdot 3.5\text{H}_2\text{O}$ has been widely used in the literature because of its relatively high dehydration temperature ($>290^\circ\text{C}$) and efficient gas phase and condensed phase flame retardancy mechanisms [20].

Zinc borate is considered to be a candidate to replace toxic flame retardants, especially halogenated compounds. During combustion, zinc borate could act both in gas phase and condensed phase. By dehydration, zinc borate releases its chemically bonded water molecules which dilute flame, and this endothermic reaction absorbs energy delaying the combustion. In addition to it, at high temperatures zinc borate can form glassy protective layer which strengthens the char. Zinc borate also acts as smoke and afterglow suppressant. Moreover, zinc borate is known to react with halogens revealing halogenated compounds which scavenge hot radicals; therefore it could also contribute to gas phase flame retardancy. In the literature, there are several studies utilizing zinc borate to improve flame retardancy of many polymeric materials.

- **Boric Acid**

Boric acid (orthoboric acid) has the chemical formula of H_3BO_3 . It is the weak acid of boron. By the application of heat, it transforms into metaboric acid ($170^\circ C$), tetraboric acid ($300^\circ C$) and boron trioxide, respectively (Reactions 1.3-1.5).



Flame retardancy mechanisms of boric acid and zinc borate are thought to be similar. By dehydration, boric acid releases its chemically bonded water molecules which dilute the flammable atmosphere. At elevated temperatures, B_2O_3 moiety forms a protective glassy layer covering the surface of burning polymer. Therefore, it has mainly condensed phase flame retardancy mechanism. In the literature, there are only a few studies investigating the flame retardancy effects of boric acid [21, 22].

- **Boron Oxide**

Boron oxide with the chemical formula of B_2O_3 mostly has amorphous structure while it could also crystallize into monoclinic form. During combustion, boron oxide could work in condensed phase by forming an insulative barrier to the flammable gases. However, there seems to be no published work, yet.

1.3 Literature Survey

1.3.1 Studies on the Flammability of LDPE and/or EVA Matrices with ATH and Boron Compounds

Zhu and Weil [23] investigated contribution of six different metal nitrates to ATH for the EVA matrix, in which specimens contained 50 phr of ATH and 3 phr of each metal nitrate. They indicated that metal nitrates increased LOI values by 2.8-7.0 $O_2\%$, while UL-94 ratings improved from fail to V-2 rating. They also stated that nitrates might lead to oxidative degradation of EVA and produce non-flammable products, which dilute the fuel.

Jiao and Chen [24] studied the synergistic effect of hydroxyl silicone oil (HSO) with ATH in EVA matrix. They used 50 wt% ATH in EVA as the reference specimen. For the other specimens ATH was replaced with 0.5, 1.0, 3.0 and 5.0 wt% HSO. They reported that increasing HSO content decreased LOI values and none of the specimens passed UL-94 flammability test. On the other hand, heat release rate (HRR) values decreased with increasing content of HSO. They claimed that this synergism was basically due to the positive effect of HSO by decreasing the accelerated rate of acetic acid release from the EVA structure.

Another study of Jiao and Chen [25] was about the use of fumed silica (SiO_2) with ATH in EVA matrix. This time 55 wt% ATH reference specimen was replaced with 2, 5, 8 and 10 wt% fumed silica. All specimens failed in UL-94 fire test, and increasing SiO_2 content decreased LOI values as much as 3 $\text{O}_2\%$. However, increasing SiO_2 amount decreased peak heat release rate (PHRR) values, for instance that decrease with 10 wt% SiO_2 was by 43%. They stated that this synergism was obtained by the condensed phase flame retardancy mechanism of SiO_2 especially due to the formation of a more thermally stable barrier, and the increase in residual char of the system.

Cross et al. [26] studied effects of zinc hydroxystannate (ZHS) with ATH in EVA matrix by replacing 150 phr ATH with 7.5 and 15 phr ZHS. They obtained increased LOI values by 2.1 and 3.3 $\text{O}_2\%$, and decreased PHRR values by 12.4 and 26.4 % for the specimens containing 7.5 and 15 phr ZHS, respectively. They concluded that 15 phr ZHS loading was very effective not only in LOI and PHRR values but also in terms of smoke suppression.

Azizi et al. [27] investigated flame retardancy of silane-crosslinked low-density polyethylene (xLDPE) containing ATH and antimony trioxide (Sb_2O_3). They compared reference material of 30 phr ATH with the specimen in which ATH was replaced with 15 phr Sb_2O_3 . They simply indicated that use of Sb_2O_3 increased LOI value by 2 $\text{O}_2\%$.

Wei et al. [28] studied fumed silica (SiO_2) with ATH in the blend of linear low density polyethylene (LLDPE) and EVA with LLDPE/EVA ratio of 80/20. Specimens were loaded with 150 phr ATH and various amounts of SiO_2 (2-12 phr). They revealed that use of SiO_2 improved LOI and PHRR values. For instance, 8 phr SiO_2 increased LOI value by 5 $\text{O}_2\%$ and decreased PHRR value by 22%. They also stated that silica-ATH synergism was basically due to the formation of more thermally stable residual chars.

Basfar et al. [29] studied zinc borate (ZB) with ATH in LDPE/EVA (40/60) blend where irradiation method was also applied after compounding with melt mixing. ATH was used as 10 phr for all specimens and ZB was loaded by 4, 6 and 8 phr. They simply indicated that the highest LOI value (25 $\text{O}_2\%$) can be achieved with 4 phr ZB at a particular irradiation rate. They also stated that this improvement was not only due to the certain combination of ZB and ATH but also due to cross-linking of the matrix chains by gamma radiation.

Bourbigot et al. [30] investigated synergistic and smoke suppressant effect of zinc borate (ZB) with ATH in the matrix of EVA. They compared reference specimen of 65 wt% ATH with the other five specimens in which ATH was replaced by 3-15 wt% ZB. They revealed that use of ZB improves many parameters. For example, 5 wt% ZB increased LOI value by 9 $\text{O}_2\%$ together with V-0 rating in UL-94 test, and resulted in very significant suppression in PHRR value. Synergism and smoke suppressant effects of ZB with ATH were discussed by their effective condensed phase mechanisms.

Isitman and Kaynak [31] studied use of another boron compound colemanite (CMT), an hydrated calcium borate, with ATH in LDPE matrix. Their reference material with 65

wt% ATH was replaced with 5, 10 and 20 wt% CMT. They revealed that use of CMT improved all flame retardancy data. For instance, replacement of ATH by 10 wt% CMT increased LOI value by 4 O₂% with UL94 V-0 rating, and the suppression in PHRR value was as much as 24%. They concluded that use of CMT with ATH resulted in better protective character and more effective fuel trapping compared to using ATH alone.

1.3.2 Studies on the Flammability of Clay Nanocomposites of LDPE and/or EVA Matrices with ATH

Zhang and Wilkie [14] investigated effects of using different nanoclays having different organic-modifications on the flammability of LDPE in the absence or presence of maleic anhydride (MA). They prepared specimens by loading 3 wt% different nanoclays and 3 wt% MA. Compared to neat LDPE, peak heat release rate (PHRR) values of all LDPE nanocomposites were suppressed by 30-40%.

Zanetti and Costa [15] studied effects of an organically-modified clay on the flammability of 10 wt% EVA loaded LDPE. They reported that loading of 5 wt% organoclay decreased mass loss rate (MLR) curve by 50% compared to neat LDPE/EVA blend. They stated that flame retardancy of the nanocomposites were due to the protective barrier action of organoclay layers.

Tang et al. [32] investigated effects of montmorillonite (MMT) clay on the flammability of neat EVA. They used two different particle sizes and two different loading contents (5 and 7 wt% MMT) with a compatibilizer called C16. They reported that loading of 5 wt% MMT with smaller particle size in the presence of C16 was the most effective case decreasing the heat release rate (HRR) value of neat EVA by 40%. They claimed that the flame retardancy mechanism of the nanocomposite was due to the gas barrier properties in the condensed phase.

Shi et al. [33] studied flammability of EVA/MMT nanocomposites which were prepared by a masterbatch process using polymer-modified clay. They used 20 wt% of two different modifiers; a cationic vinyl acetate copolymer (PVAc) and PVAc homopolymer (PVAc1). Authors observed that silicate layers in the 5.6 wt% MMT containing specimen with PVAc1 were exfoliated, while in the 5.9 wt% MMT containing specimen with PVAc they were intercalated. According to the microscale combustion calorimetry test results, intercalated and exfoliated specimens decreased heat release capacity (HRC) values by 24% and 21%, respectively.

Marosfoi et al. [34] investigated effects of non-modified, organophilized and organic-inorganic modified montmorillonites on the flammability of neat EVA. According to UL-94 tests, organophilized MMTs resulted in the most efficient contribution in hindering dripping, while organic-inorganic modified MMTs were found effective for both flame spreading and dripping. On the other hand, heat release rate (HRR) curves showed that the highest suppression in HRR was obtained by non-modified MMTs, while organophilized and organic-inorganic modified MMTs lead to similar peak values.

Yen et al. [35] studied synergistic flame retardant effect of nanoclays (NC) in EVA matrix filled with 50 wt% ATH. Nanocomposite samples were prepared by replacing ATH with 1, 2, 4 and 6 wt% NC. They obtained increased LOI values by 1.5 and 2.5 O₂% while UL-94 ratings improved from fail to V-0 rating for the specimens containing 1 and 2 wt% NC, respectively. Higher NC loadings caused reduction in LOI values. Moreover, NC loading resulted in decreased peak heat release rate (PHRR) values having the highest suppression with only 1 wt% NC. They also stated that addition of NC to EVA/ATH system lead to the formation of stacked surface layers acting as barriers to oxygen supply, heat conduction and release of flammable gases.

Chen et al. [36] investigated contribution of Fe-montmorillonite (Fe-OMT) to the flame retardancy of 50 wt% ATH filled EVA by replacing ATH amount with 0.5, 1, 2 and 3 wt% Fe-OMT. They revealed that LOI values of the nanocomposites increased as much as 6 O₂% with 3 wt% Fe-OMT replacement, while UL-94 V-0 rating and the lowest HRR value were obtained with 2 wt% Fe-OMT replacement. They claimed that these synergistic effects of Fe-OMT were based on the physical barrier mechanism and also on the formation of carbonaceous chars catalyzed by Fe-OMT.

Bee et al. [37] studied effects of montmorillonite (MMT) on the LOI values of electron beam irradiated and ATH loaded LDPE/EVA (50/50) blends. All specimens contained 150 phr ATH and different amounts of MMT (5, 10, 15, 20 wt%). They obtained increasing LOI values with increasing MMT loading levels for the nonirradiated and irradiated specimens. For instance, LOI value of 20 wt% MMT loaded nonirradiated specimen was 2.4 O₂% higher compared to 5 wt% MMT loaded one. They concluded that use of MMT promoted char formation acting as a physical barrier.

Zhang et al. [38] examined contribution of 5 wt% nanoclays on the cone calorimetric flame retardancy parameters of EVA/LDPE loaded with 68 wt% ATH. They simply indicated that NC incorporation alone suppressed HRR curves, but the lowest HRR value was achieved when NC was used together with ATH. They added that NC was especially effective on the condensed phase flame retardancy mechanism.

Ramirez-Vargas et al. [39] investigated contribution of 10 wt% organomodified montmorillonite (MMT) for the LDPE/EVA (70/30) blends loaded with 47, 43 and 38 wt% ATH by comparing with the reference blend having only 53 wt% ATH. According to LOI tests, they revealed that nanoclays should not be used with lower amounts of ATH. For instance, when ATH content was decreased from 53 wt% to 38 wt%, LOI value decreased by 1.5 O₂%. They also indicated that during UL-94 tests specimens with nanoclays had no dripping.

1.4 Aim of the Study

Owing to sufficient mechanical properties, easy processability, chemical resistance and low cost of low density polyethylene (LDPE); and high filler loading capacity and flexibility of ethylene vinyl acetate copolymer (EVA); they are both the most widely used cable insulation materials in industry. Main problem in these materials is their rather very low flame retardancy, i.e. they need very effective flame retardants [29, 40-42].

Today, due to the ban on halogen-based flame retardants by many national and international directives, the most suitable halogen-free flame retardants chosen for these materials in cable industry are metal hydroxides; particularly aluminum hydroxide (ATH). However, in order to obtain required levels of flame retardancy, very high amounts of ATH, usually between 60 and 65 wt% is required [26, 43, 44]. Therefore, researches investigating synergistic compounds with traditional ATH have been important both for the academia and the industry.

In the literature, there seems to be only six studies [23-28] investigating the possible synergism of certain materials when used together with traditional ATH for the matrices of LDPE and/or EVA. In terms of use of boron compounds with ATH in LDPE and/or EVA matrices, there are two studies conducted with zinc borate [29, 30] and only one study with colemanite [31].

Since there are only two studies about zinc borate (ZB) and no studies about boron oxide (BO) and boric acid (BA) reported so far in the literature, the first aim of this study was to investigate possible flame retardancy synergism of three boron compounds (ZB, BO and BA) with ATH in the cable insulation materials of LDPE and LDPE/EVA blends.

Recently, using “nanocomposite approach”, i.e. investigating the contribution of nano-sized materials to the traditional flame retardants is becoming crucial. However, for the cable insulation materials LDPE and EVA, the number of these studies in the literature is very limited. For example, there seems to be one work reported studying the effects of nanoclays alone on the flammability of neat LDPE [14] and LDPE/EVA [15] blends, whereas there seems to be three such studies [34-36] for neat EVA.

It is known that, although there are certain levels of improvements in some of the flame retardancy parameters of polymers via condensed phase barrier mechanism of nanoclays, these improvements are far from the required levels of industrial standards. Therefore, rather than using nanoclays alone, investigators try to obtain synergistic improvements by replacing certain amounts of traditional flame retardants with small amounts of nanoclays.

In this respect, in the literature, there seems to be no work investigating the contribution of nanoclays when used together with ATH for LDPE matrix, but there are two studies [35, 36] for EVA matrix, and three studies [37-39] for LDPE/EVA blends. For these matrices there is no study reported for the contribution of nanoclays when used together with ATH-ZB system either.

Therefore, the second aim of this study was to investigate contribution of nanoclays when used alone, and together with traditional flame retardant ATH; and also together with ATH-ZB synergistic system for these two cable insulation materials.

CHAPTER 2

EXPERIMENTAL WORK

2.1 Materials Used

Chemical structures of the materials used in this study are given in Table 2.1, while other properties are given below.

(i) Matrix Materials LDPE and EVA

Cable insulation materials used were LDPE (Argento 15803-020) and EVA (DuPont Elvax 220W) with 28 wt% vinyl acetate content. LDPE has melt flow index of 2.0 g/10 min and density of 0.919 g/cm³ and EVA has melt flow rate of 150 g/10 min and density of 0.949 g/cm³.

(ii) Compatibilizers PE-g-MA and EVA-g-MA

Maleic anhydride modified copolymers PE-g-MA (DuPont, Fusabond E226) and EVA-g-MA (DuPont, Fusabond C190) were also used as the compatibilizers to promote adhesion between matrix materials and all additives.

(iii) Traditional Flame Retardant ATH

As the halogen-free metal hydroxide flame retardant aluminum trihydroxide (ATH) (Albemarle, Martinal OL-107) with an average particle size in the range of 0.9–1.5 mm was used.

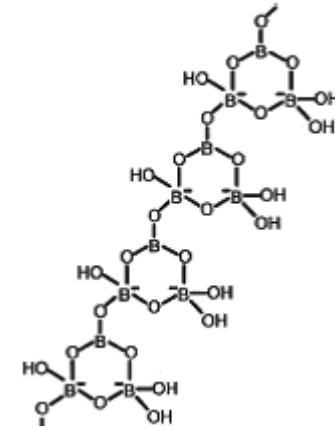
(iv) Nanoclay NC

The nanoclay (NC) used was Cloisite 20A (Southern Clay), an organically modified montmorillonite with dimethyl dehydrogenated-tallow, quaternary ammonium (2M2HT).

(v) Boron Compounds ZB, BO, BA

Three different boron compounds; zinc borate (ZB) with a formula of 2ZnO.3B₂O₃.3.5H₂O, boron oxide (BO) and boric acid (BA) were kindly provided by ETI Mine Works Inc (Turkey). ZB, BO and BA had average particle sizes of 12.4, 12.8, 33.7 μm, and purities of 97, 91, 99%, respectively.

Table 2.1 Chemical structure of the materials used

		Chemical Structure
Traditional Flame Retardant	Aluminum Hydroxide (ATH)	$ \begin{array}{c} \text{OH} \\ \\ \text{Al} \\ / \quad \backslash \\ \text{OH} \quad \text{OH} \end{array} $
Boron Compounds	Zinc Borate	 <p>(zinc atoms that complex with oxygen atoms are not displayed)</p>
	Boron Oxide	$ \text{O}=\text{B}-\text{O}-\text{B}=\text{O} $
	Boric Acid	$ \begin{array}{c} \text{H}-\text{O} \\ \\ \text{B} \\ / \quad \backslash \\ \text{O}-\text{H} \quad \text{O}-\text{H} \end{array} $
Nanoclay	Organic Modifier of Cloisite 20A	$ \begin{array}{c} \text{CH}_3 \\ \\ \text{CH}_3 - \text{N}^+ - \text{HT} \\ \\ \text{HT} \end{array} $ <p>(where HT is Hydrogenated Tallow)</p>

2.2 Production of the Specimens

As the cable insulation materials two groups of polymer matrices were investigated. The first one was only LDPE, while the latter one was a blend of LDPE/EVA with a ratio of 3:1.

In the first part of this study, in order to evaluate possible synergism of boron compounds, the reference material was chosen as LDPE or LDPE/EVA with 65 wt% ATH. Then for each matrix, amount of ATH was replaced with 10, 20, and 30 wt% ZB and BO. But, the use of BA was only 10 wt% due to the overlapping of the first dehydration temperature of BA with the compounding temperature profile of LDPE and EVA leading to significant compounding problems.

In the second part of this study, amount of the nanoclay (NC) used in all formulations was chosen as 5 wt%. In order to evaluate contribution of this NC it was first introduced into each matrix material alone without any additive, then replacing 5 wt% of the 65 wt% traditional ATH, and then replacing 5 wt% of the 55 wt% ATH-10 wt% ZB synergistic system.

Designations and compositions of the specimens produced are tabulated in Table 2.2. For the LDPE matrix group PE-g-MA was used at 5 phr (parts per hundred resin), while for LDPE/EVA group both PE-g-MA and EVA-g-MA were used at 2.5 phr. For all the groups, zinc stearate was also used at 1 phr as a lubricant to enhance processability of the compounds and nanocomposites.

Matrix polymers, all additives and nanoclay were compounded by melt mixing method in a laboratory size twin-screw extruder (Rondol Microlab 10 mm, L/D = 20). Although there were slight changes with the compound and nanocomposite composition, in general the temperature profile during extrusion for LDPE matrix compounds and nanocomposites was 88°-114°-153°-181°-186°C with 100 rpm screw speed, while for LDPE/EVA matrix compounds and nanocomposites it was 90°-110°-140°-160°-172°C with 69 rpm screw speed.

Specimens were shaped by two methods; compression and injection molding. Square plates for cone calorimeter tests were compression molded at 125°C with 6 minutes preheating followed by 90 bar pressure for 2 minutes. Injection Molding (DSM Xplore 10cc Micro) of the flammability and mechanical test specimens were done with barrel and mould temperatures of 180°C and 30°C, respectively under three step pressure of 7 bars.

Table 2.2 Designations and compositions (wt%) of the specimens

Specimens	LDPE	EVA	ATH	ZB	BO	BA	NC
LDPE	100	-	-	-	-	-	
LDPE-ATH65	35	-	65	-	-	-	
LDPE-ATH55-ZB10	35	-	55	10	-	-	
LDPE-ATH45-ZB20	35	-	45	20	-	-	
LDPE-ATH35-ZB30	35	-	35	30	-	-	
LDPE-ATH55-BO10	35	-	55	-	10	-	
LDPE-ATH45-BO20	35	-	45	-	20	-	
LDPE-ATH35-BO30	35	-	35	-	30	-	
LDPE-ATH55-BA10	35	-	55	-	-	10	
LDPE-NC	95	-	-	-	-	-	5
LDPE-ATH60-NC	35	-	60	-	-	-	5
LDPE-ATH50-ZB-NC	35	-	50	10	-	-	5
LDPE/EVA	75	25	-	-	-	-	
LDPE/EVA-ATH65	26.25	8.75	65	-	-	-	
LDPE/EVA-ATH55-ZB10	26.25	8.75	55	10	-	-	
LDPE/EVA-ATH45-ZB20	26.25	8.75	45	20	-	-	
LDPE/EVA-ATH35-ZB30	26.25	8.75	35	30	-	-	
LDPE/EVA-ATH55-BO10	26.25	8.75	55	-	10	-	
LDPE/EVA-ATH45-BO20	26.25	8.75	45	-	20	-	
LDPE/EVA-ATH35-BO30	26.25	8.75	35	-	30	-	
LDPE/EVA-ATH55-BA10	26.25	8.75	55	-	-	10	
LDPE/EVA-NC	71.25	23.75	-	-	-	-	5
LDPE/EVA-ATH60-NC	26.25	8.75	60	-	-	-	5
LDPE/EVA-ATH50-ZB-NC	26.25	8.75	50	10	-	-	5

2.3 Flammability Tests of the Specimens

Limiting Oxygen Index (LOI) measurements, UL-94 vertical burning and Mass Loss Cone Calorimeter (MLC) tests were utilized to investigate flame retardancy properties of the specimens. The procedure and the parameters obtained from these particular tests were explained in Section 1.2.1 in detail.

(i) Limiting Oxygen Index

Limiting Oxygen Index (LOI) measurements were conducted by an oxygen index apparatus (Fire Testing Technology Inc.) having a paramagnetic oxygen analyzer according to the standard of *ISO 4589 Determination of Burning Behavior by Oxygen Index*.

(ii) UL-94 Vertical Burning Test

UL-94 vertical burning tests were assessed as the procedure explained in the standard *UL-94 Tests for Flammability of Plastic Materials for Parts in Devices and Appliances* developed by Underwriters Laboratories.

(iii) Mass Loss Cone Calorimeter

Mass Loss Cone Calorimeter (Fire Testing Technology Inc.) was utilized to measure heat release rates and mass loss rates of the burning specimens having the dimensions of 100x100x4 mm according to the procedure given in the standard *ISO 13927 Simple Heat Release Test Using a Conical Radiant Heater and a Thermopile Detector*. During MLC test, in the first part of this study external heat flux was kept as 35 kW/m², while in the second part heat flux was 50 kW/m². Data were recorded using a data-acquisition system and the outcomes of the test indicated that measured heat release rates are reproducible with ±10% deviation.

2.4 Other Tests and Analysis

(i) Thermogravimetric Analysis

In order to investigate thermal degradation of the specimens, thermogravimetric analysis (TGA) (Netzsch STA 449 F3 Jupiter) was carried out under nitrogen at a flow rate of 20 ml/min and a heating rate of 10°C/min.

(ii) X-ray Diffraction Analysis

Wide angle X-ray diffraction analysis (XRD) (Rigaku D-Max 2200) with CuK α radiation (40 kV, 40 mA) was first utilized for boron compounds. Then, MLC chars were analyzed over a scanning range of 5°-80°. Finally, it was conducted in order to evaluate

dispersibility and intercalation/exfoliation state of NC silicate layers in LDPE and LDPE/EVA matrices over the continuous range of 1° - 10° .

(iii) Transmission Electron Microscopy

For the visual evidence of intercalation/exfoliation, transmission electron microscopy (TEM) (FEI Tecnai G2 Spirit Bio TWIN) was conducted at an acceleration voltage of 80 kV. To prepare samples for TEM, an ultra-microtome (Leica EM UC6) with a diamond knife was utilized. Sections having less than 100 nm thicknesses were sliced and transferred to 400 mesh copper grids.

(iv) Scanning Electron Microscopy

Morphological studies of the LOI specimen chars and fracture surfaces of tensile test specimens were conducted under scanning electron microscopy (SEM) (FEI Nova Nano 430).

(v) Tensile Testing

Mechanical behavior of the specimens were evaluated by tensile tests on at least five ISO 527 Type 1A samples using a universal testing machine (Instron 5565A, 5 kN).

CHAPTER 3

RESULTS AND DISCUSSION

As stated before, since this dissertation has two main purposes and consequently two basic experimental stages, their results are presented and discussed successively in the following two subsections:

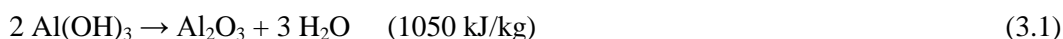
3.1 Synergistic Effects of Three Boron Compounds with ATH in LDPE and LDPE/EVA Matrices

The first purpose of this thesis was to investigate possible flame retardancy synergism of three boron compounds (ZB, BO and BA) with ATH in the cable insulation materials of LDPE and LDPE/EVA blends. Results of flammability tests and other analyses conducted for this purpose are presented and discussed below.

3.1.1 Thermal Decomposition of ATH and Boron Compounds

Before the flammability studies, thermal decomposition of ATH and three boron compounds (ZB, BO and BA) used in this study were investigated by thermogravimetric analyses. Their TG and DTG curves are given in Figure 3.1 while thermal degradation parameters determined from these curves are tabulated in Table 3.1.

Figure 3.1 and Table 3.1 show that ATH used in this study undergoes an endothermic dehydration reaction in the temperature range of 250°-350°C with 65% char yield. Byproducts of this reaction are H₂O and alumina (Al₂O₃) as given in Reaction 3.1:



Zinc borates (2ZnO.3B₂O₃.3.5H₂O) decompose endothermically usually in two steps releasing water, boric acid and boron oxide (B₂O₃) and zinc oxide (ZnO₂). It is seen in Figure 3.1 and Table 3.1 that ZB used in this study decomposes mainly between 350°-450°C leading to a formation of 86% residue. The initial degradation peak at around 242°C is not significant leading to only 1 wt% mass loss.

Table 3.1 Thermal degradation parameters of ATH and boron compounds determined from TG and DTG curves

Materials	T_{DTG-Peak 1}^a (°C)	T_{DTG-Peak 2}^b (°C)	T_{DTG-Peak 3}^c (°C)	% Residue at 600°C^d
ATH	317	-	-	65.0
ZB	242	415	-	85.8
BO	106	161	292	81.1
BA	153	213	265	55.9

^aT_{DTG-Peak 1}: First peak temperature in DTG curve.

^bT_{DTG-Peak 2}: Second peak temperature in DTG curve.

^cT_{DTG-Peak 3}: Third peak temperature in DTG curve.

^d% Residue at 600°C: % Char yield at 600 °C.

Boron Oxide (B₂O₃) softens around 350°C and flows above 500°C forming a protective vitreous layer. Figure 3.1 and Table 3.1 show that there are three small decomposition peaks for BO used in this study. BO is very susceptible to moisture; therefore the first small decomposition peak at 106°C with 1.7 wt% mass loss should correspond to the evaporation of adsorbed water. The other two small decomposition peaks at 161°C and 292°C could be explained with the possible reaction between BO and evaporated water resulting in formation and then decomposition of metaboric acid (HBO₂) or tetraboric acid (H₂B₄O₇). Above 400°C, the remaining 81 wt% phase should be vitreous boron oxide.

Boric acid (H₃BO₃) liberates water at around 150°C and produces metaboric acid (Reaction 3.2) or also tetraboric acid, and then the second water liberation occurs at around 265°C with the formation of boron oxide (Reaction 3.3):



It is seen in Figure 3.1 and Table 3.1 that the main decomposition occurs at 153°C for the BA used in this study, followed by other decomposition peaks at 213°C and 265°C corresponding to the liberation of chemically bonded water molecules. At the end above 400°C, the remaining 56 wt% char should be again vitreous boron oxide.

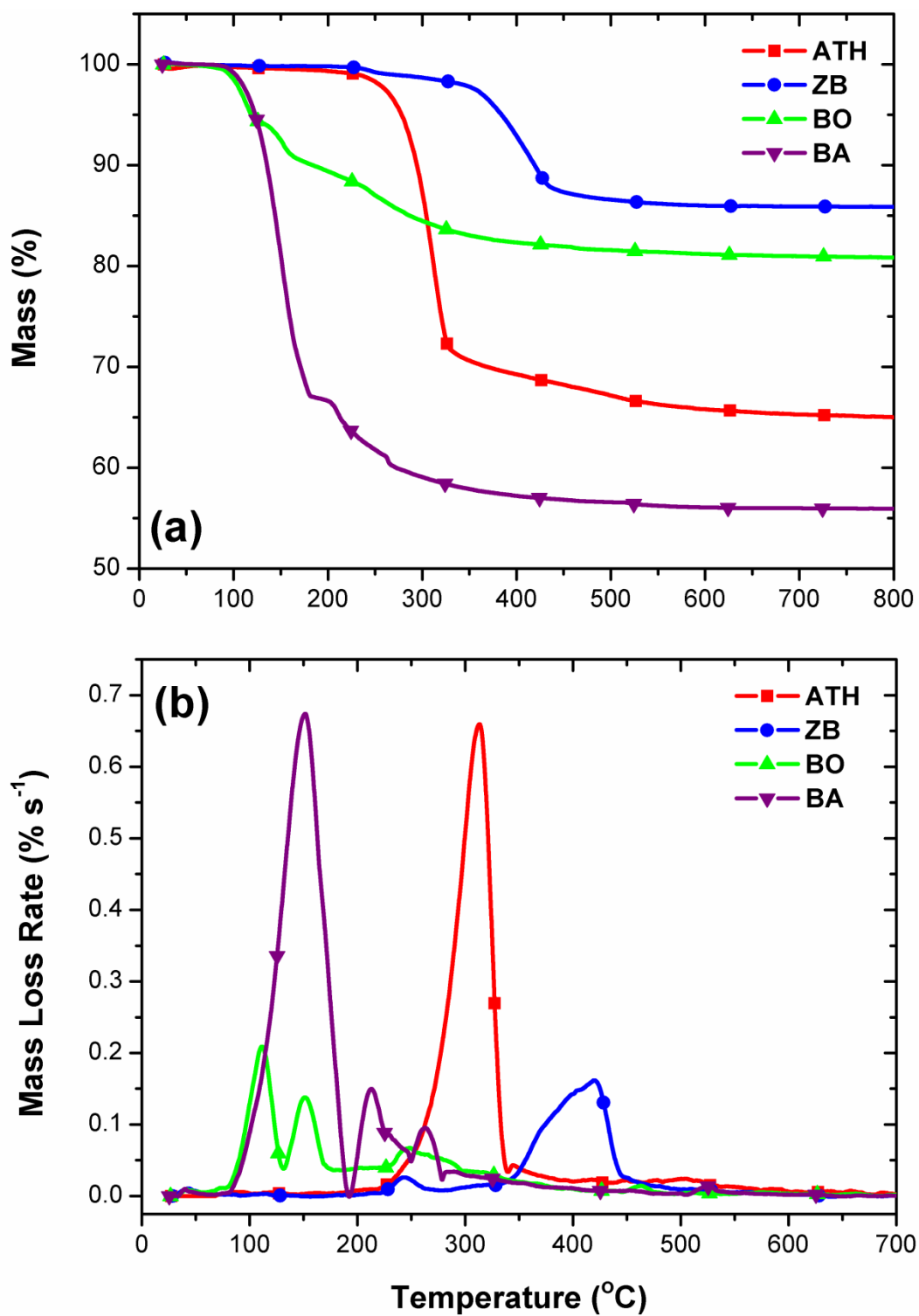


Figure 3.1 (a) Thermogravimetric (TG) and (b) Differential Thermogravimetric (DTG) curves of ATH and boron compounds

3.1.2 UL-94 and LOI Flammability Tests

Results of UL-94 and LOI flammability tests are given in Table 3.2. It is seen that both cable insulation matrices LDPE and LDPE/EVA fail from UL-94 rating with also very low LOI values of 19 and 18 O₂%, respectively. When they are loaded with 65 wt% traditional flame retardant ATH, they obtain the best rating (V-0) of UL-94; and significant increases of LOI values up to 30 and 31 O₂%, respectively.

It is well established in the literature [16] that; the basic flame retardancy mechanism of ATH is physical barrier action in both gas and condensed phases. As discussed in the previous section, ATH decomposes endothermically liberating H₂O molecules at the end of the reaction. During combustion, temperature of the polymer matrix decreases due to this endothermic reaction; and by product H₂O molecules dilute the combustion fuel, i.e. barrier mechanism in the gas phase. Moreover, Al₂O₃ which is the other product of the decomposition reaction forms a thermal insulating protective layer on the polymer, i.e. barrier mechanism in the condensed phase.

Table 3.2 shows that, for both matrices, when 10, 20 and 30 wt% ATH was replaced with boron compounds ZB, BO, and BA, all specimen formulations keep their UL-94 rating of V-0. In terms of LOI values, although there were very slight decreases for a few specimens, many of them had equal or higher values compared to the reference specimens with 65 wt% ATH. For example, the increase in LDPE matrix was from 30 to 31 O₂%, while in LDPE/EVA matrix from 31 up to 36 O₂%, respectively.

Therefore, it can be concluded that, for both matrix materials, replacement of certain amount of ATH with boron compounds ZB, BO, BA not only keep V-0 UL-94 rating, but also leads to synergistic increases in the LOI values of the specimens. Synergism especially takes place with 10 wt% replacements, increasing the replacement amount decreases the synergistic effect.

Table 3.2 Results of UL-94 and LOI flammability tests

Specimens	UL-94 rating^a	LOI (O₂ %)^b
LDPE	Fail	19
LDPE-ATH65	V-0	30
LDPE-ATH55-ZB10	V-0	30
LDPE-ATH45-ZB20	V-0	28
LDPE-ATH35-ZB30	V-0	27
LDPE-ATH55-BO10	V-0	31
LDPE-ATH45-BO20	V-0	27
LDPE-ATH35-BO30	V-0	27
LDPE-ATH55-BA10	V-0	31
LDPE/EVA	Fail	18
LDPE/EVA-ATH65	V-0	31
LDPE/EVA-ATH55-ZB10	V-0	32
LDPE/EVA-ATH45-ZB20	V-0	30
LDPE/EVA-ATH35-ZB30	V-0	29
LDPE/EVA-ATH55-BO10	V-0	36
LDPE/EVA-ATH45-BO20	V-0	33
LDPE/EVA-ATH35-BO30	V-0	30
LDPE/EVA-ATH55-BA10	V-0	33

^aMaterials flammability classifications for stringent vertical orientation; Fail (flame extinguishing $t > 30$ s), V-2 (flaming drips, material self-extinguishes at $10 < t < 30$ s), V-1 (material self-extinguishes at $10 < t < 30$ s, without dripping), V-0 (material self-extinguishes at $t < 10$ s)

^bOxygen level required for sustained flaming combustion.

3.1.3 Mass Loss Cone Calorimetry

Fire performances of the cable insulation materials based on LDPE and LDPE/EVA matrices were evaluated by using mass loss cone calorimeter. Figure 3.2 and 3.3 show heat release rate (HRR) and mass loss rate (MLR) curves only for the specimens with ATH and 10 wt% boron compounds for each matrix, while important fire parameters determined for all specimens are given in Table 3.3.

These figures simply reveal that both cable insulation materials LDPE and LDPE/EVA have high single peaks with very large areas under, i.e. they both have very high levels of peak heat release rate (PHRR) and total heat evolved (THE). When both matrices were loaded with 65 wt% ATH, Table 3.3 shows that PHRR and THE values decrease drastically. For example, suppressions in PHRR values were 92% and 90%, while in THE values 83% and 59%, for the LDPE and LDPE/EVA matrices, respectively.

Table 3.3 also indicates that, when certain amount of ATH was replaced with boron compounds there were no significant differences in PHRR and THE values. Only, replacements with 10 wt% boron compounds resulted in certain level of synergism. For instance, PHRR value of the LDPE specimen with 65 wt% ATH was suppressed further by 38% with 10 wt% BO replacement, and by 13% with 10 wt% BA replacement. In the LDPE/EVA matrix, there seems to be slight synergism in the values of PHRR and THE with 10 wt% ZB replacement.

Figures 2 and 3 also show that HRR curves of ATH loaded specimens have two distinct peaks. The first HRR peak is attributed to the material combustion prior to charring while the part between first and second HRR peaks represent gradual burning of the specimen through the thickness after the formation of initial char layer. The second peak should be due to the diminishing mass of fuel being subject to more rapid heating toward the end of combustion. These multiple HRR peaks have been also reported by [34] and [45]. Due to basically their similar flame retardancy mechanism (i.e. physical barrier formation), HRR curves of the specimens with boron compounds had also two peaks.

In terms of time to ignition (TTI) values, Table 3.3 reveals that use of ATH prolong the ignition time, while replacement of certain amount of ATH with boron compounds leads to synergism by delaying the ignition time further in many specimens.

Contribution of a material to the flame spread can be evaluated by fire growth index (FGI) which is the ratio of PHRR/TTI. FGI values tabulated in Table 3.3 indicate that ATH decreases fire propagation rate of both matrices significantly, and replacement of certain amounts of ATH with boron compounds lead to similar influences, again having synergism in many specimens.

The ratio of THE/TML (total heat evolved/total mass loss) and % Char Yield data might give information about the flame retardancy mechanisms of specimens. Table 3.3 reveals that values of these two parameters for the specimens loaded with only ATH and ATH

with boron compounds are very similar, i.e. physical barrier mechanism basically in the condensed phase.

On the other hand, it is known that ATH, ZB and BA liberate their chemically bonded water molecules during combustion and lead to the dilution of combustible fuel. Therefore, it can be said that ATH, ZB and BA might contribute physical barrier mechanism also in the gas phase.

For both cable insulation materials, it can be simply summarized that replacement of certain amount of ATH with boron compounds leads to similar mass loss cone calorimeter (MLC) parameters with similar mechanisms. Synergisms in the parameters of PHRR, TTI, FGI and % Char Yield could be obtained with the replacements of especially 10 wt% ZB, BO and BA. Another advantage of these boron compounds, especially ZB, would be their very good ability of smoke and afterglow suppression.

Table 3.3. Mass Loss Cone Calorimeter parameters of the specimens

Specimens	PHRR (kW/m²)	THE (MJ/m²)	TTI (s)	FGI (kW/m².s)	THE/TML (MJ/m².g)	Char Yield (%)
LDPE	1040	178	108	9.6	5.4	1
LDPE-ATH65	82	30	111	0.7	0.9	43
LDPE-ATH55-ZB10	94	49	86	1.1	1.7	49
LDPE-ATH45-ZB20	83	45	108	0.8	1.6	50
LDPE-ATH35-ZB30	132	113	102	1.3	3.5	46
LDPE-ATH55-BO10	51	31	149	0.4	1.1	53
LDPE-ATH45-BO20	120	92	148	0.8	2.8	47
LDPE-ATH35-BO30	140	120	164	0.9	3.5	45
LDPE-ATH55-BA10	71	38	158	0.5	1.2	47
LDPE/EVA	1247	165	89	14.0	4.9	2
LDPE/EVA-ATH65	123	67	98	1.3	2.0	44
LDPE/EVA-ATH55-ZB10	121	65	104	1.2	1.9	44
LDPE/EVA-ATH45-ZB20	128	79	95	1.4	2.4	45
LDPE/EVA-ATH35-ZB30	133	81	91	1.5	2.4	46
LDPE/EVA-ATH55-BO10	142	73	130	1.1	2.2	43
LDPE/EVA-ATH45-BO20	144	74	200	0.7	2.3	46
LDPE/EVA-ATH35-BO30	151	77	198	0.8	2.4	47
LDPE/EVA-ATH55-BA10	145	72	143	1.0	2.2	41

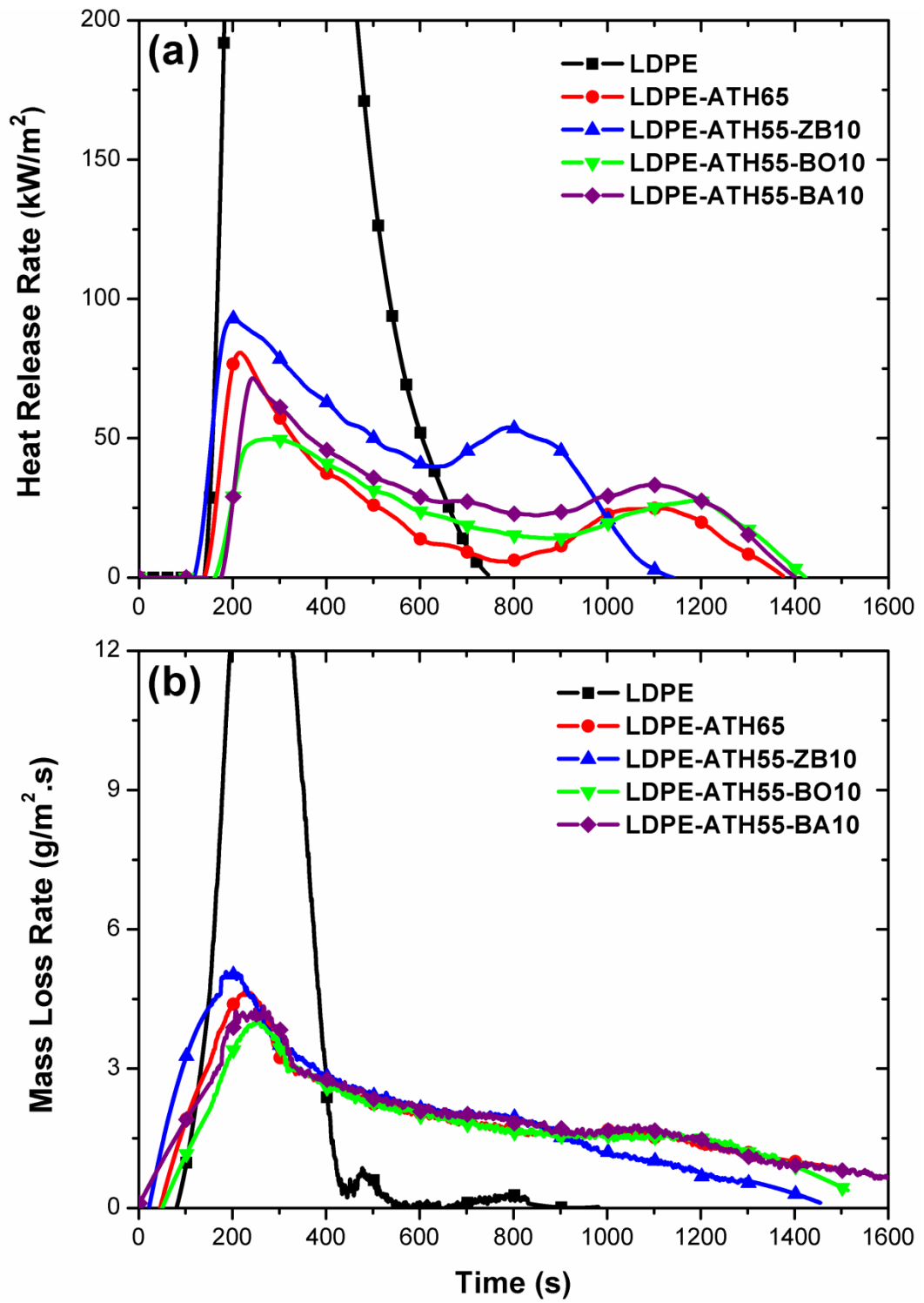


Figure 3.2. (a) Heat Release Rate and (b) Mass Loss Rate curves of the specimens with LDPE matrix

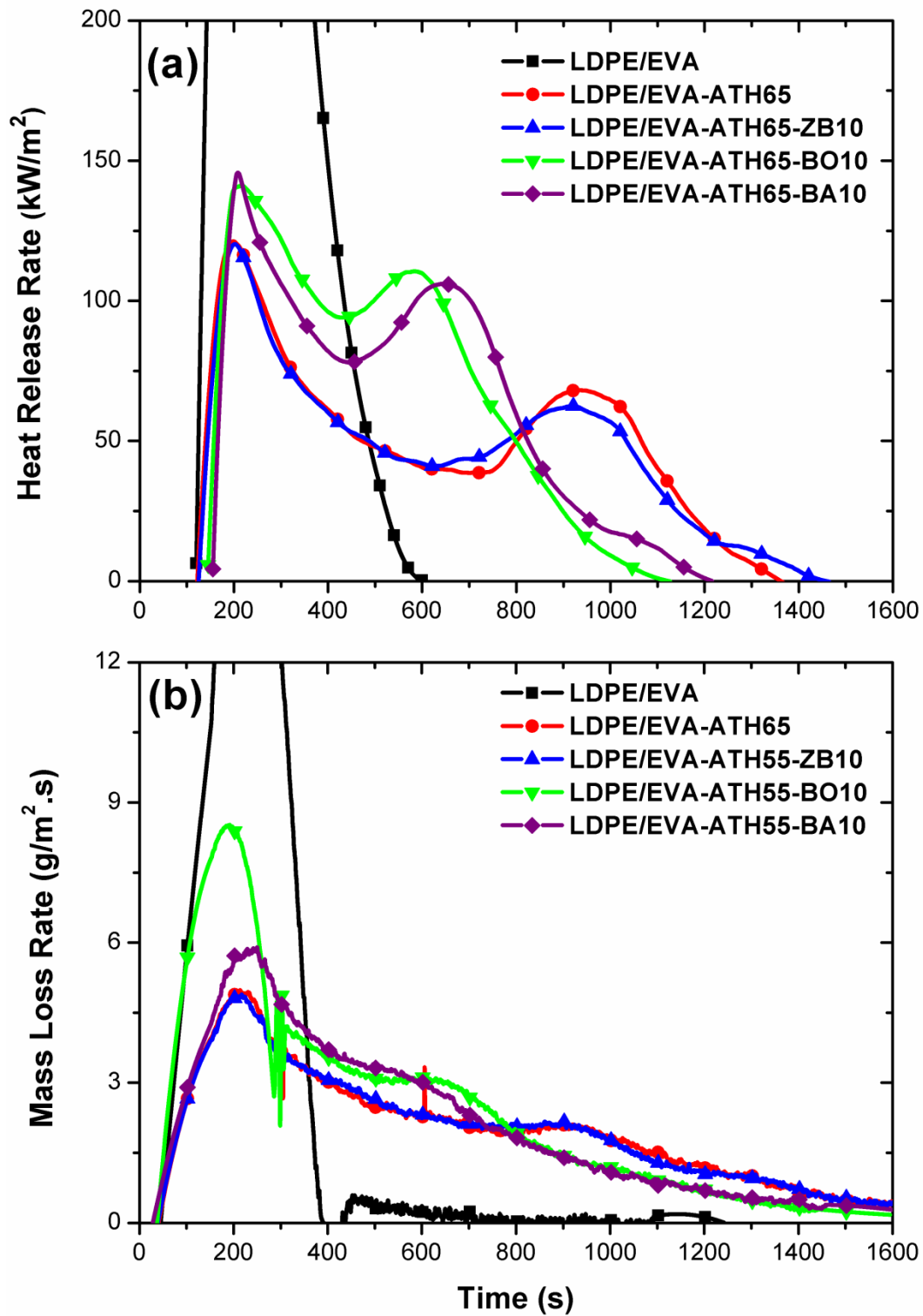


Figure 3.3. (a) Heat Release Rate and (b) Mass Loss Rate curves of the specimens with LDPE/EVA matrix

3.1.4 Thermogravimetric Analysis

Thermogravimetric (TG) and Differential Thermogravimetric (DTG) curves of the specimens based on LDPE and LDPE/EVA matrices are given in Figure 3.4 and 3.5, respectively, while the thermal degradation parameters derived from these curves are tabulated in Table 3.4.

These curves show that neat LDPE matrix decomposes in one step at around 480°C with nearly no residue formation. On the other hand, due to the EVA content LDPE/EVA blend decomposes in two steps, the first step being around 357°C, again without residue formation. It is known that thermal decomposition of EVA proceeds first by losing acetic acid and formation of unsaturated polyenes followed by random chain scission of the remaining material, releasing unsaturated vapour species such as butane and ethylene [3].

When ATH was incorporated into LDPE matrix, first, an initial peak appeared around 329°C due to endothermic dehydration reaction of ATH leading to 16 wt% overall mass loss, while there was no change in the LDPE decomposition peak of 480°C. When ATH was loaded into LDPE/EVA matrix, there was no change in the second peak of 478°C, while the first peak decreased from 357°C down to 336°C due to again early decomposition of ATH.

In terms of 10 wt% and 50 wt% degradation temperatures ($T_{10\text{wt}\%}$ and $T_{50\text{wt}\%}$), Table 3.4 indicates that $T_{10\text{wt}\%}$ values of both matrix materials decreases significantly, due to the early dehydration reactions of ATH. On the other hand, $T_{50\text{wt}\%}$ values of the matrices increased by 7°C and 14°C, respectively. However, the most significant contribution of ATH loading was the formation of residue which was 38 wt% for LDPE matrix and 40 wt% for LDPE/EVA matrix.

When certain amount of ATH loading was replaced with 10 wt% boron compounds ZB, BO and BA, it was observed that there were no significant changes in the values of DTG peak temperatures and 10 wt% and 50 wt% thermal degradation temperatures. However, there were synergistic increases in the percent residue formation for each matrix, for example, ZB replacement resulted in as much as 5 wt% extra residue formation.

Table 3.4 Thermal degradation parameters of the specimens determined from TG and DTG curves

Specimens	T_{DTG-Peak 1}^a (°C)	T_{DTG-Peak 2}^b (°C)	T_{10wt%}^c (°C)	T_{50wt%}^d (°C)	% Residue at 600°C^e
LDPE	-	480	451	477	0.2
LDPE-ATH65	329	480	324	484	38.4
LDPE-ATH55-ZB10	322	475	320	481	43.4
LDPE-ATH55-BO10	343	444	323	449	43.8
LDPE-ATH55-BA10	335	450	322	455	38.6
LDPE/EVA	357	478	431	473	0.3
LDPE/EVA-ATH65	336	478	329	487	40.2
LDPE/EVA-ATH55-ZB10	335	478	330	489	45.5
LDPE/EVA-ATH55-BO10	336	463	303	464	43.5
LDPE/EVA-ATH55-BA10	340	458	313	464	42.0

^aT_{DTG-Peak 1}: First peak temperature in DTG curve.

^bT_{DTG-Peak 2}: Second peak temperature in DTG curve.

^cT_{10wt%}: Thermal degradation temperature for 10% mass loss.

^dT_{50wt%}: Thermal degradation temperature for 50% mass loss.

^e% Residue at 600°C: % Char yield at 600 °C.

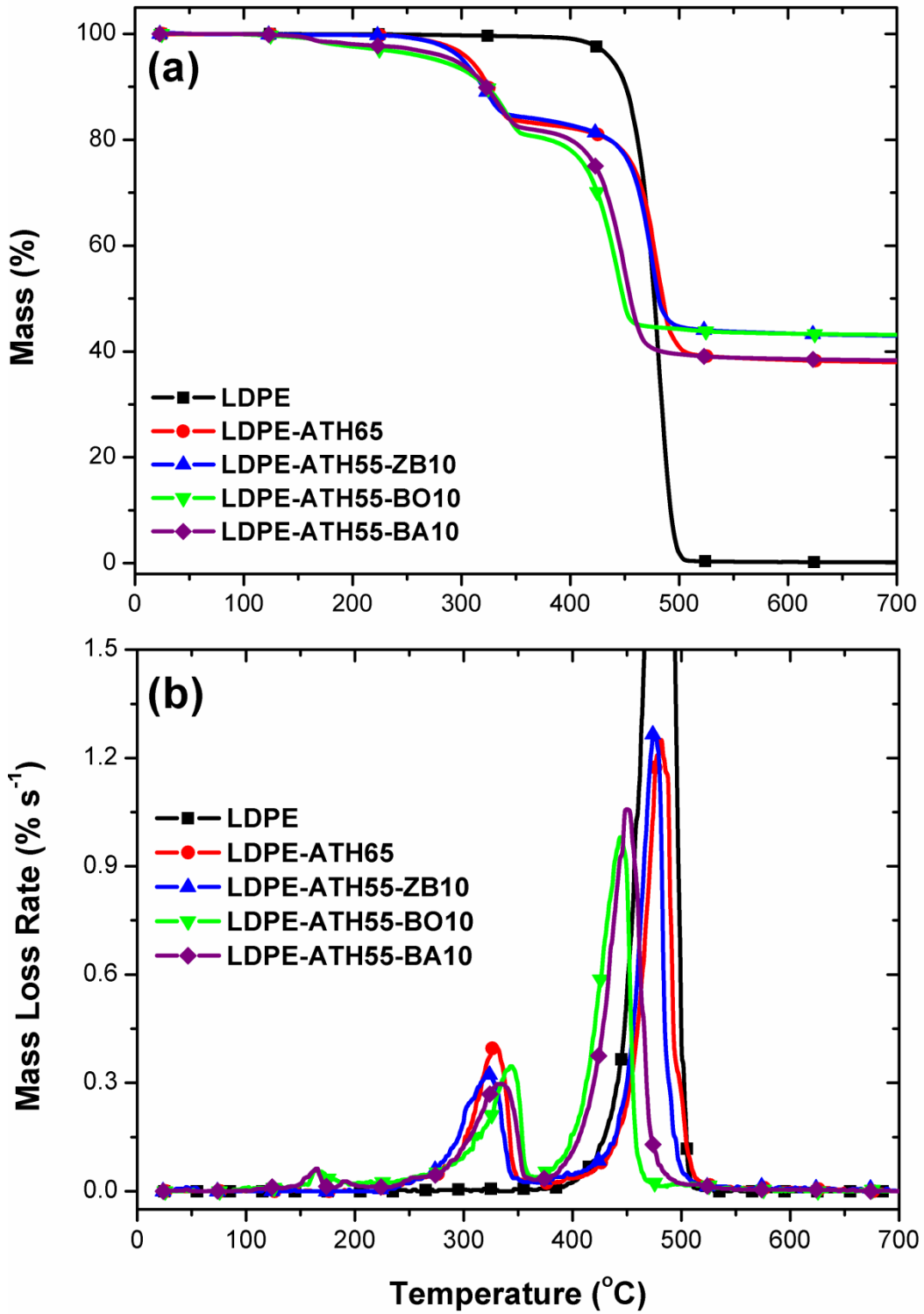


Figure 3.4 (a) Thermogravimetric (TG) and (b) Differential Thermogravimetric (DTG) curves of the specimens with LDPE matrix

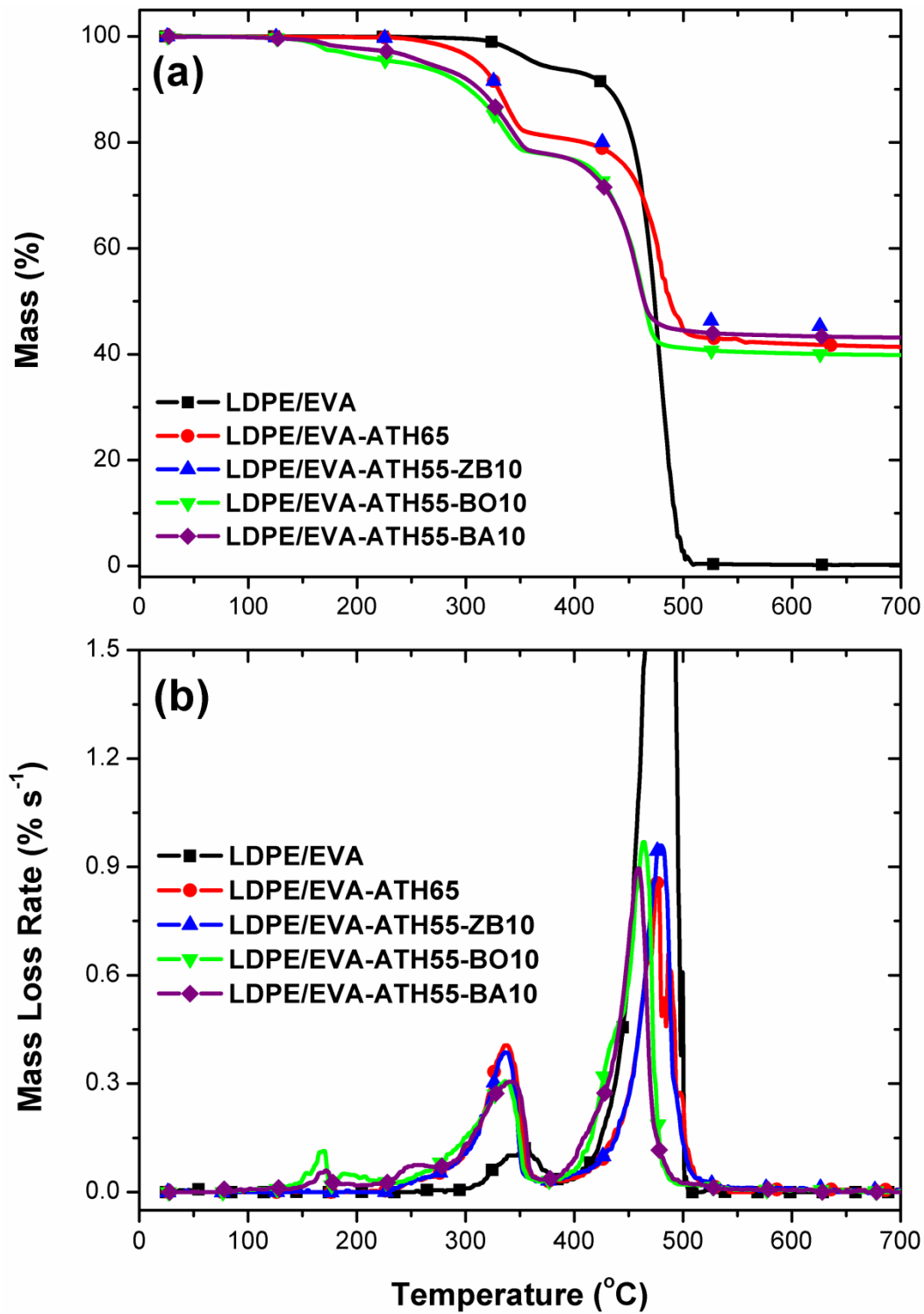


Figure 3.5 (a) Thermogravimetric (TG) and (b) Differential Thermogravimetric (DTG) curves of the specimens with LDPE/EVA matrix

3.1.5 Residue Analysis

Residue analysis was first performed with the macro-scale visual examination of the surface char layers of all MLC specimens just after the test. Surface char layer images of the specimens with LDPE and LDPE/EVA matrices are given in Figures 3.6 and 3.7, respectively.

Figures 3.6(a) and 3.7(a) show that using only ATH leads to formation of continuous and rather cohesive char layer with almost no cracking. On the other hand, when boron compounds ZB, BO and BA were incorporated, it was observed that (Figures 3.6(b,c,d) and Figures 3.7(b,c,d)) there was not only formation of several cracks through surface char layers, but also certain levels of intumescence occurred. Although cracking is a disadvantage, intumescence character of the char layers resulted in certain synergism in the physical barrier mechanism.

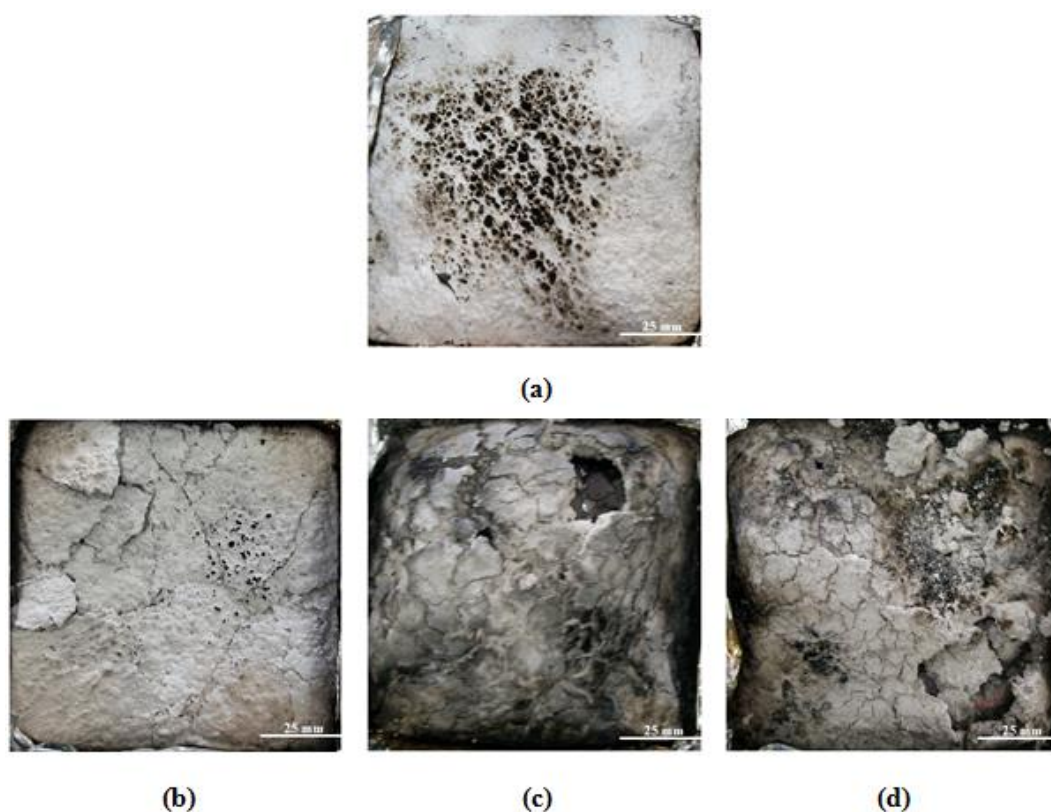


Figure 3.6 Macroscale appearances of the surface char layers of MLC specimens with LDPE matrix; (a) LDPE-ATH65, (b) LDPE-ATH55-ZB10, (c) LDPE-ATH55-BO10, (d) LDPE-ATH55-BA10

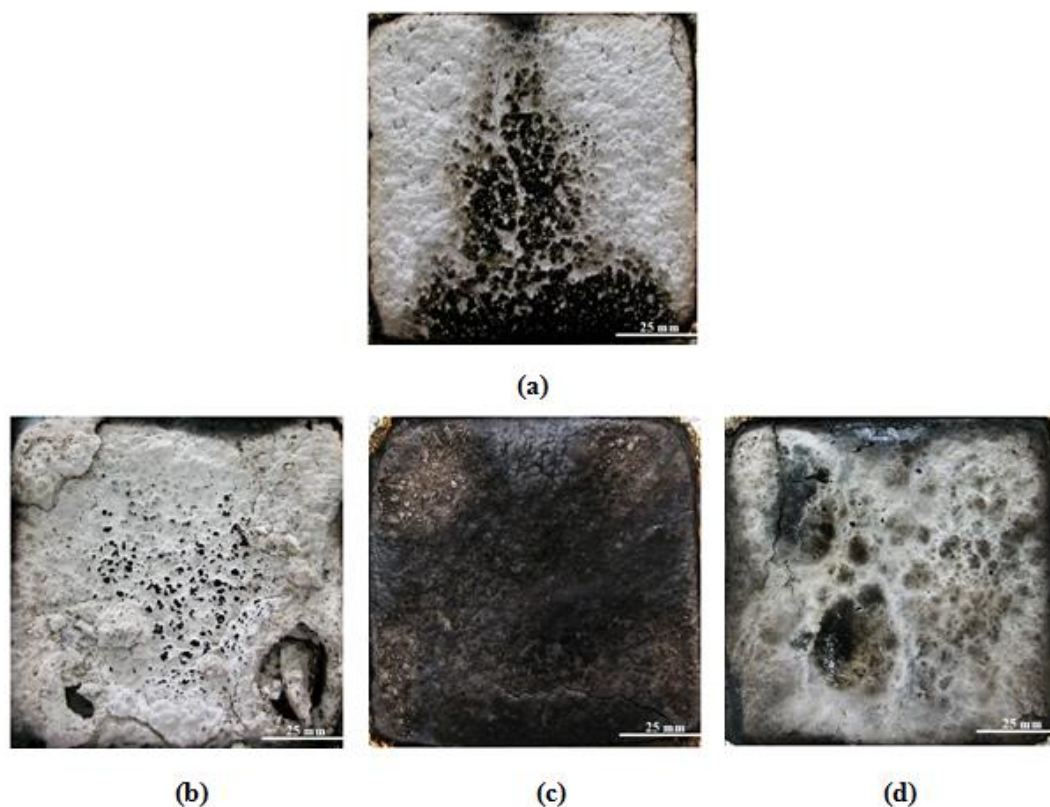


Figure 3.7 Macroscale appearances of the surface char layers of MLC specimens with LDPE/EVA matrix; (a) LDPE/EVA-ATH65, (b) LDPE/EVA-ATH55-ZB10, (c) LDPE/EVA-ATH55-BO10, (d) LDPE/EVA-ATH55-BA10

Apart from the expected ones, in order to reveal whether there is any other ceramic structure formed in the char layers, XRD analyses were conducted on the MLC chars of all specimens. XRD diffractograms of the specimens with each matrix are given in Figures 3.8 and 3.9, respectively.

Figures 3.8 and 3.9 show that when only ATH was loaded, typical crystal peaks of alumina, the main byproduct of the decomposition, were appeared. When ZB was added, two more peaks corresponding to its decomposition byproducts; dehydrated zinc borate and zinc oxide, were also formed. Similarly, when BO and BA were added, typical peaks of boron oxide also appeared.

Thus, it can be stated that, apart from the expected decomposition byproducts, no other phases were formed in the chars of the MLC specimens. This could be interpreted as another confirmation of the physical barrier mechanism of ATH and boron compounds.

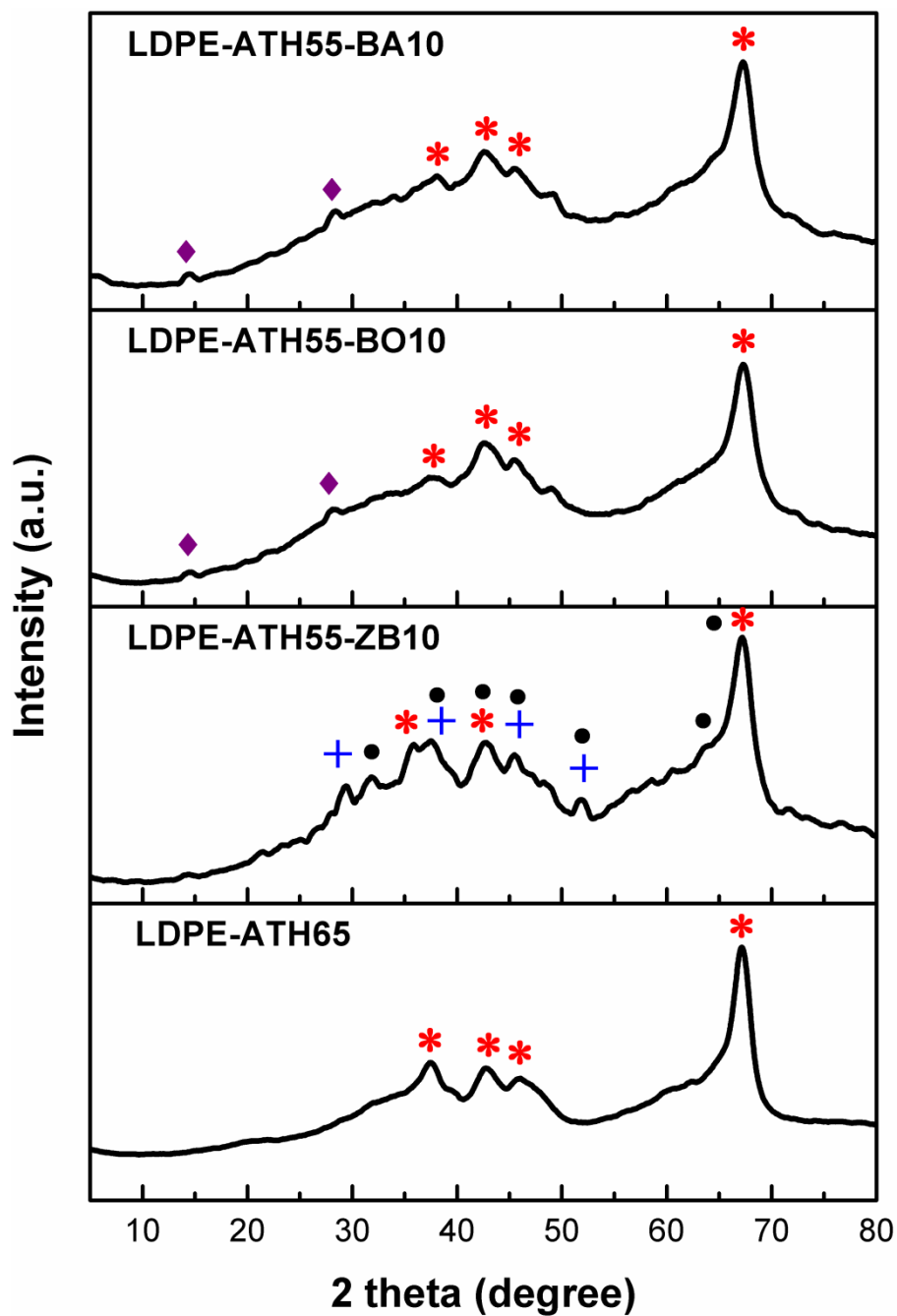


Figure 3.8 XRD patterns of the chars of the MLC specimens with LDPE matrix

- * **Aluminum oxide:** Al_2O_3 (Card no: 04-0880)
- + **Dehydrated zinc borate:** $\text{Zn}(\text{BO}_2)_2$ (Card no: 39-1126)
- **Zinc oxide:** ZnO_2 (Card no: 13-0311)
- ◆ **Boron oxide:** B_2O_3 (Card no: 06-0297)

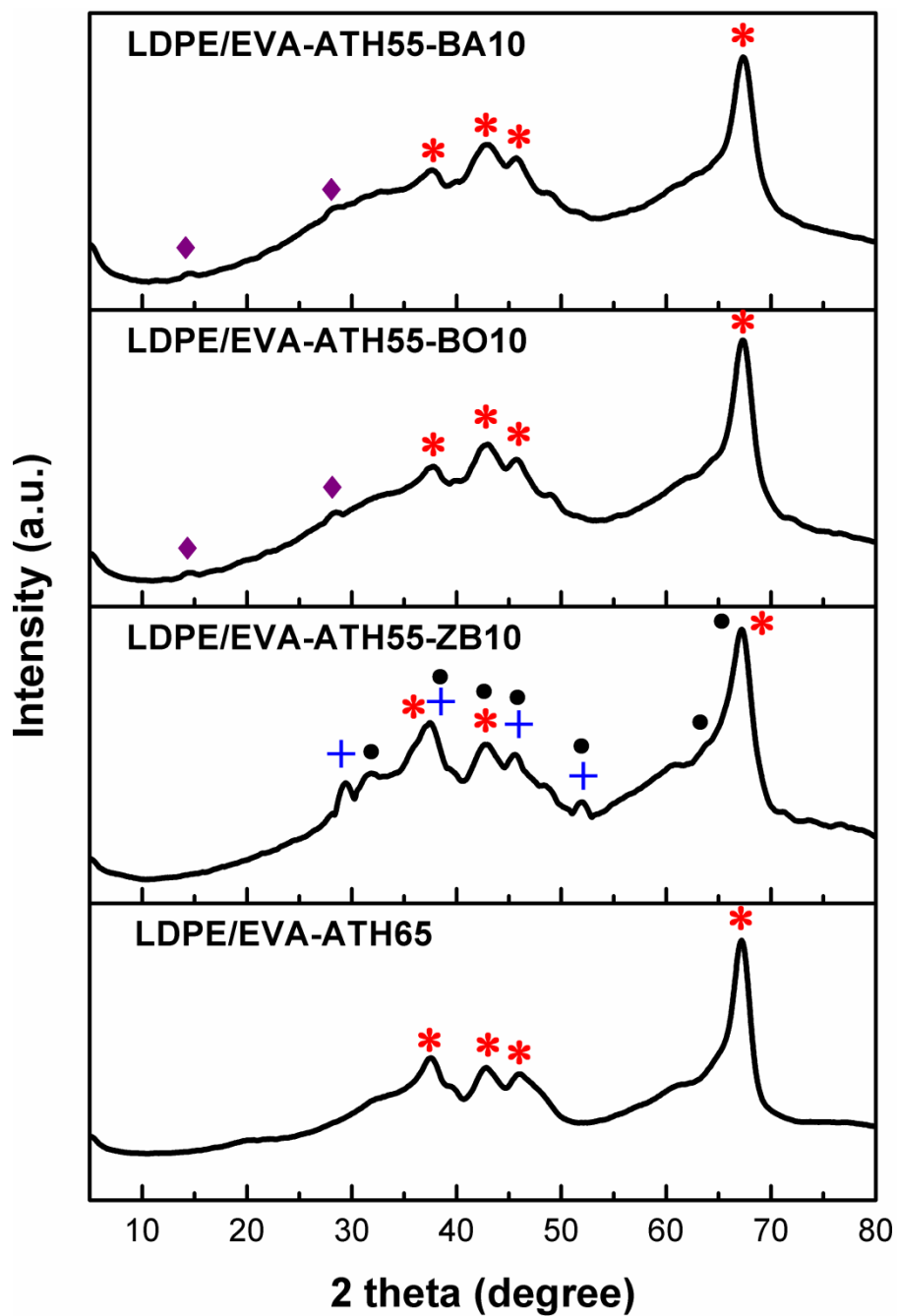


Figure 3.9 XRD patterns of the chars of the MLC specimens with LDPE/EVA matrix

- * Aluminum oxide: Al₂O₃ (Card no: 04-0880)
- + Dehydrated zinc borate: Zn(BO₂)₂ (Card no: 39-1126)
- Zinc oxide: ZnO₂ (Card no: 13-0311)
- ◆ Boron oxide: B₂O₃ (Card no: 06-0297)

3.1.6 Mechanical Behavior

In order to observe effects of traditional flame retardant ATH and boron compounds on the mechanical performance of cable insulation materials LDPE and LDPE/EVA, at least five specimens for each formulation were investigated by tensile tests. Figures 3.10 and 3.11 show tensile stress-strain behavior of the specimens with ATH and 10 wt% boron compounds for each matrix, while mechanical properties determined for all specimens are tabulated in Table 3.5.

Figures 3.10 and 3.11, and Table 3.5 indicate that incorporation of 65 wt% ATH increases both modulus and strength of cable insulation materials, which is due to the decreased chain mobility of the polymer matrices by the very rigid inorganic fillers. For example, the increases in Young's Modulus are as much as 5 times for LDPE matrix, and 4 times for LDPE/EVA matrix, respectively. Increases in tensile strength are only 20% for both LDPE matrix and LDPE/EVA matrix.

On the other hand, it is seen that ductility (i.e. % elongation at break) values of both matrix polymers drop drastically due to the extreme stiffening effect of the required very large quantity of flame retardant additive. Table 3.5 indicates that, 65 wt% ATH decreases ductility of LDPE matrix by 5 times, while that decrease is as much as 11 times for LDPE/EVA matrix.

Figures 3.10 and 3.11, and Table 3.5 also show that replacement of certain amounts of ATH with boron compounds ZB, BO, BA leads to very similar influences on the mechanical properties of both matrix materials, i.e. they all lead to similar increases in the values of Young's Modulus and Tensile Strength, and similar decreases in the % Elongation at break values.

In order to clarify these similar influences, fracture surfaces of the tensile test specimens were examined under SEM. Fracture surface morphology of each matrix are given in Figures 3.12 and 3.13, respectively. Fractographs revealed that all flame retardants (ATH, ZB, BO, BA) were homogeneously dispersed, with similar levels of interfacial bonding.

Therefore, it can be concluded that replacement of certain amounts of ATH with boron compounds (ZB, BO, BA) result in similar changes in the mechanical properties of the both cable insulation materials.

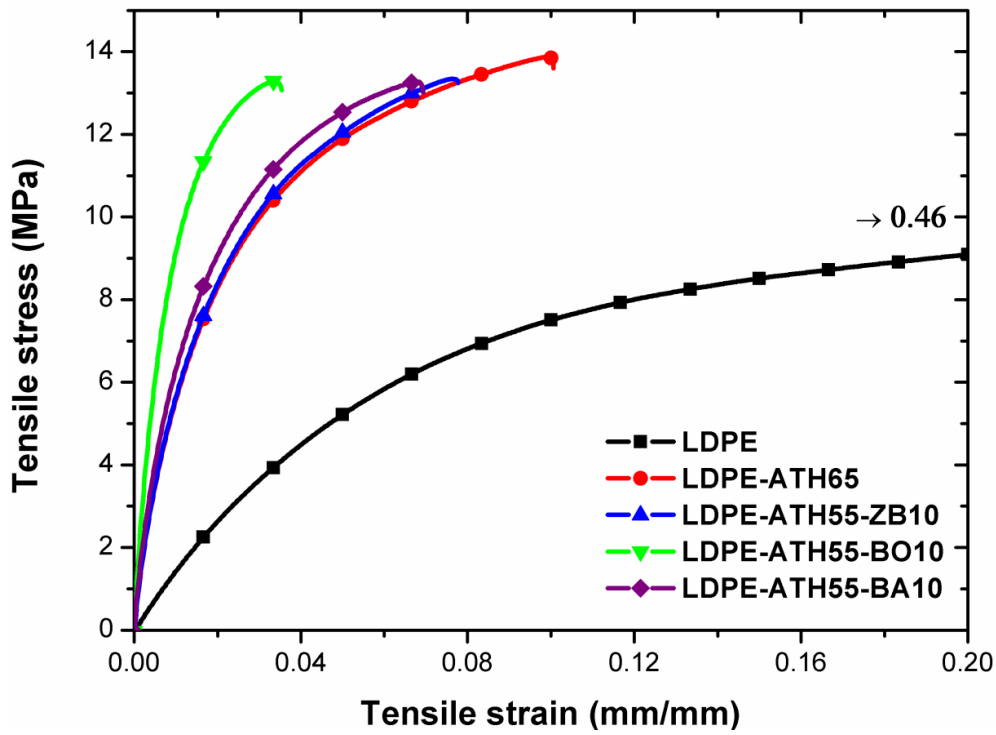


Figure 3.10 Tensile stress-strain curves of the specimens with LDPE matrix

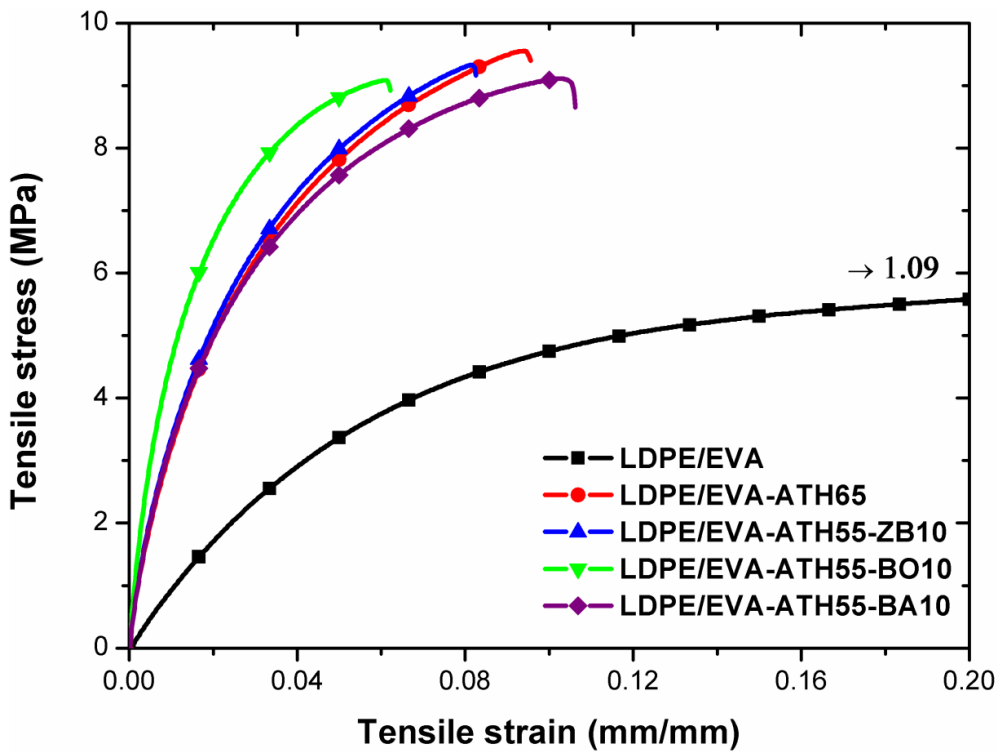


Figure 3.11 Tensile stress-strain curves of the specimens with LDPE/EVA matrix

Table 3.5 Mechanical properties of the specimens

Specimens	Young's Modulus (GPa)	Tensile Strength (MPa)	% Elongation at break
LDPE	0.19±0.01	11.1±0.3	46±3
LDPE-ATH65	0.93±0.01	13.6±0.4	9±1
LDPE-ATH55-ZB10	0.80±0.07	13.4±0.2	8±1
LDPE-ATH45-ZB20	0.95±0.12	12.4±0.1	7±1
LDPE-ATH35-ZB30	1.03±0.03	12.5±0.1	7±1
LDPE-ATH55-BO10	1.49±0.12	13.0±0.5	4±1
LDPE-ATH45-BO20	2.12±0.11	12.3±0.5	2±1
LDPE-ATH35-BO30	2.15±0.20	11.0±0.5	2±0
LDPE-ATH55-BA10	1.03±0.04	13.3±0.3	7±1
LDPE/EVA	0.13±0.01	7.8±0.3	109±28
LDPE/EVA-ATH65	0.53±0.02	9.5±0.3	10±1
LDPE/EVA-ATH55-ZB10	0.55±0.03	9.3±0.3	9±1
LDPE/EVA-ATH45-ZB20	0.54±0.03	9.1±0.2	9±1
LDPE/EVA-ATH35-ZB30	0.53±0.02	9.1±0.4	10±2
LDPE/EVA-ATH55-BO10	0.73±0.08	9.1±0.1	7±1
LDPE/EVA-ATH45-BO20	0.91±0.12	8.6±0.4	5±1
LDPE/EVA-ATH35-BO30	1.05±0.06	8.7±0.4	4±1
LDPE/EVA-ATH55-BA10	0.56±0.03	9.0±0.2	10±1

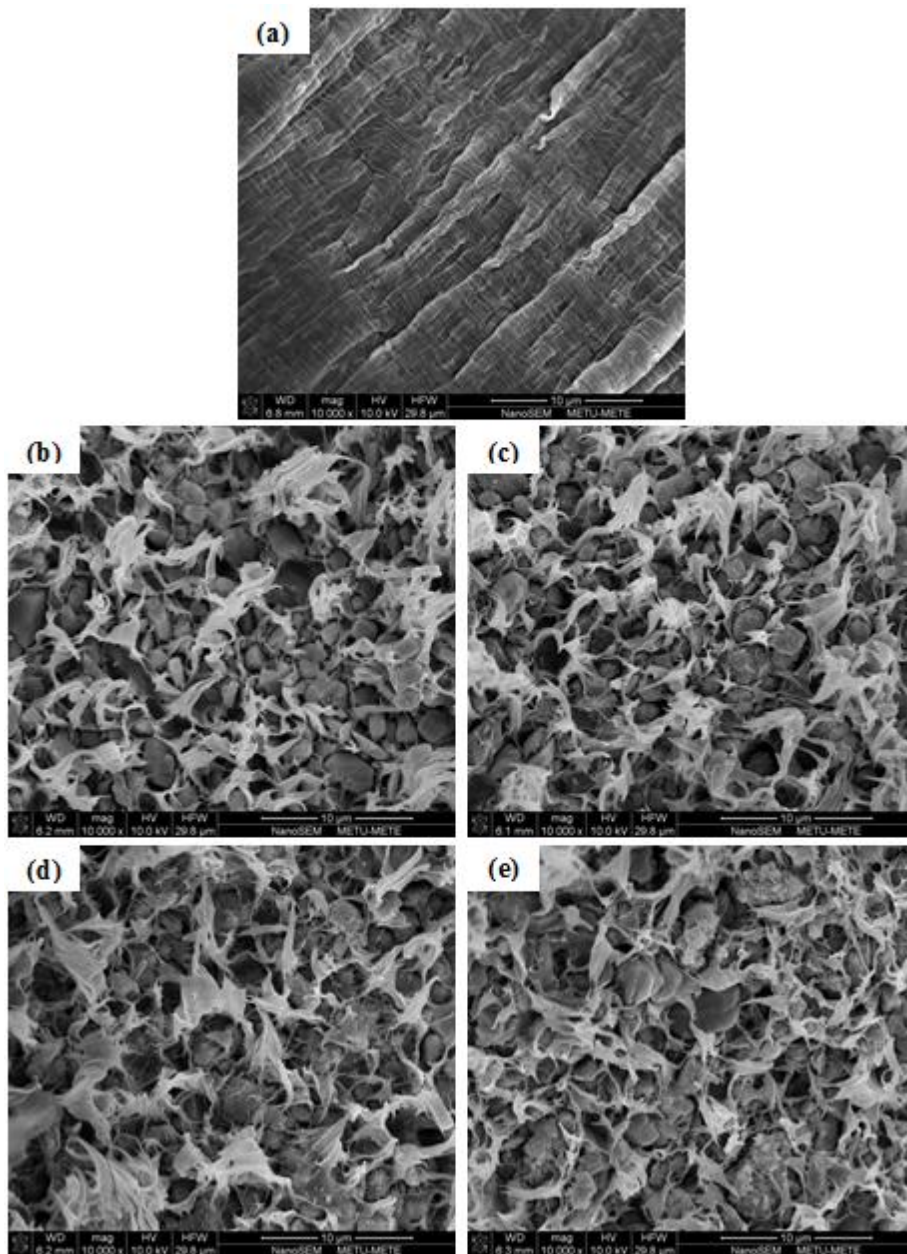


Figure 3.12 SEM fractographs of the specimens with LDPE matrix; (a) LDPE, (b) LDPE-ATH65, (c) LDPE-ATH55-ZB10, (d) LDPE-ATH55-BO10, (e) LDPE-ATH55-BA10

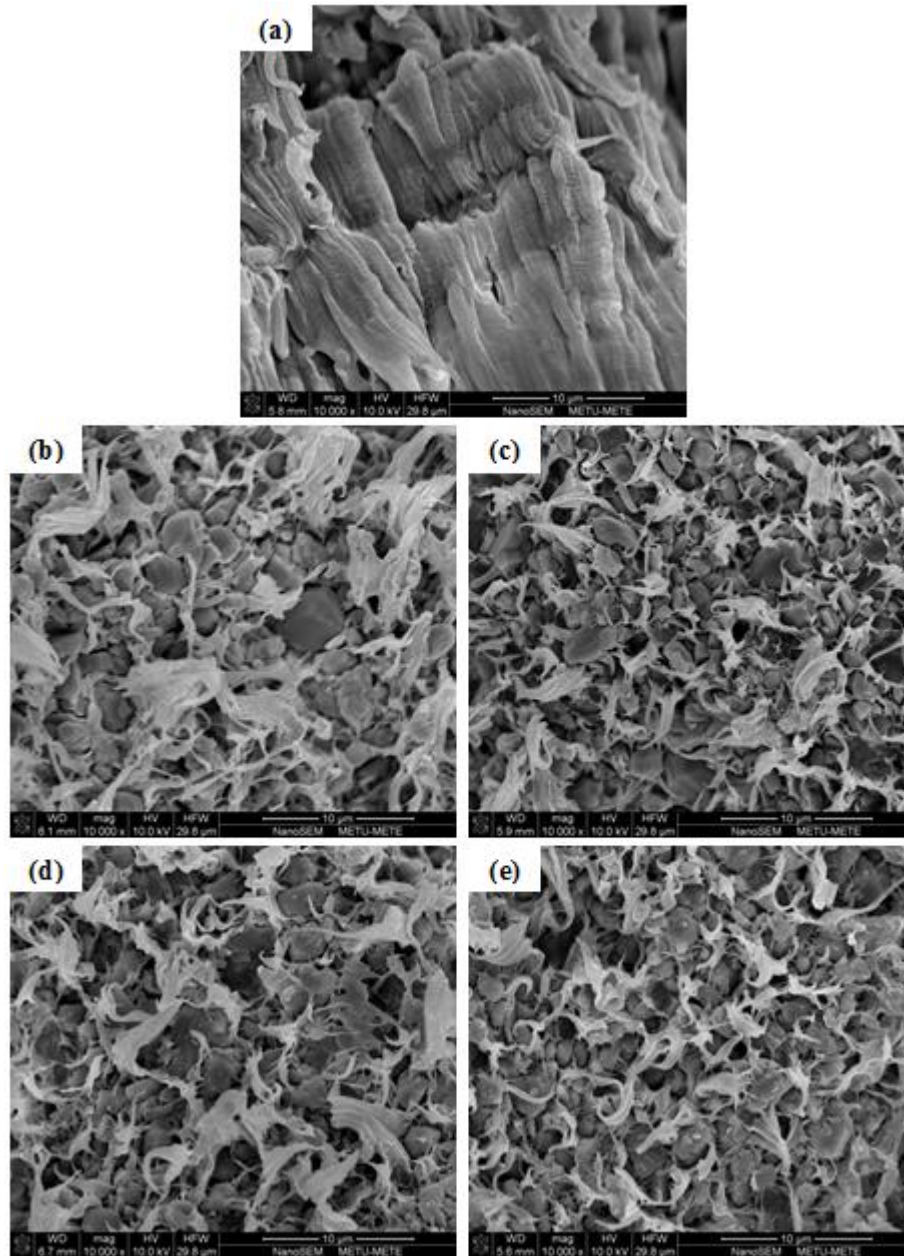


Figure 3.13 SEM fractographs of the specimens with LDPE/EVA matrix; (a) LDPE/EVA, (b) LDPE/EVA-ATH65, (c) LDPE/EVA-ATH55-ZB10, (d) LDPE/EVA-ATH55-BO10, (e) LDPE/EVA-ATH55-BA10

3.2 Contribution of Nanoclays with ATH and Zinc Borate in LDPE and LDPE/EVA Matrices

The second purpose of this thesis was to investigate contribution of nanoclays when used alone, and together with traditional flame retardant ATH; and also together with ATH-ZB synergistic system for LDPE and LDPE/EVA cable insulation materials. Results of flammability tests and other analyses conducted for this purpose are presented and discussed below.

3.2.1 Nanocomposite Formation

Before flammability analysis, it was necessary to determine whether nanocomposite structure was achieved or not. For this reason, first of all X-ray diffraction analysis (XRD) and transmission electron microscopy (TEM) were conducted in order to evaluate dispersibility and intercalation/exfoliation level of nanoclay (NC) silicate layers in each matrix.

It is known that Cloisite 20A nanoclay gives a sharp XRD peak at $2\theta=3.4^\circ$ corresponding to an interlayer spacing of 2.4 nm. XRD patterns of the nanocomposite specimens in Figure 3.14 show that loading 5% NC into LDPE and LDPE/EVA matrices resulted in three XRD peaks. In LDPE-NC specimen (Figure 3.14(a)) the first sharp peak at $2\theta=2.38^\circ$ corresponds to the interlayer spacing of 3.7 nm. Therefore, increase of gallery distance from 2.4 nm to 3.7 nm indicates that silicate layers are very well intercalated by the LDPE molecular chains. The second and third peaks (at $2\theta=4.72^\circ$ and $2\theta=6.80^\circ$, respectively) are rather broad with low intensity. These peaks should be due to the second-order and third-order reflections corresponding to the same d -spacing of the first-order reflection.

Similarly, in LDPE/EVA-NC specimen (Figure 3.14(b)) the gallery distance was increased from 2.4 nm to 4.5 nm (at $2\theta=1.98^\circ$) which reveals that LDPE/EVA blend can intercalate into the silicate layers more effectively due to the more polar structure of EVA. The second and third peaks (at $2\theta=4.30^\circ$ and $2\theta=6.42^\circ$, respectively) should be again due to the higher (second and third) order basal reflections.

On the other hand, Figure 3.14(a) also shows that basal reflections disappear in the specimens with ATH and ATH-ZB. Due to the intercalation efficiency of EVA, Figure 3.14(b) shows that there could be very low intensity, very broad peaks in ATH and ATH-ZB loaded LDPE/EVA specimens, corresponding to 3.9 nm and 4.0 nm gallery distances, respectively. However, this situation should not be interpreted as the complete exfoliation of silicate layers. Loss of these sharp peaks should be due to the attenuation and absorption of the reflections by the very high amount of elements in the flame retardants used (such as aluminum in ATH, and zinc and boron in ZB) having high levels of absorption coefficients.

In order to support XRD results, NC loaded LDPE and LDPE/EVA specimens were also investigated under TEM. Lower magnification images (Figures 15(a) and 16(a)) show that

nanoclays were homogeneously distributed in both matrices. Medium and higher magnification images (Figures 15(b, c) and 16(b, c)) revealed that NC silicate layers were very well intercalated with certain level of exfoliation.

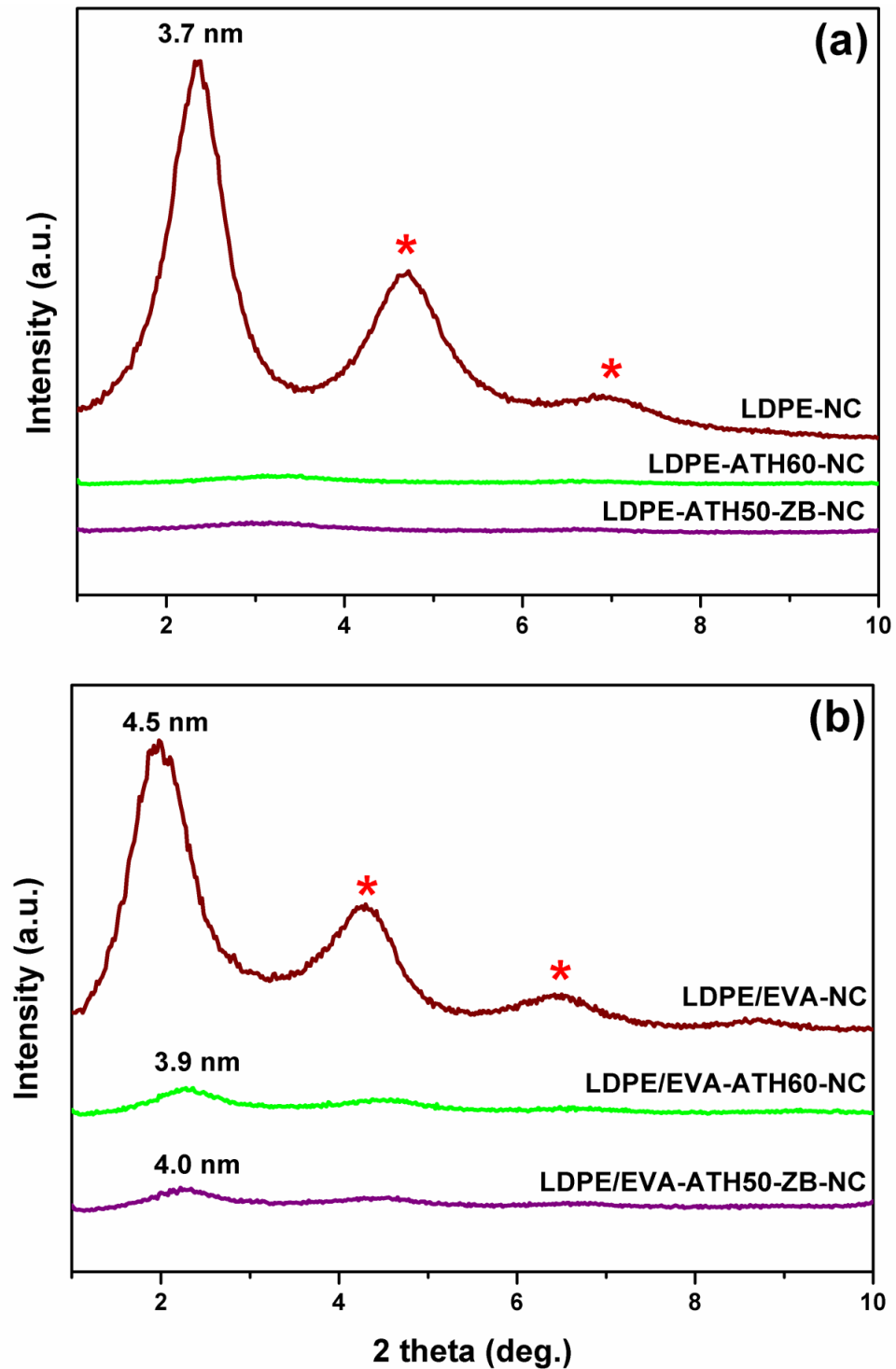


Figure 3.14 XRD patterns of nanocomposite specimens with (a) LDPE matrix and (b) LDPE/EVA matrix. Asterisks (*) designate second and third order reflections.

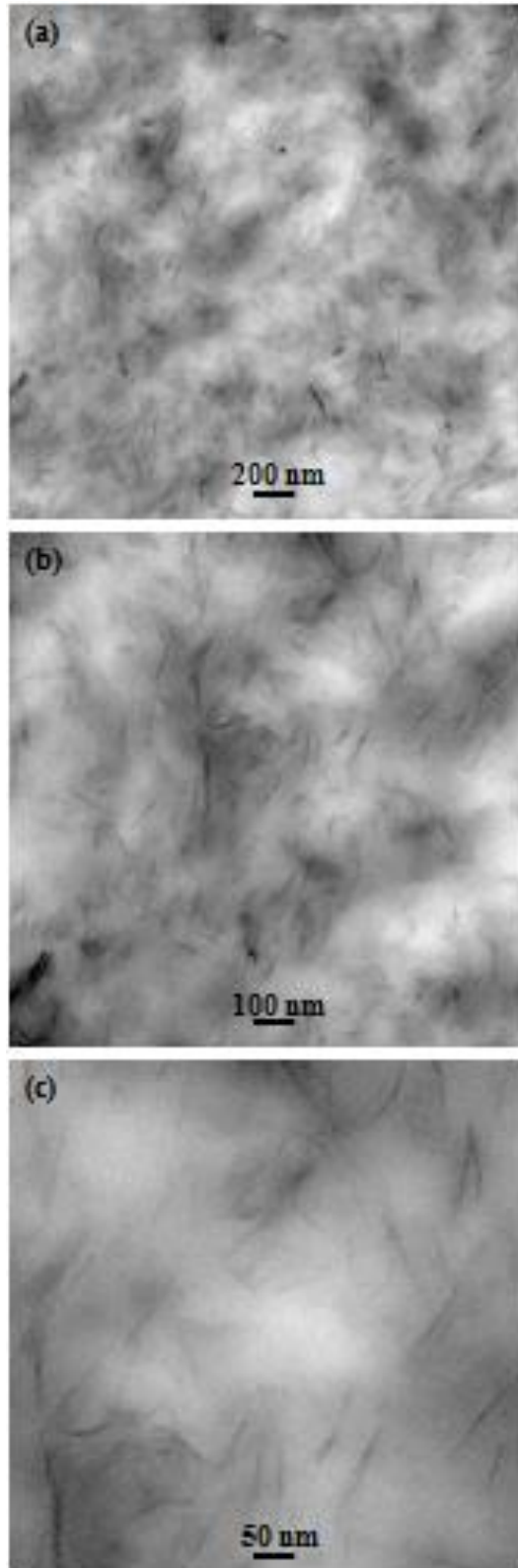


Figure 3.15 TEM images showing (a) uniform distribution, (b) and (c) intercalated and partly exfoliated structure of NC silicate layers in LDPE matrix

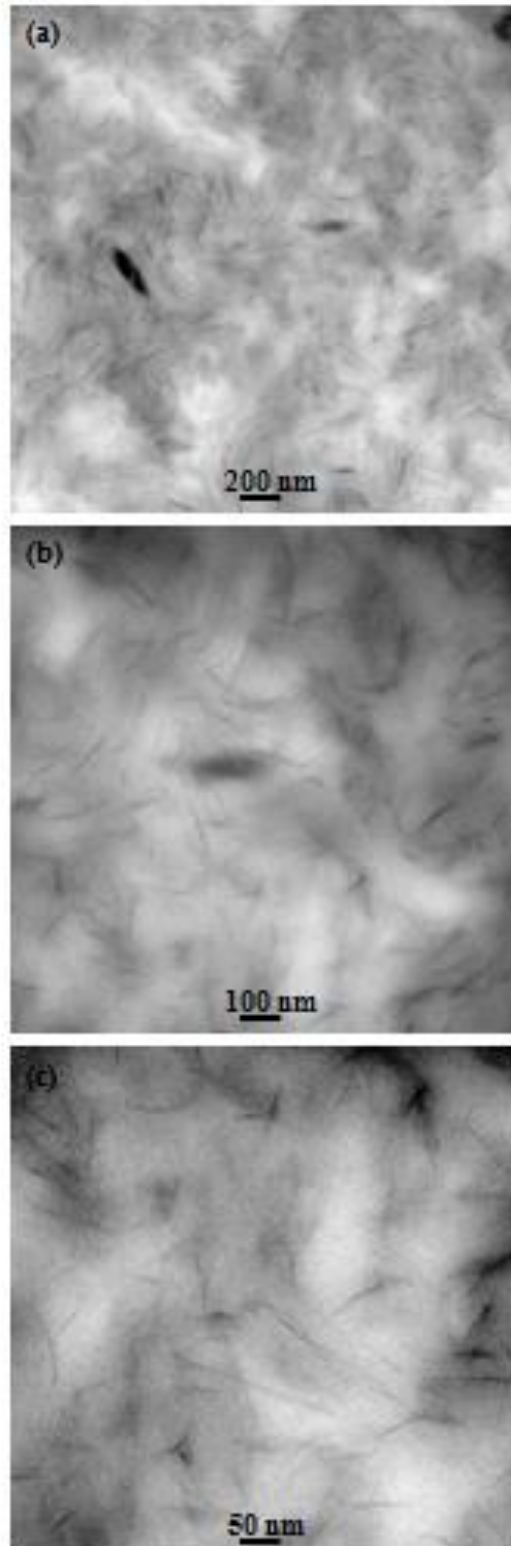


Figure 3.16 TEM images showing (a) uniform distribution, (b) and (c) intercalated and partly exfoliated structure of NC silicate layers in LDPE/EVA matrix

3.2.2 UL-94 and LOI Flammability Tests

Table 3.6 tabulating the results of UL-94 and LOI flammability tests of each compound and nanocomposites show that both cable insulation matrices LDPE and LDPE/EVA fail from UL-94 rating with low LOI values of 19 and 18 O₂%, respectively. It is seen in Table 3.6 that, addition of 5 wt% NC alone into LDPE and LDPE/EVA matrices increased LOI values by 2 and 4 O₂%, respectively. Although, addition of nanoclays alone did not contribute to the UL-94 rating of each matrix material, it was observed that NC loading decreased the level of dripping and increased the amount of char formation during the test.

Table 3.6 Results of UL-94 and LOI flammability tests

Specimens	UL-94 rating^a	LOI (O₂ %)^b
LDPE	Fail	19
LDPE-NC	Fail	21
LDPE-ATH65	V-0	30
LDPE-ATH60-NC	V-0	34
LDPE-ATH55-ZB	V-0	30
LDPE-ATH50-ZB-NC	V-0	33
LDPE/EVA	Fail	18
LDPE/EVA-NC	Fail	22
LDPE/EVA-ATH65	V-0	31
LDPE/EVA-ATH60-NC	V-0	38
LDPE/EVA-ATH55-ZB	V-0	32
LDPE/EVA-ATH50-ZB-NC	V-0	34

^aMaterials flammability classifications for stringent vertical orientation; Fail (flame extinguishing $t > 30$ s), V-2 (flaming drips, material self-extinguishes at $10 < t < 30$ s), V-1 (material self-extinguishes at $10 < t < 30$ s, without dripping), V-0 (material self-extinguishes at $t < 10$ s)

^bOxygen level required for sustained flaming combustion.

As expected, when the polymer matrices were loaded with 65 wt% traditional flame retardant ATH, they both obtained V-0 rating of UL-94; and significant increases of LOI values from 19 and 18 O₂% up to 30 and 31 O₂%, respectively. Table 3.6 indicates that, when 5 wt% of ATH was replaced with NC, both matrices not only keep their UL-94 V-0 rating, but their LOI values further increased significantly up to 34 and 38 O₂%, respectively.

It was shown in the previous Section 3.1 that use of ATH together with ZB lead to synergism in many flammability properties of LDPE and LDPE/EVA matrices. Table 3.6 also shows that, for both matrices, when 5 wt% of ATH-ZB system was replaced with NC, specimens again keep their UL-94 rating of V-0 and increases LOI values further by 3 and 2 O₂% for LDPE and LDPE/EVA matrices, respectively.

It can be concluded that use of nanoclays with traditional ATH or ATH-ZB system keep UL-94 rating of both matrix materials, and contributes their LOI values by further increases as much as 7 O₂%. Flame retardancy mechanisms of ATH and ZB were discussed in the previous Section 3.1, here it can be added that contribution of NC was especially due to the further physical barrier mechanism of intercalated silicate layers, which will be discussed more in the following sections.

3.2.3 Mass Loss Cone Calorimetry

Flammability parameters determined by mass loss cone calorimeter (MLC) for all specimens are listed in Table 3.7 while Figures 3.17 and 3.18 give their heat release rate (HRR) and mass loss rate (MLR) curves. Note that these data were determined under an external heat flux of 50 kW/m², which was 35 kW/m² in the previous Section 3.1.

It is seen that both cable insulation matrix materials have very high values of peak heat release rate (PHRR) and total heat evolved (THE). When 5 wt% NC was introduced alone into LDPE and LDPE/EVA matrices, their PHRR values were suppressed by 26% and 40%, respectively. On the other hand, suppressions in THE values were only 2% for each matrix. This can be interpreted that use of nanoclays alone would be not very satisfactory.

As expected, loading of 65 wt% traditional ATH into LDPE and LDPE/EVA matrices decreased both PHRR and THE values drastically. For example, suppressions in PHRR values were 90% and 91%, while in THE values 58% and 53%, for the LDPE and LDPE/EVA matrices, respectively. When 5 wt% of ATH was replaced by NC, Table 3.7 shows that PHRR values were suppressed further by 23% in LDPE and by 20% in LDPE/EVA, while further suppressions in THE values were 7% and 15%, respectively.

Table 3.7 reveals that further synergistic contribution of nanoclays in the values of PHRR and THE were obtained when ATH was used together with ZB. In this formulation when 5 wt% ATH was replaced with NC, further decreases in PHRR and THE values were 29% and 17% respectively in LDPE matrix, while these decreases were 35% and 24% in LDPE/EVA matrix.

Figures 3.17 and 3.18 also show that HRR curves of ATH and ATH-ZB loaded specimens have two distinct peaks. The first HRR peak indicates combustion prior to charring while the part between first and second HRR peaks are attributed to gradual burning of the specimen through the thickness after the formation of initial char layer. The second peak should be due to the diminishing mass of fuel being subject to more rapid heating toward the end of combustion. These multiple HRR peaks have been also reported in Section 3.1 and [16, 34]. Due to their similar flame retardancy mechanism (i.e. physical barrier formation), Figures 3.17 and 3.18 indicate that when nanoclays were used together with ATH and ATH-ZB, HRR curves of these specimens have also double peaks.

Table 3.7 also reveals that incorporation of NC extended time to ignition (TTI) values slightly in all specimens. Fire growth index (FGI) which is the ratio of PHRR/TTI can be used to evaluate the contribution of a material to the flame spread. FGI values tabulated in Table 3.7 indicate that, not only loading of NC alone suppresses fire propagation rate of both matrices significantly, but replacement of 5 wt% of ATH or ATH-ZB with NC also contribute lower FGI values.

The ratio of THE/TML (total heat evolved/total mass loss) and % Char Yield might give information about the type of flame retardancy mechanisms of specimens. Table 3.7 reveals that values of these two parameters for the specimens without NC and with NC are very similar, i.e. basic flame retardancy mechanism of ATH, ZB, and NC are physical barrier in the condensed phase. On the other hand, as discussed in the previous Section 3.1, ATH and ZB liberate their chemically bonded water molecules during combustion and lead to the dilution of combustible fuel. Thus, it can be stated that ATH and ZB might contribute physical barrier mechanism also in the gas phase.

For both cable insulation materials, it can be simply summarized that contribution of nanoclays alone or together with ATH and ATH-ZB especially takes place in the values of PHRR and THE by further synergistic suppressions. These contributions should be due to the intercalated silicate layers acting as a barrier during combustion which inhibits flow of heat and flammable gases.

Table 3.7 Mass Loss Cone Calorimeter parameters of the specimens (under 50 kW/m² heat flux)

Specimens	PHRR (kW/m²)	THE (MJ/m²)	TTI (s)	FGI (kW/m².s)	THE/TML (MJ/m².g)	Char Yield (%)
LDPE	1565	2075	45	34.8	59.4	-
LDPE-NC	1166	2032	54	20.7	57.1	2
LDPE-ATH65	163	864	60	2.7	24.1	36
LDPE-ATH60-NC	125	802	65	1.9	22.1	35
LDPE-ATH55-ZB	148	976	58	2.6	25.6	38
LDPE-ATH50-ZB-NC	105	813	68	1.5	20.9	36
LDPE/EVA	1620	1969	42	38.6	57.5	-
LDPE/EVA-NC	975	1937	52	18.8	54.6	2
LDPE/EVA-ATH65	154	934	58	2.7	23.7	37
LDPE/EVA-ATH60-NC	124	790	67	2.4	21.4	35
LDPE/EVA-ATH55-ZB	145	932	56	2.6	24.1	39
LDPE/EVA-ATH50-ZB-NC	94	713	79	1.2	18.4	37

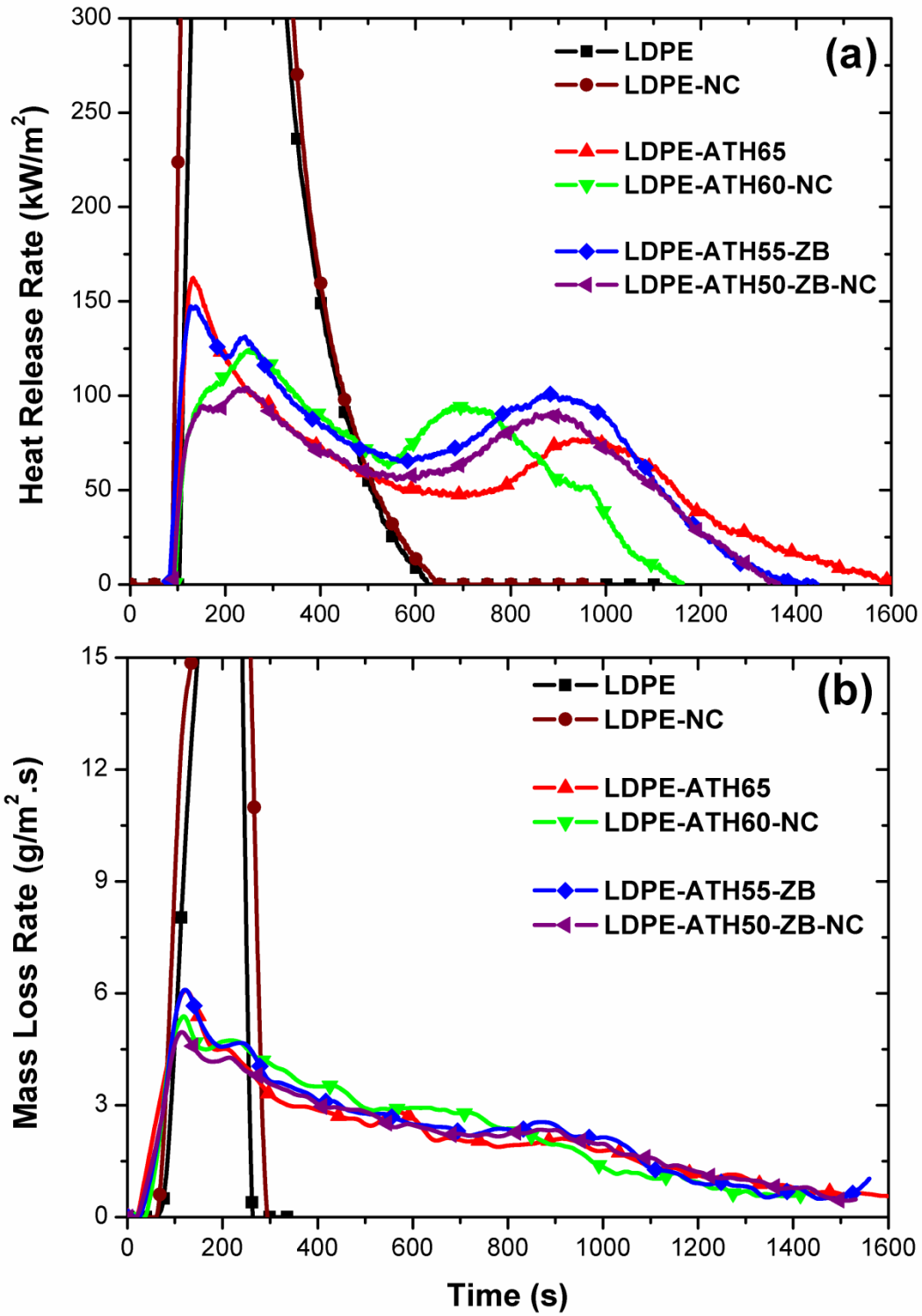


Figure 3.17 (a) Heat Release Rate and (b) Mass Loss Rate curves of the specimens with LDPE matrix

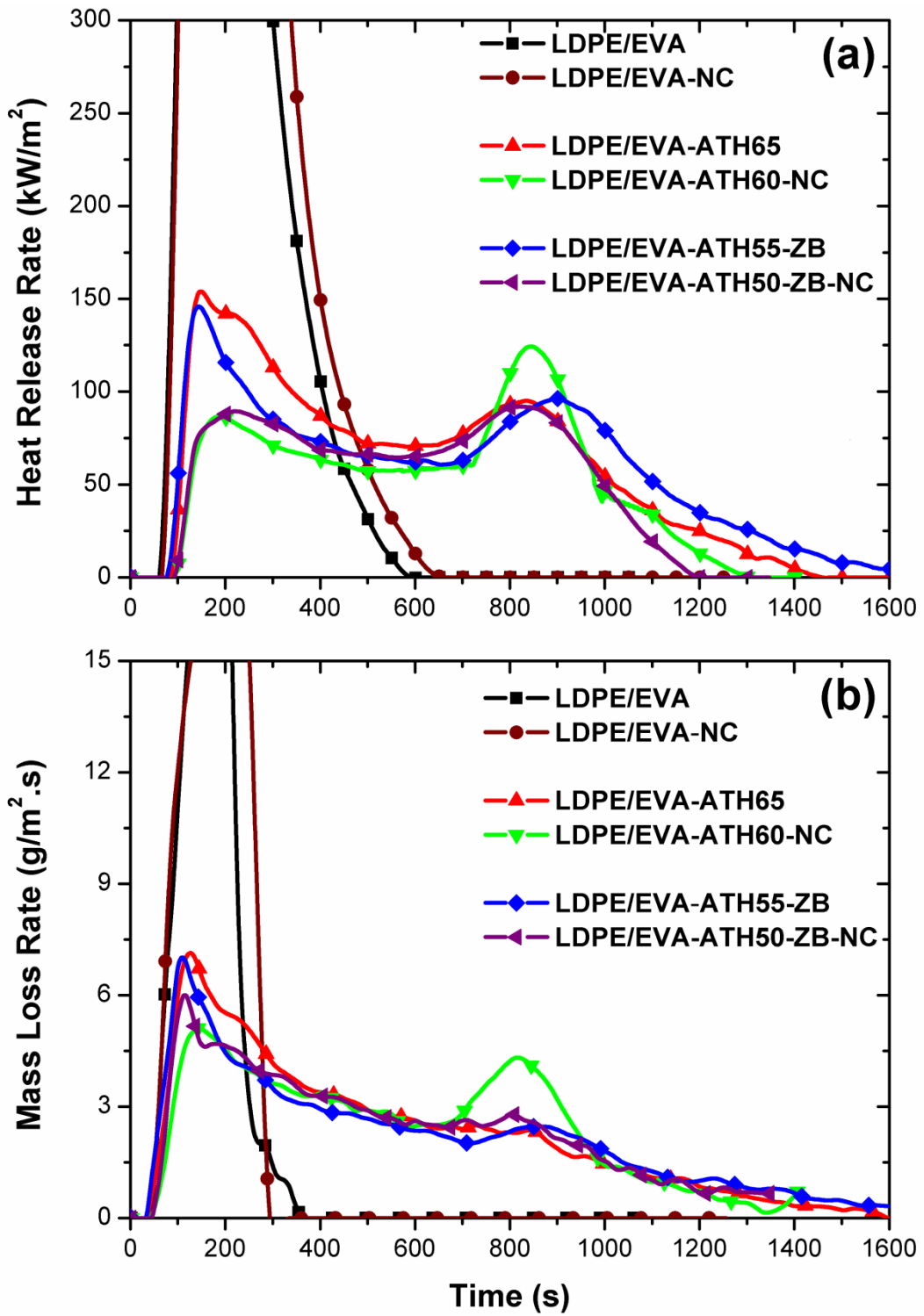


Figure 3.18 (a) Heat Release Rate and (b) Mass Loss Rate curves of the specimens with LDPE/EVA matrix

3.2.4 Thermogravimetric Analysis

Figures 3.19 and 3.20 show thermogravimetric (TG) and differential thermogravimetric (DTG) curves of the specimens with LDPE and LDPE/EVA matrices, respectively, while their thermal degradation parameters derived from these curves are tabulated in Table 3.8.

These curves show that neat LDPE matrix decomposes in one step while neat LDPE/EVA blends in two steps, both having no residue formation. Their degradation mechanisms were discussed in detail in Section 3.1 and [45]. It is seen that incorporation of 5 wt% nanoclays alone into these matrices had no significant influences on the TG and DTG parameters. The basic contribution of 5 wt% NC alone was the formation of 2.6 and 3.0 wt% residue, respectively. It is known that, after evaporation of organic modifiers in the nanoclay structure, the remaining silicate layers normally leads to formation of around 3 wt% residue.

Thermal degradation mechanisms of each matrix when loaded with ATH and ATH-ZB system were also discussed in detail in the previous Section 3.1. Figures 3.19 and 3.20, and Table 3.8 show that, replacement of 5 wt% ATH with NC also results in no significant improvements in TG and DTG parameters, except a slight contribution in the residue amount.

Table 3.8 Thermal degradation parameters determined from TG and DTG curves

Specimens	T_{DTG-Peak 1}^a (°C)	T_{DTG-Peak 2}^b (°C)	T_{10wt%}^c (°C)	T_{50wt%}^d (°C)	% Residue at 600°C^e
LDPE	-	480	451	477	0.2
LDPE-NC	-	484	455	481	2.6
LDPE-ATH65	329	480	324	484	38.4
LDPE-ATH60-NC	329	441	321	447	41.9
LDPE-ATH55-ZB	322	475	320	481	43.4
LDPE-ATH50-ZB-NC	331	437	326	444	43.9
LDPE/EVA	357	478	431	473	0.3
LDPE/EVA-NC	339	484	420	477	3.0
LDPE/EVA-ATH65	336	478	329	487	40.2
LDPE/EVA-ATH60-NC	337	443	330	457	43.2
LDPE/EVA-ATH55-ZB	335	478	330	489	45.5
LDPE/EVA-ATH50-ZB-NC	340	444	334	465	45.7

^a T_{DTG-Peak 1}: First peak temperature in DTG curve.

^b T_{DTG-Peak 2}: Second peak temperature in DTG curve.

^c T_{10wt%}: Thermal degradation temperature for 10% mass loss.

^d T_{50wt%}: Thermal degradation temperature for 50% mass loss.

^e % Residue at 600°C: % Char yield at 600 °C.

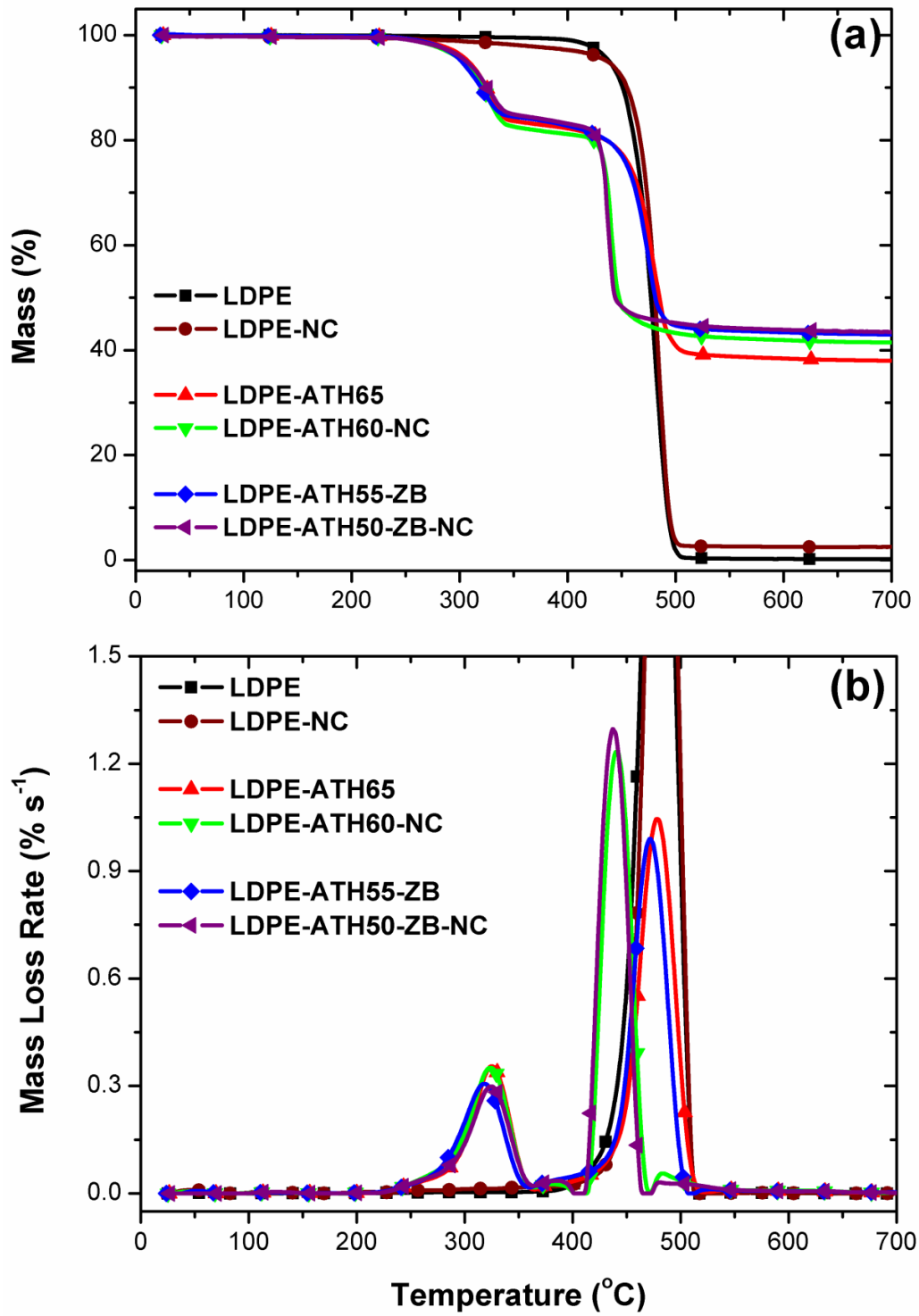


Figure 3.19 (a) Thermogravimetric (TG) and (b) Differential Thermogravimetric (DTG) curves of the specimens with LDPE matrix

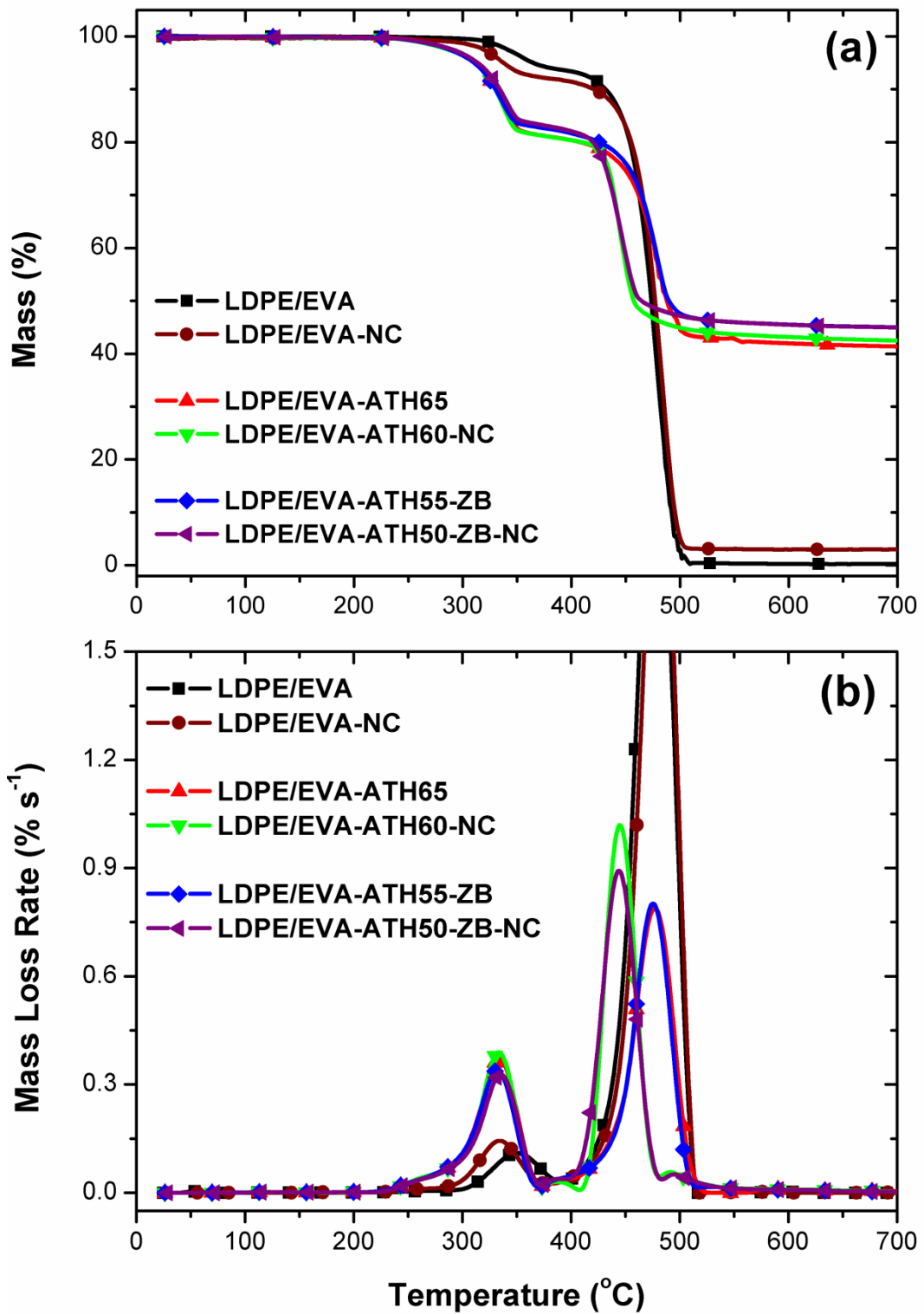


Figure 3.20 (a) Thermogravimetric (TG) and (b) Differential Thermogravimetric (DTG) curves of the specimens with LDPE/EVA matrix

3.2.5 Residue Analysis

In the previous Section 3.1 it was not possible to investigate surface char layers of LOI specimens under SEM due to their very loose and weak structure. However, incorporation of nanoclays into each matrix caused microscopic examination of LOI char layers with SEM as shown in Figure 3.21 for the specimens with LDPE matrix. Since there were no significant differences, images for LDPE/EVA matrices were not shown.

Low magnification smooth surface image in Figure 3.21(a) indicates that when 5 wt% NC was used alone, there was almost no carbonaceous char layer formation. On the other hand, when 5 wt% NC was used together with ATH and ATH-ZB system, high magnification images in Figure 3.21(b) and (c) show that rather a continuous surface char barrier could be formed protecting the underlying polymer from heat and flammable gas transfer.

The second step of the residue analysis was performed with the macro-scale visual examination of the surface char layers of all MLC specimens just after the test. Since there were no significant differences between LDPE and LDPE/EVA specimens, surface char layer images of only LDPE specimens are given in Figure 3.22.

Figure 3.22(a) and (b) reveal that incorporation of nanoclays alone into neat matrices lead to only increased char content. When NC was used together with ATH (Figure 3.22(c, d)) and ATH-ZB system (Figure 3.22(e, f)), it was seen that there was no significant differences in the top view macro scale appearances of the surface char layers of MLC specimens.

However, it is known that addition of nanoclays result in strong, tough and tight carbonaceous structure through the char layer thickness due to basically the stacks of well-dispersed clay silicate layers, which shield the underlying polymer by restricting heat and mass transfer. Besides, the tortuous pathway formed by nano-dispersed high-aspect-ratio silicate layers could hinder the diffusion of volatiles within the melt during fire. These two contributions of nanoclays, i.e. strong and tough carbonaceous char formation and hindered diffusion are simply named as “barrier effects”.

As the third step, residue analysis was conducted by XRD of MLC chars of all specimens in order to reveal whether there is any other ceramic structure formed apart from the expected ones. XRD diffractograms are given in Figures 3.23 and 3.24 for the specimens with LDPE and LDPE/EVA matrices, respectively.

Figures 3.23 and 3.24 show that when NC was used alone, typical crystal peaks of montmorillonite clay mineral were appeared. When NC was used together with ATH, then typical peaks of alumina which is the main byproduct of its decomposition were also appeared. Similarly, when NC was used together with ATH-ZB system, then two more peaks corresponding to decomposition byproducts of ZB; i.e. dehydrated zinc borate and zinc oxide, were also formed.

Thus, it can be stated that, apart from the expected decomposition byproducts, no other phases were formed in the chars of MLC specimens. This could be interpreted as another confirmation of the physical barrier mechanism of ATH, ZB and NC.

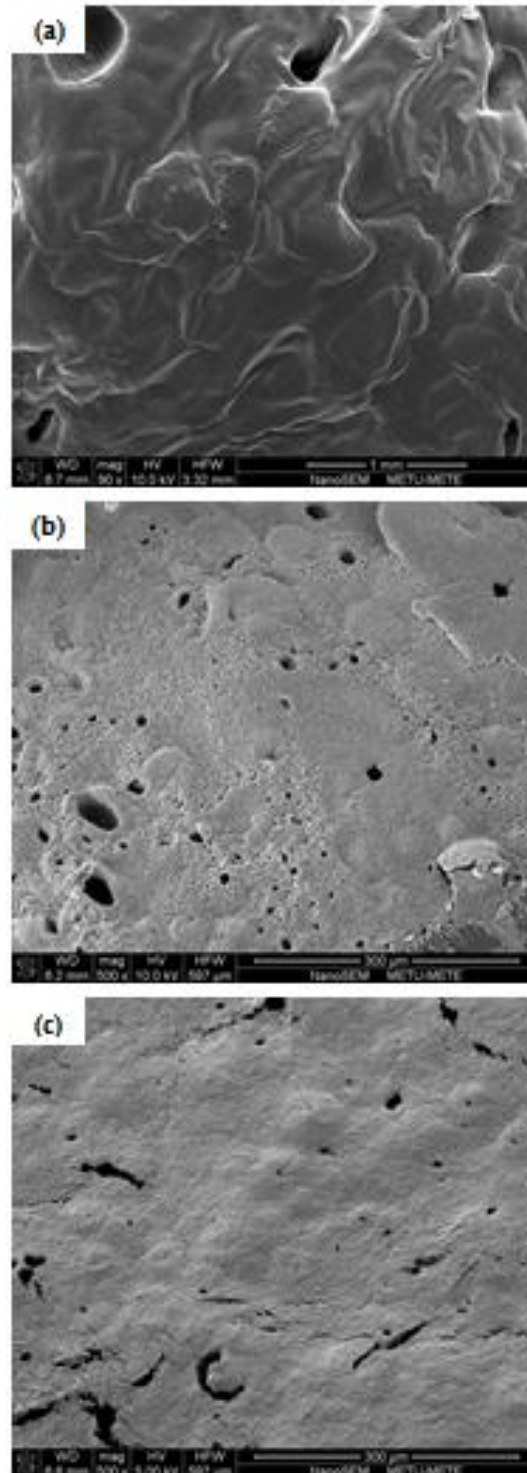


Figure 3.21 SEM images showing surface char barriers of the specimens with LDPE matrix after LOI test; (a) LDPE-NC, (b) LDPE-ATH60-NC, (c) LDPE-ATH50-ZB-NC

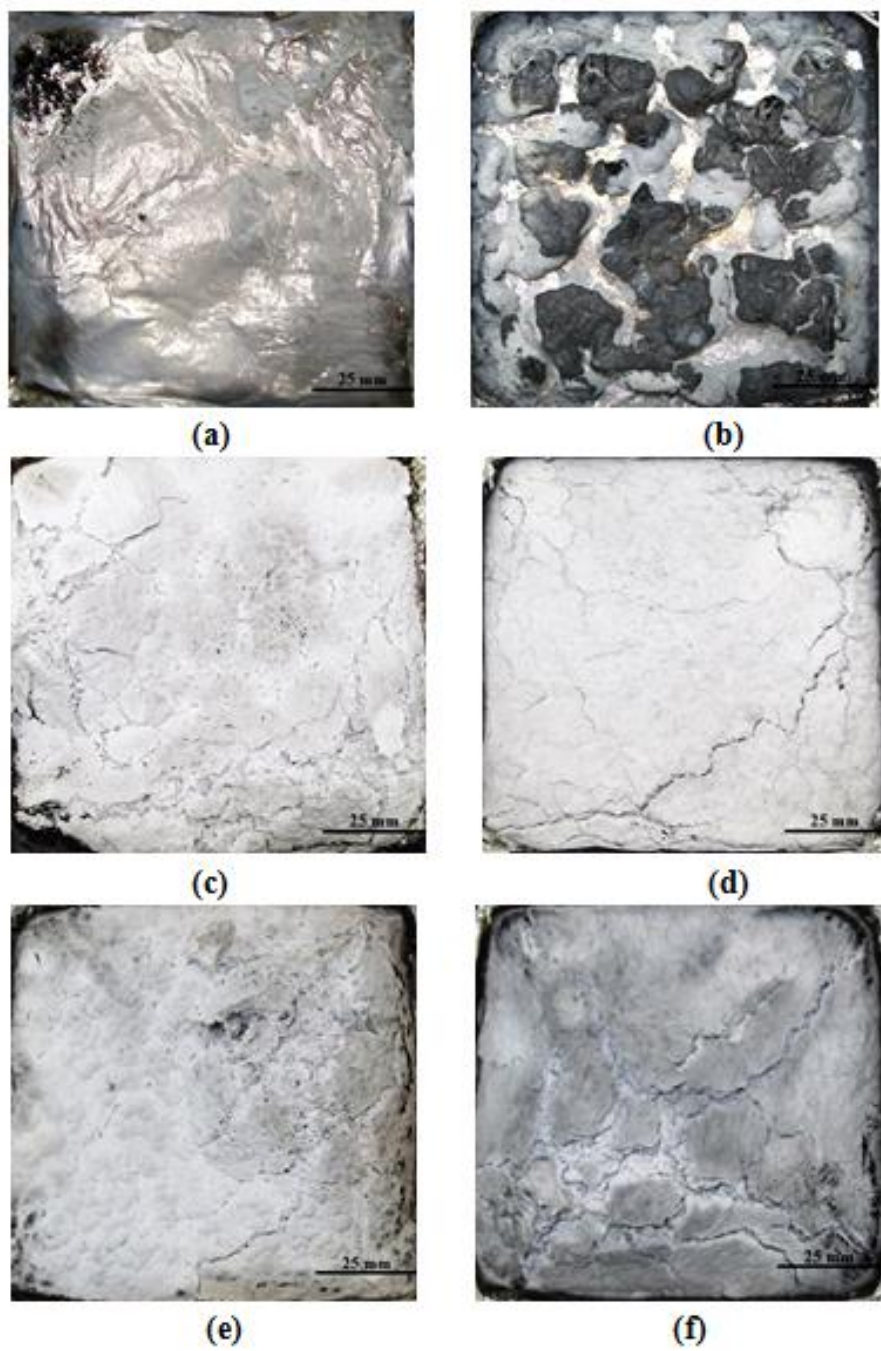


Figure 3.22 Macroscale appearances of the surface char layers of MLC specimens with LDPE matrix; (a) LDPE, (b) LDPE-NC, (c) LDPE-ATH65, (d) LDPE-ATH60-NC, (e) LDPE-ATH55-ZB, (f) LDPE-ATH50-ZB-NC

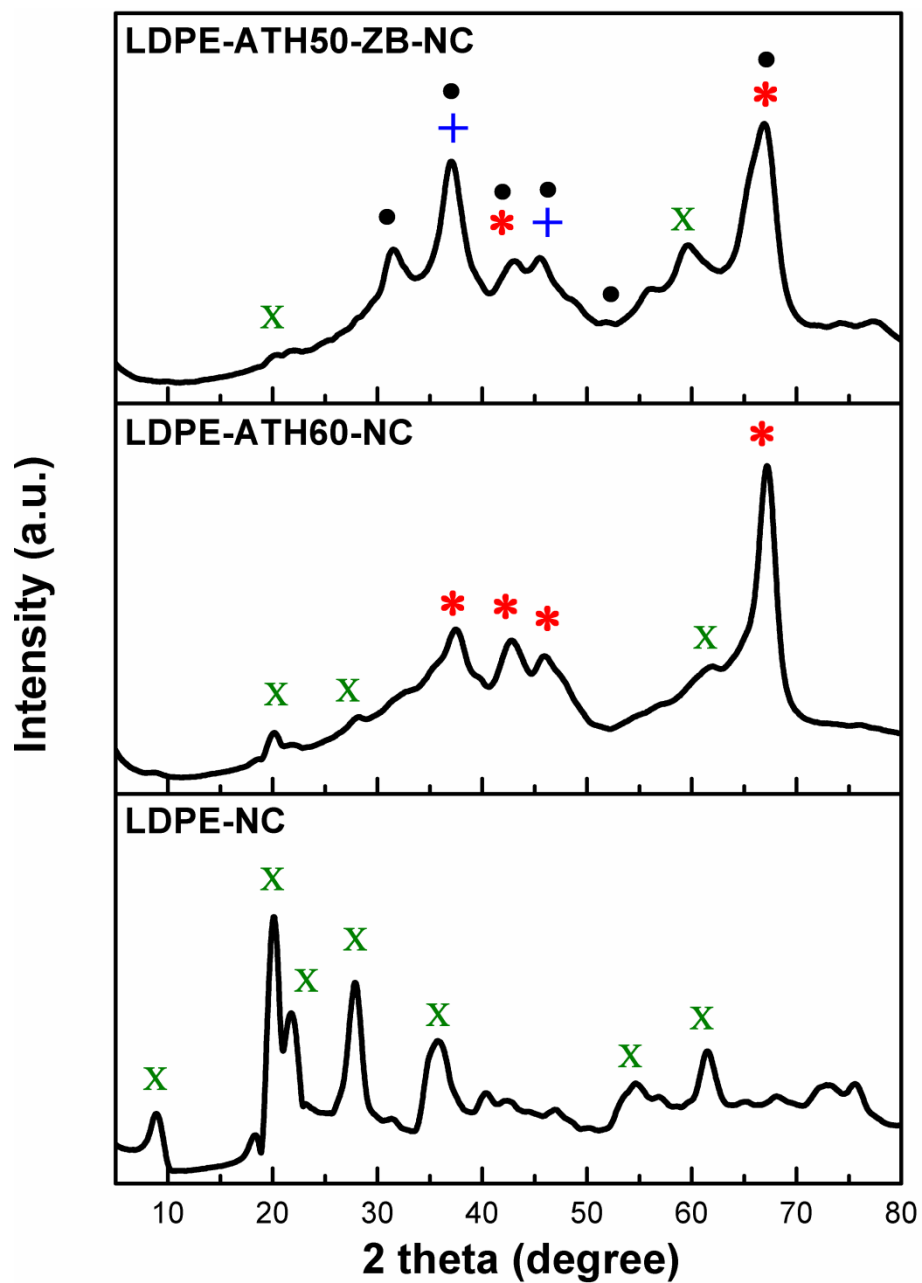


Figure 3.23 XRD patterns of the chars of the MLC nanocomposite specimens with LDPE matrix

X Montmorillonite

* Aluminum oxide: Al_2O_3 (Card no: 04-0880)

+ Dehydrated zinc borate: $\text{Zn}(\text{BO}_2)_2$ (Card no: 39-1126)

• Zinc oxide: ZnO_2 (Card no: 13-0311)

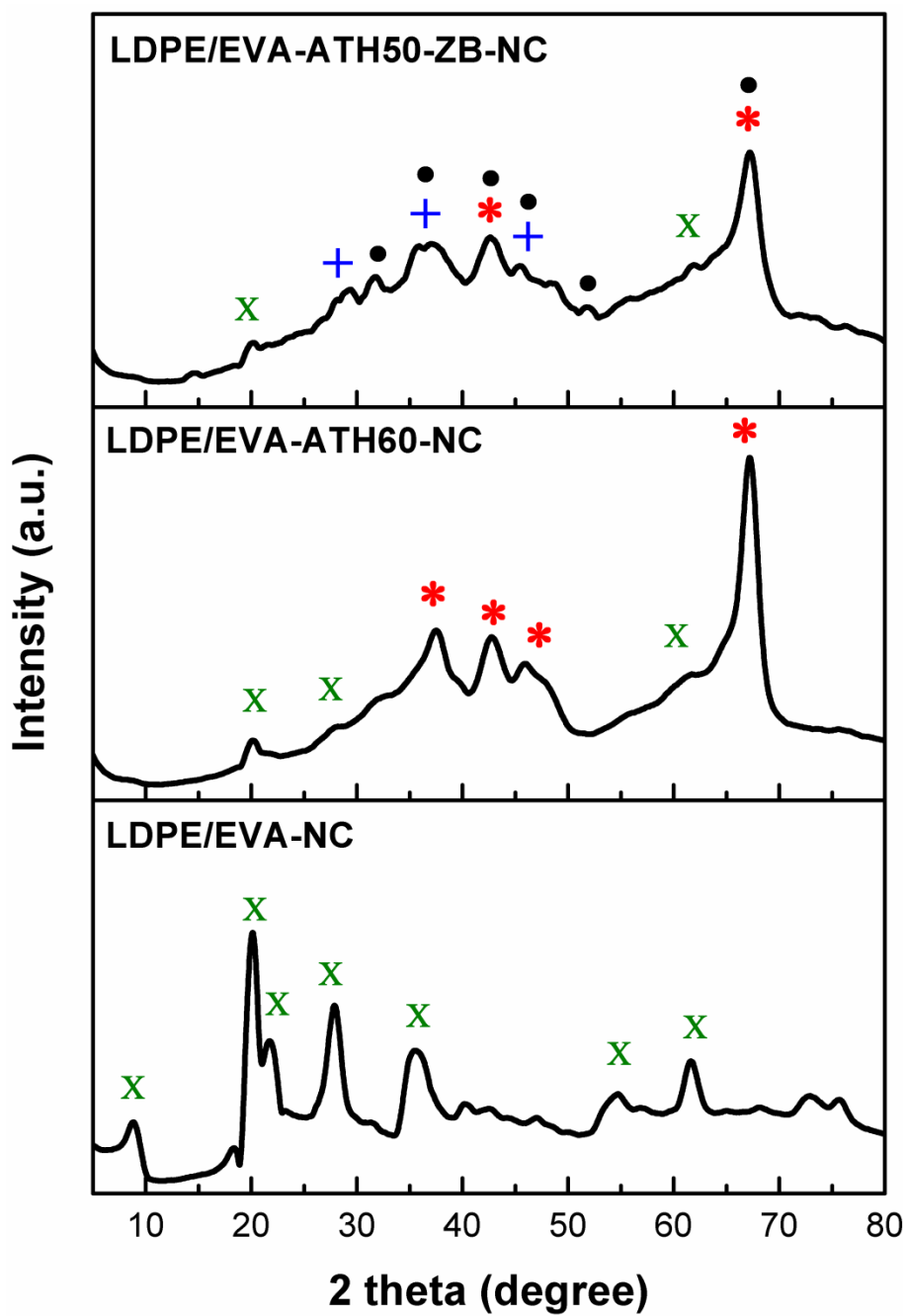


Figure 3.24 XRD patterns of the chars of the MLC nanocomposite specimens with LDPE/EVA matrix

X Montmorillonite

* Aluminum oxide: Al_2O_3 (Card no: 04-0880)

+ Dehydrated zinc borate: $\text{Zn}(\text{BO}_2)_2$ (Card no: 39-1126)

• Zinc oxide: ZnO_2 (Card no: 13-0311)

3.2.6 Mechanical Behavior

Effects of nanoclays (NC) alone and together with ATH and ATH-ZB flame retardants on the mechanical performance of cable insulation materials LDPE and LDPE/EVA were investigated by tensile tests. Figures 3.25 and 3.26 show tensile stress-strain behavior of the specimens for each matrix, while mechanical properties determined for all specimens are tabulated in Table 3.9.

These figures and Table 3.9 show that due to the decreased chain mobility of the polymer matrices, use of ATH and ATH-ZB flame retardants increases both Young's modulus and tensile strength of cable insulation materials as much as by 500% and 20%, respectively. On the other hand, ductility values (i.e. % elongation at break) of both matrices drop drastically due to the extreme stiffening effect of the required very large quantity of these flame retardants.

Figures 3.25 and 3.26, and Table 3.9 also indicate that when NC was incorporated alone or together with ATH and ATH-ZB flame retardants, there were further increases in Young's modulus values, but slight decreases in tensile strength and % elongation at break values. However, these slight decreases were traded-off with the improvements in many flammability parameters.

In order to observe distribution of additives, fracture surfaces of the tensile test specimens were also examined under SEM. Fractographs of LDPE and LDPE/EVA specimens are given in Figures 3.27 and 3.28, respectively.

Figures 3.27(a) and 3.28(a) revealed rather rough and ductile fracture surface of neat LDPE. Due to its nanosize, distribution of NC alone could not be observed (Figures 3.27(b) and 3.28(b)). Figures 3.27(c, e) and 3.28(c, e) show that ATH and ATH-ZB particles were uniformly distributed with certain level of interfacial bonding with the matrix. Incorporation of NC together with ATH and ATH-ZB had no detrimental effect on the distribution of these particles, as indicated in Figures 3.27(d, f) and 3.28(d, f).

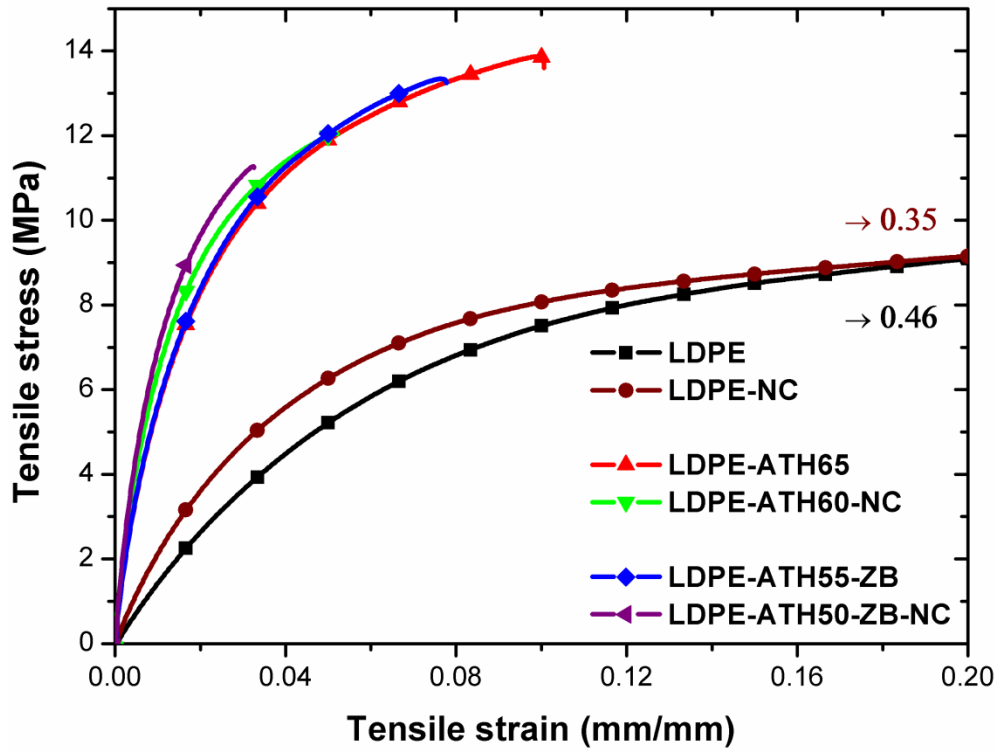


Figure 3.25 Tensile stress-strain curves of the specimens with LDPE matrix

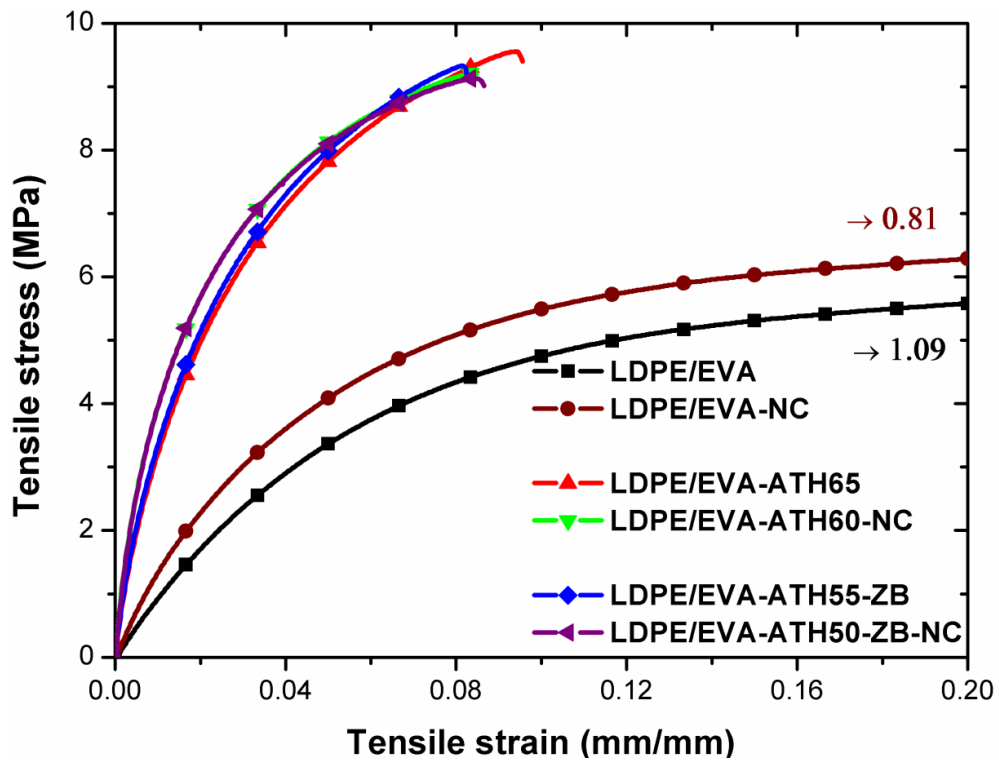


Figure 3.26 Tensile stress-strain curves of the specimens with LDPE/EVA matrix

Table 3.9 Mechanical properties of the specimens

Specimens	Young's Modulus (GPa)	Tensile Strength (MPa)	% Elongation at break
LDPE	0.19±0.01	11.1±0.3	46±3
LDPE-NC	0.30±0.01	10.8±0.3	35±2
LDPE-ATH65	0.93±0.01	13.6±0.4	9±1
LDPE-ATH60-NC	1.13±0.00	12.0±0.2	5±1
LDPE-ATH55-ZB	0.80±0.07	13.4±0.2	8±1
LDPE-ATH50-ZB-NC	1.21±0.02	12.2±0.4	5±1
LDPE/EVA	0.13±0.01	7.8±0.3	109±28
LDPE/EVA-NC	0.18±0.01	7.8±0.1	81±1
LDPE/EVA-ATH65	0.53±0.02	9.5±0.3	10±1
LDPE/EVA-ATH60-NC	0.75±0.02	9.4±0.1	9±0
LDPE/EVA-ATH55-ZB	0.55±0.03	9.3±0.3	9±1
LDPE/EVA-ATH50-ZB-NC	0.73±0.03	9.2±0.1	9±0

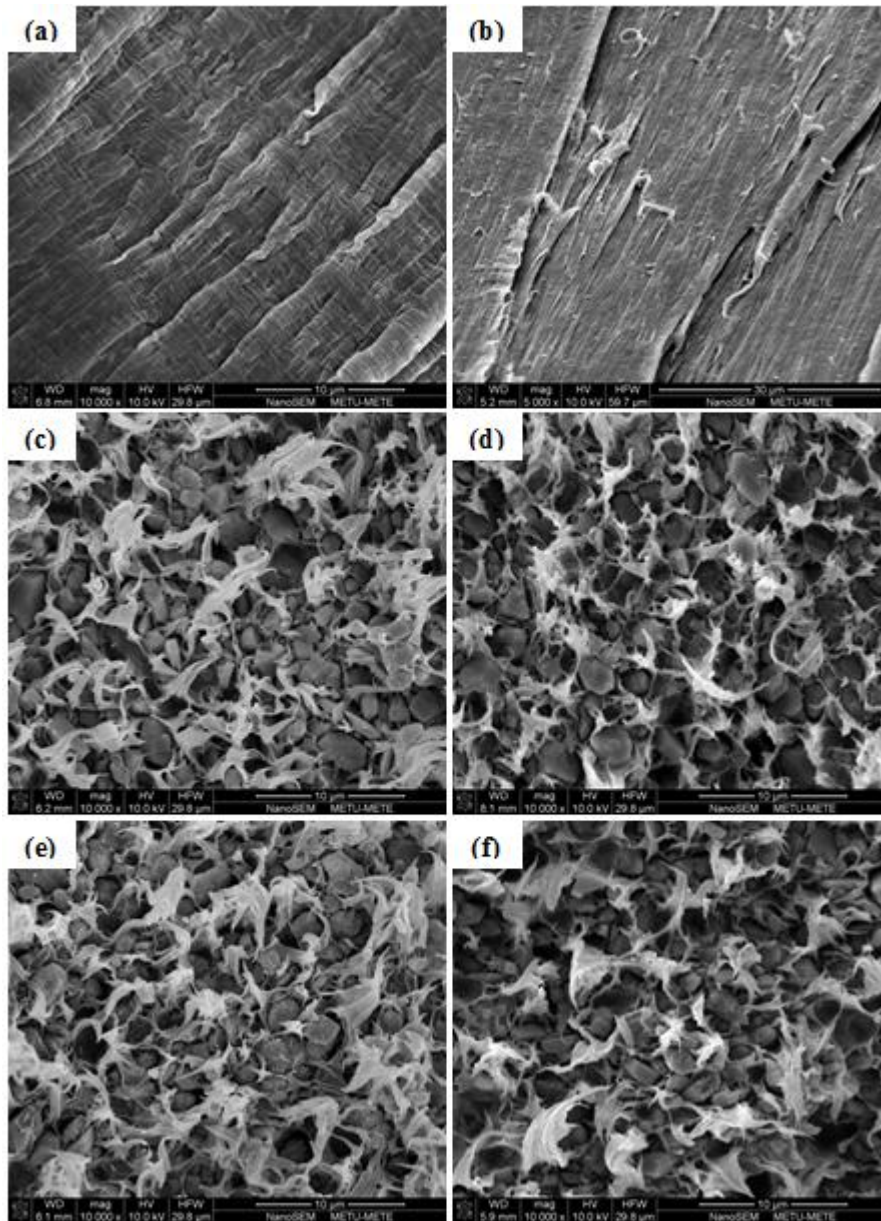


Figure 3.27 SEM fractographs of the specimens with LDPE matrix; (a) LDPE, (b) LDPE-NC, (c) LDPE-ATH65, (d) LDPE-ATH60-NC, (e) LDPE-ATH55-ZB, (f) LDPE-ATH50-ZB-NC

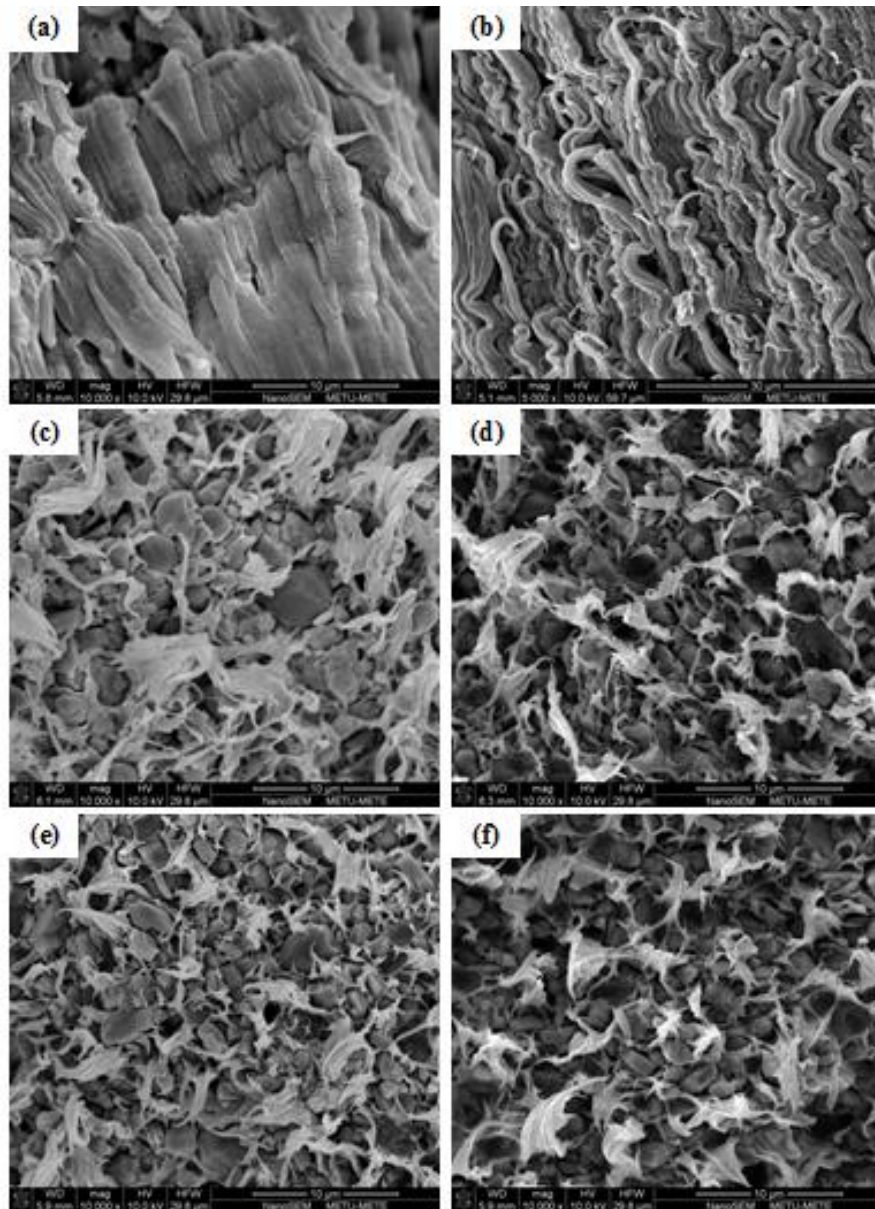


Figure 3.28 SEM fractographs of the specimens with LDPE matrix; (a) LDPE/EVA, (b) LDPE/EVA-NC, (c) LDPE/EVA-ATH65, (d) LDPE/EVA-ATH60-NC, (e) LDPE/EVA-ATH55-ZB, (f) LDPE/EVA-ATH50-ZB-NC

CHAPTER 4

CONCLUSIONS

The main conclusions drawn from the two basic parts of this thesis can be summarized as follows:

(i) Synergistic Effects of Three Boron Compounds with ATH in LDPE and LDPE/EVA Matrices

- UL-94 vertical burning tests indicated that in both matrix materials, replacement of certain amount of ATH with 10, 20 and 30 wt% boron compounds ZB, BO, BA keep the best rating of V-0. In terms of LOI values, replacements especially with 10 wt% boron compounds resulted in synergistic effects.
- In each matrix materials, replacement of certain amount of ATH with boron compounds resulted in similar mass loss cone calorimeter (MLC) behaviour with similar flame retardancy mechanism of physical barrier formation both in the condensed and gas phases. Synergisms in the parameters of PHRR, TTI, FGI and % Char Yield were obtained with the replacements of especially 10 wt% ZB, BO and BA.
- Thermogravimetric analysis revealed that replacement of certain amount of ATH with boron compounds had no significant influences on the values of DTG peak temperatures and 10 wt% and 50 wt% thermal degradation temperatures. On the other hand, there were synergistic increases in the percent residue formation for each matrix.
- Macro-scale visual examination of MLC chars showed that using only ATH resulted in continuous char layer while addition of boron compounds caused formation of not only several cracks but also certain levels of intumescence. Thus, intumescence character of the char layers resulted in synergism in the physical barrier mechanism.
- XRD diffractograms of MLC chars indicated that, apart from the expected decomposition products, no other phases were formed, which could confirm the physical barrier mechanism of ATH and boron compounds.

- Tensile tests revealed that replacement of certain amounts of ATH with boron compounds resulted in similar mechanical behaviour in each matrix, i.e. similar increases in modulus and strength and similar decreases in ductility values.
- (ii) Contribution of Nanoclays with ATH and Zinc Borate in LDPE and LDPE/EVA Matrices**
- XRD and TEM analyses revealed that nanoclays can be homogeneously distributed in both matrices, where silicate layers were mainly intercalated with certain level of exfoliation.
 - Use of nanoclays with traditional ATH or ATH-ZB system keep UL-94 rating of both matrix materials, and contributes their LOI values by further increases as much as 7 O₂%.
 - Mass loss cone calorimetry analyses indicated that for both matrix materials, use of nanoclays alone could improve many flammability parameters including PHRR, THE, TTI, FGI, etc.
 - Contribution of nanoclays were much more significant when 5 wt% ATH or ATH-ZB flame retardants were replaced with NC. For example, contribution of NC in the further suppression of PHRR and THE values could be as much as 35% and 24%, respectively.
 - Residue analyses clarified that contribution of nanoclays to the flame retardancy mechanisms of ATH and ZB was basically via formation of strong and tough char structure by the stacks of well-dispersed and intercalated/exfoliated silicate layers, which protect the underlying polymer by preventing heat and mass transfer.
 - Thermogravimetric analyses and tensile tests also indicated that use of nanoclays had no detrimental effects on the thermal and mechanical properties of the specimens with each matrix materials.

REFERENCES

- [1] Vasile C, Pascu M. Practical Guide to Polyethylene. *RAPRA Technology, Shrewsbury* 2005.
- [2] Harper CA. Modern Plastics Handbook. *McGraw-Hill, USA* 2000.
- [3] McGarry K, Zilberman J, Hull TR, Woolley WD. Decomposition and Combustion of EVA and LDPE Alone and When Fire Retarded with ATH. *Polymer International* 2000; (49): 1193-1198.
- [4] Jana RN, Mukunda PG, Nando GB. Thermogravimetric Analysis of Compatibilized Blends of Low Density Polyethylene and Poly(dimethyl siloxane) Rubber. *Polymer Degradation and Stability* 2003; (80): 75-82.
- [5] Fink JK. Handbook of Engineering and Specialty Thermoplastics: Polyolefins and Styrenics, *Wiley, USA* 2010.
- [6] Faker M, Rezavi Aghjeh MK, Ghaffari M, Seyyedi SA. Rheology, Morphology and Mechanical Properties of Polyethylene/Ethylene Vinyl Acetate Copolymer (PE/EVA) Blends. *European Polymer Journal* 2008; (44): 1834-1842.
- [7] Takidis G, Bikiaris DN, Papageorgiou GZ, Achilias DS, Sideridou I. Compatibility of Low-Density Polyethylene/Poly(Ethylene-co-vinyl Acetate) Binary Blends Prepared by Melt Mixing. *Journal of Applied Polymer Science* 2003; (90): 841-852.
- [8] Koo JH. Polymer Nanocomposites: Processing, Characterization, and Applications. *McGraw-Hill, New York* 2006.
- [9] Haurie L, Fernandez AI, Valesco JI, Chimenos JM, Lopez Cuesta JM, Espiell F. Thermal Stability and Flame Retardancy of LDPE/EVA Blends Filled with Synthetic Hydromagnesite/Aluminium Hydroxide/Montmorillonite and Magnesium Hydroxide/Aluminium Hydroxide/Montmorillonite Mixtures. *Polymer Degradation and Stability* 2007; (92): 1082-1087.
- [10] Morawiec J, Pawlak A, Slouf M, Galeski A, Piorowska E, Krasnikowa N. Preparation and Properties of Compatibilized LDPE/Organo-Modified Montmorillonite Nanocomposites. *European Polymer Journal* 2005; (41): 1115-1122.

- [11] Wang S, Hu Y, Zhongkai Q, Wang Z, Chen Z, Fan W. Preparation and Flammability Properties of Polyethylene/Clay Nanocomposites by Melt Intercalation Method from Na⁺ Montmorillonite. *Material Letters* 2003; (57): 2675-2678.
- [12] Lee J, Jung D, Hong C, Rhee KY, Advani SG. Properties of Polyethylene-Layered Silicate Nanocomposites Prepared by Melt Intercalation with a PP-g-MA Compatibilizer. *Composites Science and Technology* 2005; (65): 1996-2002.
- [13] Alexandre M, Dubois P. Polymer-Layered Silicate Nanocomposites: Preparation, Properties and Uses of a New Class of Materials. *Materials Science and Engineering* 2000; (28): 1-63.
- [14] Zhang J, Wilkie CA. Preparation and Flammability Properties of Polyethylene-Clay Nanocomposites. *Polymer Degradation and Stability* 2003; (80): 163-169.
- [15] Zanetti M, Costa L. Preparation and Combustion Behavior of Polymer/Layered Silicate Nanocomposites Based upon PE and EVA. *Polymer* 2004; (45): 4367-4373.
- [16] Laoutid F, Bonnaud L, Alexandre M, Lopez-Cuesta JM, Dubois Ph. New Prospects in Flame Retardant Polymer Materials: From Fundamentals to Nanocomposites. *Materials Science and Engineering: R: Reports* 2009; (63): 100-125.
- [17] Scharrel B, Hull TR. Development of Fire-Retarded Materials-Interpretation of Cone Calorimeter Data. *Fire and Materials* 2007; (31): 327-354.
- [18] Beyler CL, Hirschler MM. Thermal Decomposition of Polymers: Handbook of Fire Protection Engineering. *National Fire Protection Association, Quincy, MA* 1988.
- [19] Bourbigot S, Duquesne S. Fire Retardant Polymers: Recent Developments and Opportunities. *Journal of Materials Chemistry* 2007; (17): 2283-2300.
- [20] Kelvin K, Kochesfahani S, Jouffret F. Zinc Borates as Multifunctional Polymer Additives. *Polymers for Advanced Technologies* 2008; (19): 469-474.
- [21] Demirel M, Pamuk V, Dilsiz N. Investigation of Flame Retardancy and Physical-Mechanical Properties of Zinc Borate/Boric Acid Polyester Composites. *Journal Of Applied Polymer Science* 2010; (115): 2550-2555.
- [22] Nyambo C, Kandare E, Wilkie CA. Thermal Stability and Flammability Characteristics of Ethylene Vinyl Acetate (EVA) Composites Blended with a Phenyl Phosphonate-Intercalated Layered Double Hydroxide (LDH), Melamine Polyphosphate and/or Boric Acid. *Polymer Degradation and Stability* 2009; (94): 513-520.
- [23] Zhu W, Weil ED. A Paradoxical Flame-Retardant Effect of Nitrates in ATH-Filled Ethylene-Vinyl Acetate Copolymer. *Journal Of Applied Polymer Science* 1995; (56):925-933.

- [24] Jiao CM, Chen XL. Flame Retardant Synergism of Hydroxy Silicone Oil and $\text{Al}(\text{OH})_3$ in EVA Composites. *Polymer-Plastics Technology and Engineering* 2009; (48):665-670.
- [25] Jiao CM, Chen XL. Influence of Fumed Silica on the Flame-Retardant Properties of Ethylene Vinyl Acetate/Aluminum Hydroxide Composites. *Journal Of Applied Polymer Science* 2011; (120):1285-1289.
- [26] Cross MS, Cusack PA, Hornsby PR. Effects of Tin Additives on the Flammability and Smoke Emission Characteristics of Halogen-free Ethylene-Vinyl Acetate Copolymer. *Polymer Degradation and Stability* 2003; (79):309-318.
- [27] Azizi H, Barzin J, Morshedian J. Silane Crosslinking of Polyethylene: The Effects of EVA, ATH and Sb_2O_3 on Properties of the Production in Continuous Grafting of LDPE. *Express Polymer Letters* 2007; (1):378-384.
- [28] Wei P, Han Z, Xu X, Li Z. Synergistic Flame Retardant Effect of SiO_2 in LLDPE/EVA/ATH Blends. *Journal of Fire Sciences* 2006; (24):487-498.
- [29] Basfar AA. Flammability of Radiation Cross-linked Low Density Polyethylene as an Insulating Material for Wire and Cable. *Radiation Physics and Chemistry* 2002; (63):505-508.
- [30] Bourbigot S, Bras ML, Leeuwendal R, Shen KK, Schubert D. Recent Advances in the Use of Zinc Borates in Flame Retardancy of EVA. *Polymer Degradation and Stability* 1999; (64):419-425.
- [31] Isitman NA, Kaynak C. Effect of Partial Substitution of Aluminum Hydroxide with Colemanite in Fire Retarded Low-Density Polyethylene. *Journal of Fire Sciences* 2012; (31):73-84.
- [32] Tang Y, Hu Y, Wang SF, Gui Z, Chen Z, Fan WC. Preparation and Flammability of Ethylene-Vinyl Acetate Copolymer/Montmorillonite Nanocomposites. *Polymer Degradation and Stability* 2002; (78):555-559.
- [33] Shi Y, Kashiwagi T, Walters RN, Gilman JW, Lyon RE, Sogah DY. Ethylene Vinyl Acetate/Layered Silicate Nanocomposites Prepared by a Surfactant-Free Method: Enhanced Flame Retardant and Mechanical Properties. *Polymer* 2009; (50):3478-3487.
- [34] Marosfoi BB, Marosi GJ, Szep A, Anna P, Keszei S, Nagy BJ, Martvonova H, Sajo IE. Complex Activity of Clay and CNT Particles in Flame Retarded EVA Copolymer. *Polymers for Advanced Technologies* 2006; (17):255-262.

- [35] Yen YY, Wang HT, Guo WJ. Synergistic Flame Retardant Effect of Metal Hydroxide and Nanoclay in EVA Composites. *Polymer Degradation and Stability* 2012; (97):863-869.
- [36] Chen X, Jiao C, Zhang J. Thermal and Combustion Behavior of Ethylene-Vinyl Acetate/Aluminum Trihydroxide/Fe-Montmorillonite Composites. *Polymer Engineering and Science* 2012; (52):414-419.
- [37] Bee ST, Hassan A, Ratman CT, Tee TT, Sin LT. Effects of Montmorillonite on the Electron Beam Irradiated Alumina Trihydrate Added Polyethylene and Ethylene Vinyl Acetate Nanocomposite. *Polymer Composites* 2012; (33):1883-1892.
- [38] Zhang J, Hereid J, Hagen M, Bakirtzis D, Delichatsios MA, Fina A, Castrovinci A, Camino G, Samyn F, Bourbigot S. Effects of Nanoclay and Fire Retardants on Fire Retardancy of a Polymer Blend of EVA and LDPE. *Fire Safety Journal* 2009; (44):504-513.
- [39] Ramirez-Vargas E, Sanchez-Valdes S, Parra-Tabla O, Castaneda-Gutierrez S, Mendez-Nonell J, Ramos-de Valle LF, Lopez-Leon A, Lujan-Acosta R. Structural Characterization of LDPE/EVA Blends Containing Nanoclay-Flame Retardant Combinations. *Journal of Applied Polymer Science* 2012; (123):1125-1136.
- [40] Wu Z, Shu W, Hu Y. Synergist Flame Retarding Effect of Ultrafine Zinc Borate on LDPE/IFR System. *Journal of Applied Polymer Science* 2007; (103):3667-3674.
- [41] Nie S, Zhang M, Yuan S, Dai G, Hong N, Song L, Hu Y, Liu X. Thermal and Flame Retardant Properties of Novel Intumescent Flame Retardant Low-density Polyethylene (LDPE) Composites. *Journal of Thermal Analysis and Calorimetry* 2012; (109):999-1004.
- [42] Witkowski A, Stec AA, Hull TR. The Influence of Metal Hydroxide Fire Retardants and Nanoclay on the Thermal Decomposition of EVA. *Polymer Degradation and Stability* 2012; (97):2231-2240.
- [43] Lu SY, Hamerton I. Recent Developments in the Chemistry of Halogen-free Flame Retardant Polymers. *Progress in Polymer Science* 2002; (27):1661-1712.
- [44] Wu K, Shen MM, Hu Y. Combustion Behavior and Thermal Oxidative Degradation of EVA Containing Intumescent Flame Retardant. *Polymer-Plastics Technology and Engineering* 2010; (49):1527-1533.
- [45] Grexa O, Lübke H. Flammability Parameters of Wood Tested on a Cone Calorimeter. *Polymer Degradation and Stability* 2001; (74):427-432.